MICROFLUIDIC FLOW CELL ARRAY INTEGRATED WITH SURFACE PLASMON RESONANCE MICROSCOPY FOR MICROARRAY ANALYSIS

by

Jianping Liu

A dissertation submitted to the faculty of
The University of Utah
in partial fulfillment of the requirements for the degree of

Doctor of Philosophy

Department of Chemistry

The University of Utah

May 2012

The University of Utah Graduate School

STATEMENT OF DISSERTATION APPROVAL

The dissertation of **Jianping Liu**

has been approved by the following supervisory committee members:

Jennifer S. Shumaker-Parry	, Chair	**5/5/2011** Date Approved
John C. Conboy	, Member	**5/5/2011** Date Approved
Joel M. Harris	, Member	**5/5/2011** Date Approved
Jon D. Rainier	, Member	**5/5/2011** Date Approved
Vladimir Hlady	, Member	**5/5/2011** Date Approved

and by **Henry S. White** , Chair of the Department of **Chemistry**

and by Charles A. Wight, Dean of The Graduate School.

ABSTRACT

This dissertation describes the integration of a microfluidic flow cell array (MFCA) with surface plasmon resonance microscopy (SPRM) and the application of MFCA-SPRM system for microarray analysis of biomolecule interactions.

The design and construction of a SPR microscope with a sensing area that is compatible with the fluidics footprint of the MFCA is described first. Antibody-antibody interactions are used as the model system to demonstrate the capability of the integrated MFCA-SPRM for in situ microarray fabrication and analysis. Impacts of physicochemical parameters, such as reactant concentrations, reaction constants and the flow rate, on the performance of the MFCA-SPRM are investigated by experiments and modeling. Optimized experimental conditions will support the future application of the MFCA-SPRM. Statistical analysis of microarray data (24 micro spots) shows that the spot-to-spot coefficient of variation is within 15%. Major sources of signal variance are from the deviation of light incident angle, heterogeneous sensing surface and the mass transport.

Next, a proof-of-principle experiment demonstrates the potential of the MFCA-SPRM system for immunogenicity assays of Daclizumab to analyze anti-drug antibodies (ADA) from serum samples. Daclizumab is a monoclonal antibody drug for treatment of multiple sclerosis patients. Biotinylated-Daclizumab immobilized on a streptavidin monolayer is used to assess the presence of ADA in serum samples of three patients with multiple

sclerosis. The result shows that the sample from a patient without the treatment of Daclizumab generates the highest SPR signal. In the future, more samples are required to generate statistically significant data to evaluate the immunogenicity of Daclizumab. Matrix-assisted laser desorption/ionization mass spectrometer (MALDI MS) is an ideal tool to be combined with SPR for protein analysis. An antibody microarray created by MFCA and coupled to MS is utilized to demonstrate the potential of microarray analysis with SPR-MS.

Finally, we apply MFCA-SPRM system for characterization of in situ immobilized vesicles on solid surfaces. Hydrophilicity of surface, vesicle size and composition are investigated as factors that affect the structure of vesicles adsorbed on surfaces. A model for the calculation of the surface area of the bilayer is proposed to correlate the SPR response with vesicle structures at the surface.

Dedicated to my parents, sister and Jing for their endless love and support

CONTENTS

LIST OF FIGURES

LIST OF TABLES

Table Page

ACKNOWLEDGMENTS

I am particularly grateful to my mentor Professor Jennifer S. Shumaker-Parry for her guidance throughout my graduate studies at the University of Utah. She has provided me an optimal research environment. Her constant encouragement, support, and invaluable suggestions made my research success.

I would like to thank all of my committee members, Dr. Henry S. White, Dr. Joel M. Harris, Dr. John C. Conboy, Dr. Jon D. Rainier and Dr. Vladimir Hlady, for their guidance and suggestions. I am grateful for the help and support from my research collaborators, Dr. Bruce K. Gale, Dr. Mark A. Eddings and the Wasatch Microfluidics team.

I would like to appreciate the help and friendship from all the members of Shumaker-Parry group and the IBAC groups. Thank you Rostislav, Jong-won, Patrick, Cindy, Cara and Aixiang. Thank you Eric and Chaoxiong in the Harris group; Jin, Dayi and Trang in the Conboy group and anyone else I might have forgotten.

Finally, I would like to acknowledge my family. I thank my parents, Kehua Liu and Xianjin Gao, for teaching me how to live life and enjoy it. I thank my sister Meiling Gao for being my closest friend. I thank my husband Jing Liu for his overwhelming love and unconditional support.

CHAPTER 1

INTRODUCTION

Surface Plasmons

Surface plasmons (SPs) are electromagnetic waves propagating along a dielectric and metal interface. They are generated by the interaction between the free electrons of the metal and an electromagnetic field.[1] The phenomenon of SPs was first observed by Wood in the beginning of the 20th century by reporting anomalous diffraction of light with metallic gratings.[2] In 1957, the concept of a plasmon was introduced by Ritchie to theoretically explain the energy loss experienced by fast electrons traveling through thin metal foils.[3] In the late 1960s, optical excitation of SPs based on attenuated total reflection (ATR) was demonstrated by Otto and Kretschmann.[1] Recently, with the development of nanotechnology, manipulating optical properties of SPs on the nanoscale has attracted intense interest of applying SPs in electronics, photonics, sensing and many other research areas.[4-6]

Based on the excitation mode of SPs, the study of SPs can be divided into localized surface plasmons (LSPs) and surface plasmon polaritons (SPPs).[7] LSPs are charge density oscillations confined to metallic nanoparticles or nanostructures, resulting in strong light scattering and absorption as well as enhanced local electromagnetic field.[8] The field enhancement of LSPs has been used to enhance signals in surface-enhanced

Raman spectroscopy (SERS).[9, 10] The loss of light due to absorption and scattering is characterized by peaks in SPs extinction spectra. Properties of the extinction peaks, such as frequency and intensity, depend on the nanostructure materials, size, shape, distribution and surrounding environment, which promotes the development of LSPs-based waveguide and sensors.[11] However, we will focus on excitation of SPPs at a metal film-dielectric interface with light in an ATR configuration for biosensing. The dependence of the properties of SPPs on the dielectric constant of the local environment is the fundamental basis for SPR sensing.[12-14]

SPPs are surface-bound electromagnetic waves propagating at a metal-dielectric planar interface as shown in Figure 1.1a.[5] They are transverse waves with the electric field perpendicular to the traveling direction in the positive *x*-direction shown in the Figure 1.1a. Figure 1.1b illustrates the electric field being enhanced in the surface and decaying exponentially into the metal and dielectric medium. By solving Maxwell's equations and using the physical parameters of a gold-water interface with an excitation wavelength of 630 nm, the decay lengths of SPPs in water and gold are 162 and 29 nm, respectively.[2] The propagation length of SPPs in the x-y plane is 3 μm. The decay and propagation lengths of SPPs determine the spatial detection limit and resolution of SPR microscope because SPR sensing depends on the excitation of SPPs. Figure 1.1c compares the dispersion curves of SPPs and a free space photon to excite SPPs. It shows that there is always a momentum mismatch between SPPs and the light photon for the same frequency. Some strategies are needed to overcome the momentum mismatch. Grating and prism coupling are two major configurations used in the setup of SPR microscopes.[2] Next I will discuss details of SPR biosensing based on the prism coupling.

Surface Plasmon Resonance Sensing

Surface plasmon resonance (SPR) sensing has been widely used in biomedical, pharmaceutical, food and environmental research to study biomolecular interactions at solid-liquid interfaces.[2, 15] The principle of SPR sensing is characterized by the dispersion relation of SPPs at a planar dielectric-metal interface. Under appropriate boundary conditions shown in Figure 1.2, solving Maxwell's equation yields the dispersion relation of SPPs. The SPPs wave vector k_{sp} can be expressed as:

$$k_{SP} = \frac{\omega}{c}\sqrt{\frac{\varepsilon_d \varepsilon_m}{\varepsilon_d + \varepsilon_m}} \tag{1.1}$$

where ω is the angular frequency of incident light, c is the speed of light in vacuum, and ε_d and ε_m are the dielectric constants of the dielectric and metal, respectively. As discussed above, the incidence light wave vector of $k = w/c$ can't match that of SPPs. One strategy to overcome the mismatch is to utilize the evanescent wave generated through ATR with prism coupling (wave vector shown in Equation 1.2) to match the momentum required by SPPs. A scheme of the experimental arrangement is shown in Figure 1.2. The wave vector of the evanescent wave k_{EW} is:

$$k_{EW} = \frac{\omega}{c} sin\theta \sqrt{\varepsilon_p} \tag{1.2}$$

where ε_p is the dielectric constant of the prism and θ is the light incident angle. With high refractive index of the prism and proper angle of incident light, if the metal film is brought within the range of the evanescent wave, SPPs can be excited when $k_{SP} = k_{EW}$. Due to the coupling, the energy of evanescent wave is transferred to SPPs. According to

energy conservation, the energy of incident light is equal to the energy of light absorbed by SPPs and reflected from the interface. As a result, the reflected light intensity drops and the dropped intensity depends on the coupling conditions. When proteins or other biomolecules bind to the metal surface, the dielectric constant ε_d will be changed, which will also cause following changes of the wave vector of SPPs, SPR coupling conditions and light intensity of reflected light as expressed in Equations 1.1 and 1.2. Therefore, the change of dielectric constant can be indirectly detected via measuring the reflected light properties. Since the refractive index ($n = \sqrt{\varepsilon_p}$) is proportional to the dielectric constant ε_d, it is also possible to measure the change of refractive index caused by the adsorption of biomolecules in the same manner.

Depending on the detection mode, a prism-based SPR system can be set up for either SPR spectroscopy or SPR microscopy (also called SPR imaging). SPR spectroscopy typically relies on measuring a SPR curve with either a spectrophotometer or a position-sensitive detector, which is a plot of the reflected light intensity versus the light wavelength or incident angle. SPR microscopy uses a CCD camera as a detector to monitor the reflected light intensity from the entire sensing region to form a digital image. The intensity values for selected pixels in the generated gray-scale images can be correlated with the amount of material adsorbed on the sensor surface.[16, 17] The microscopy format provides spatially-resolved measurements which offer opportunities for multiple, simultaneous control experiments and parallel processing of larger data sets, which will be further discussed in Chapter 2.

Microfluidic Flow Cell Array-Surface Plasmon Resonance Microscope

SPR microscopy is an ideal tool for probing large microarrays of biomolecular binding interactions and can provide label-free, real-time analysis of binding kinetics. Creation of a high-density and high-activity microarray on the SPR sensing surface is a key step in SPRM analysis. Various microarray fabrication techniques, such as protein pin spotting, ink jet printing and micro contact printing, have been used to create large numbers of densely arrayed spots.[18, 19] However, disadvantages of these *ex situ* arraying methods include poor spot quality, extensive sample processing, and the requirement for expensive robotic control.[17, 20, 21]

Microfluidic technology provides an alternative approach to *in situ* array fabrication and biomolecule immobilization.[22, 23] A continuous flow microspotter (CFM) is a 3D microfluidic system that was developed by Gale and coworkers for microarray fabrication with continuous flow.[24] The confinement of protein deposition to specific locations on the substrate with CFM can minimize sample depletion in 2D microfluidic channels and increase the array density. When CFM was integrated with SPR microscope for the first time in our lab, the capability to perform sequential assay steps with continuous flow enabled the integrated system for *in situ* immobilization of probe molecules and analysis of target in solution in a microarray format. In addition to the advantages of real-time, label-free and high-throughput analysis with SPR microscope, the *in situ* method shows improved deposition quality,[24] and maintaining a humid condition at the reaction surface can prevent protein denaturation. In this dissertation

research, we will focus on the setup of the integrated system, optimization of experiment conditions and applications in analyses of various biomolecular interactions.

In Chapter 2, we demonstrate the integration of the CFM as a microfluidic flow cell array (MFCA) with an SPR microscope (SPRM) for *in situ* microarray fabrication and real-time analysis. Antibody-antibody interactions are chosen as the model system to demonstrate the capability of the combined MFCA-SPRM system.

In order to optimize conditions for array-based biomolecular interaction analysis with the MFCA-SPRM, binding kinetics of biotin-streptavidin and Daclizumab (a humanized monoclonal antibody drug)-IgG are studied as model systems in Chapter 3 to probe the impact of physicochemical parameters, such as concentration of reactants in solution and on the surface, flow rate and geometry of flow cell, on the performance of MFCA-SPRM system. The study is based on both experiments and numerical modeling. The modeling is useful for the evaluation of factors that impact different biomolecular interactions under a variety of conditions. Sources that cause signal variations among microspots are also identified in Chapter 3.

The application of the MFCA-SPRM system for biomolecule analysis is described in Chapters 4-6. In Chapter 4, a preliminary investigation of applying the MFCA-SPRM to detect and measure antidrug antibodies (ADAs) from serum samples of multiple sclerosis patients treated with Daclizumab is reported. Measurement of ADAs is one of the approaches to evaluate the immunogenicity of biological drugs. The assessment and monitoring of immunogenicity are necessary in clinical trials of new drugs for safety and efficacy. Bioanalytical methods including radiolabeling, enzymatic, fluorescence, electrochemical luminescence detection and SPR have been used to develop

immunogenicity assays in various formats, such as direct, indirect, bridging and competitive. In addition to reported label-free, real-time immunogenicity assays with SPR, MFCA-SPRM provides more channels for high-throughput analysis and opportunities for multiple simultaneous control experiments.

Chapter 5 describes a versatile method to use MFCA to fabricate antibody arrays and then identify surface-bound antibodies after SPR analysis with a commercial MALDI-TOF mass spectrometry. The ultimate goal is to combine SPR and MALDI MS for array-based qualitative and quantitative analyses of protein interactions. Chapter 6 presents the characterization of intact vesicles immobilization on SPR sensing surface, which could be applied in protein-membrane interaction analysis. The interfacial energy of vesicles adsorption depends on several factors including the hydrophilicity of the surface as well as the composition and size of vesicles. A calculation model is proposed to relate SPR signals with structures of the vesicles on the solid surfaces.

References

1. Raether, H., *Surface Plasmons on Smooth and Rough Surfaces and on Gratings;* Springer: 1988.

2. Homola, J.; Yee, S. S.; Gauglitz, G., Surface plasmon resonance sensors: review. *Sens. Actuators B Chem.* **1999**, *54*, 3-15.

3. Ritchie, R. H., Plasma losses by fast electrons in thin films. *Phys. Rev.* **1957**, *106*, 874.

4. Ozbay, E., Plasmonics: Merging photonics and electronics at nanoscale dimensions. *Science* **2006**, *311*, 189-193.

5. Barnes, W. L.; Dereux, A.; Ebbesen, T. W., Surface plasmon subwavelength optics. *Nature* **2003**, *424*, 824-830.

6. Maier, S. A.; Brongersma, M. L.; Kik, P. G.; Meltzer, S.; Requicha, A. A. G.; Atwater, H. A., Plasmonics - A route to nanoscale optical devices. *Adv. Mater.* **2001**, *13*, 1501-1505.

7. Maier, S., *Plasmonics: Fundamentals and Applications*; Springer: 2007.

8. Hutter, E.; Fendler, J. H., *Exploitation of Localized Surface Plasmon Resonance*; WILEY-VCH Verlag: 2004; Vol. *16*, pp 1685-1706.

9. Moskovits, M., Surface-enhanced spectroscopy. *Rev. Mod. Phys.* **1985**, *57*, 783-826.

10. Mulvaney, P., Surface plasmon spectroscopy of nanosized metal particles. *Langmuir* **1996**, *12*, 788-800.

11. Hutter, E.; Fendler, J. H., Exploitation of localized surface plasmon resonance. *Adv. Mater.* **2004**, *16*, 1685-1706.

12. Liedberg, B.; Nylander, C.; Lunstrom, I., Surface plasmon resonance for gas detection and biosensing. *Sens. Actuators* **1983**, *4*, 299-304.

13. Rothenhausler, B.; Knoll, W., Surface-plasmon microscopy. *Nature* **1988**, *332*, 615-617.

14. Knoll, W., Interfaces and thin films as seen by bound electromagnetic waves. *Annu. Rev. Phys. Chem.*, **1998**, *49*, 569-638.

15. Campbell, C. T.; Kim, G., SPR microscopy and its applications to high-throughput analyses of biomolecular binding events and their kinetics. *Biomaterials* **2007**, *28*, 2380-2392.

16. Jung, L. S.; Shumaker-Parry, J. S.; Campbell, C. T.; Yee, S. S.; Gelb, M. H., Quantification of tight binding to surface-immobilized phospholipid vesicles using surface plasmon resonance: binding constant of phospholipase A2. *J. Am. Chem. Soc.* **2000**, *122*, 4177-4184.

17. Shumaker-Parry, J. S. *Quantitative Aspects of SPR Spectroscopy and SPR Microscopy:Applications in Protein Binding to Immobilized Vesicles and dsDNA Array;* University of Washington: 2002.

18. Singh, B. K.; Hillier, A. C., Multicolor surface plasmon resonance imaging of ink jet-printed protein microarrays. *Anal. Chem.* **2007**, *79*, 5124-5132.

19. Wilkop, T.; Wang, Z.; Cheng, Q., Analysis of micro-contact printed protein patterns by SPR imaging with a LED light source. *Langmuir* **2004**, *20*, 11141-11148.

20. Barbulovic-Nad, I.; Lucente, M.; Sun, Y.; Zhang, M.; Wheeler, A. R.; Bussman, M., Bio-microarray fabrication techniques - A review. *Critical Reviews in Biotechnology* **2006**, *26*, 237-259.

21. Wu, P.; Grainger, D. W., Comparison of hydroxylated print additives on antibody microarray performance. *J. Proteome* **2006**, *5*, 2956-2965.

22. Whitesides, G. M., The origins and the future of microfluidics. *Nature* **2006**, *442*, 368-373.

23. Delamarche, E.; Bernard, A.; Schmid, H.; Bietsch, A.; Michel, B.; Biebuyck, H., Microfluidic networks for chemical patterning of substrates: design and applications to bioassays. *J. Am. Chem. Soc.* **1998**, *120*, 500-508.

24. Natarajan, S.; Miles, A.; Eckman, J.; Rich, R.; Gale, B. K.; Myszka, D., Continuous-flow microfluidic printing of proteins for array-based applications including surface plasmon resonance imaging. *Anal. Biochem.* **2008**, *373*, 141-146.

Figure 1.1. Properties of surface plasmon polaritons at a dielectric-metal interface. (a) SPPs are transverse electromagnetic waves propagating in the *x*-positive direction. (b) The exponentially decayed electric fields of SPPs in metal and dielectric medium. (c) The dispersion curves of SPPs and a photon in free space. Reprinted by permission from Macmillan Publishers Ltd: [Nature] (Barnes et al. *Nature* **2003,** 424, 824-830.), copyright (2003)

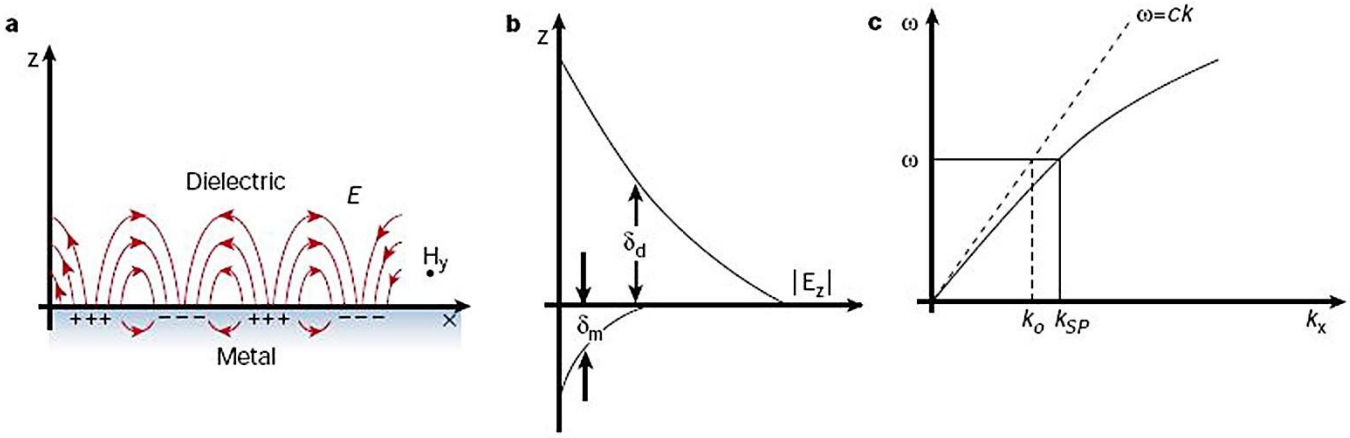
a
z
Dielectric
E
H_y
+++ −−− +++ −−−
Metal
b
z
δ_d
$|E_z|$
δ_m
c
ω
ω=ck
ω
k_o k_{SP}
k_x

Figure 1.2. Schematic of excitation of SPPs with light based on Kretschmann configuration.

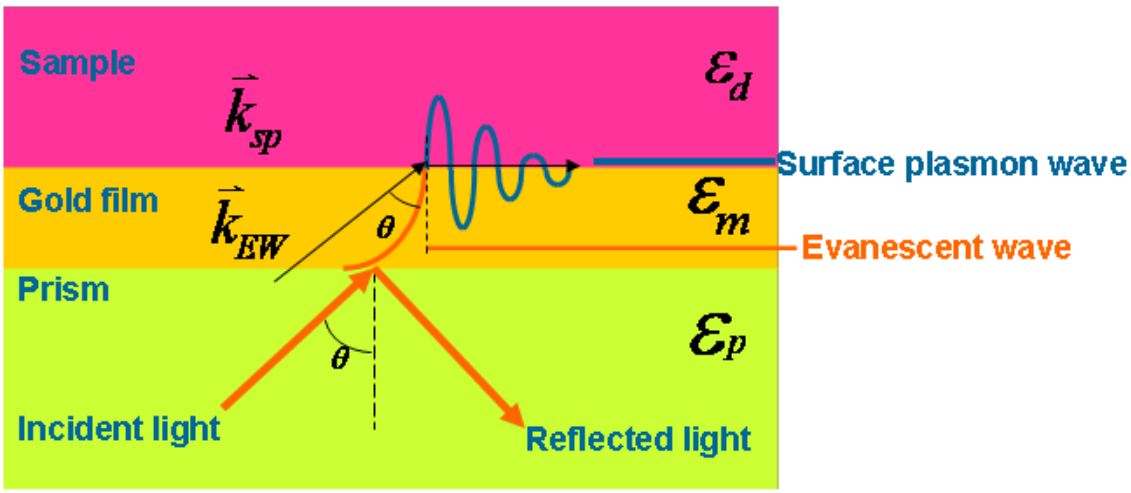
Sample
ε_d
$\vec{k}_{sp}$
Surface plasmon wave
Gold film
$\vec{k}_{EW}$
θ
ε_m
Evanescent wave
Prism
ε_p
θ
Incident light
Reflected light

CHAPTER 2

MFCA-SPRM SYSTEM FOR *IN SITU* MICROARRAY FABRICATION AND THE STUDY OF BIOMOLECULE INTERACTIONS

Introduction

In this chapter, the integration of a microfluidic flow cell array (MFCA) with a surface plasmon resonance microscope (SPRM) is described. After integration and initial characterization, a high-throughput approach to SPRM calibration, microarray fabrication and biomolecular interaction analysis demonstrates the multiplexing capability of the integrated MFCA-SPRM system.

SPR-Based Biosensors

SPR-based sensors have been widely used in analyses of biomolecular interactions in biomedical, pharmaceutical, food and environmental research.[1] Based on the coupling approaches leading to excitation of surface plasmons,[2] SPR sensors can be categorized into three types: prism, grating and waveguide coupled. The most common SPR sensors are built with a prism coupler because of the simple configuration. Depending on the detection modulation, a prism-based SPR system can be set up in either SPR spectroscopy or SPR microscopy (also called SPR imaging) modes.[3, 4] SPR spectroscopy typically relies on measuring the minimum intensity of reflected light versus

wavelength or angle of the incident light.[5] However, this spectroscopy mode is often limited in terms of running multiple experiments simultaneously. The image based microscopy format provides spatially-resolved measurements and has extended SPR-based sensing to a microarray format. In addition to the label-free and real-time analysis provided by SPR spectroscopy, microarray with SPRM increases the throughput for rapid and multiplexed analysis.[6-10]

SPR Microscopy

SPR Microscopy (SPRM) is based on using an expanded and collimated light source to probe a large region of a sensor surface and a CCD camera to monitor the reflected light intensity from the entire sensing region to form a digital image (Figure 2.1a).[11] The intensity values for selected pixels in the generated gray-scale images can be correlated with the amount of material adsorbed on the sensor surface.[9, 12] The microscopy format provides parallel processing advantages of larger data sets, opportunities for multiple simultaneous control experiments, and improved statistically significant results.

The ability to analyze biomolecular interactions in a real-time, label-free and high-throughput manner has made SPRM an attractive option for protein microarray studies.[9, 13-15] In order to apply SPRM, deposition and arraying technology must be used to functionalize the sensing surface and create the microarray. Protein pin spotting, ink jet printing, microcontact printing and other surface patterning techniques have been used to create microarrays of biomolecules, such as DNA,RNA and protein microarrays shown in the top row of Figure 2.1b.[9, 16, 17] Typically, these microarray fabrication is done ex situ, introducing potential protein denaturation and conformation changes due to drying of the surface.[18] Other disadvantages of traditional arraying include poor spot quality, extensive

sample processing, and the requirement for expensive robotic control.[9, 19, 20] In addition, array fabrication suffers from inadequate methods to characterize protein immobilization and to quantify immobilized probe molecules.

Microfluidic Flow Cell Array

Microfluidic technology provides an alternative approach to address challenges related to array fabrication and biomolecule immobilization.[21, 22] When a microfluidic system is used to deliver biomolecules, mass transport to regions of the sensor surface is significantly enhanced as diffusion lengths are minimized and convective transport replenishes sample across the surface.[23] Two-dimensional (2D) microfluidic approaches have been used in conjunction with SPRM as shown in the bottom row of Figure 2.1b.[24-28] 2D microchannels or two sets of perpendicular microchannels are used to deliver biomolecules to the functionalized SPR sensing surface. However, these microfluidic systems are limited by the density that can be achieved and the extended lengths of the regions that are created leading to sample depletion problems. Sample adsorption to the surface of the microchannels can be reduced through blocking agents; however, sample depletion during immobilization still occurs leading to a decrease in sample near the end of the reaction zone due to the large reactive surface region defined by the microfluidic lanes. The large regions of immobilized probe also can lead to a low target surface density which may impact detection limits. Due to these problems, high probe concentration is needed for immobilization to avoid the formation of a gradient of probe densities on the sensor surface.

Recent microfluidic developments have focused on three-dimensional (3D) microfluidic networks to confine deposition to specific locations on the substrate in order

to minimize sample depletion and increase array density. One example is the development of the 3D continuous flow microspotter (CFM). Gale and co-workers demonstrated a dramatic increase in spot uniformity and quality for the CFM compared with standard pin-spotting microarray fabrication.[29, 30] Despite the advantages of the CFM, the problem of performing the spotting step *ex situ* and separate from the detection step remains, and can lead to potential protein denaturation, contamination, and delayed assay time. Also the ability to perform large numbers of separate, simultaneous experiments is eliminated due to the use of a single or limited-channel flow cell used for the detection step of array-based assays.[31, 32]

In this chapter, we demonstrate the integration of the CFM as a microfluidic flow cell array (MFCA) directly with an SPR microscope for *in situ* microarray fabrication and real-time analysis. The MFCA enables simultaneous operation of 48 separate microfluidic cells to address 48 individual sensing regions on a SPR sensor surface using an SPR microscope as the detector. We used 24 of the available microfluidic cells; however, a modification to the fluidics control would allow addressing all 48 cells. Even larger numbers of channels could be used in a 96-channel MFCA that is under development.

The MFCA-SPRM system enables microarray based analysis using both SPR intensity and angular modulations. The SPR microscope is set up in the Kretschmann configuration. The circular sensing area has a diameter of approximately 1 cm, which is well suited to integration of the microfluidic flow cell array (MFCA), which has a rectangular area of 0.5 × 1 cm. A multichannel peristaltic pump is adopted to load samples into each flow cell of the MFCA simultaneously at the same flow rate.

Continuous-flow deposition of biomolecules on the SPR sensing surface can be used for *in situ* microarray fabrication and multiplexed biomolecular interaction analysis. Ethanol and water mixtures are used to test the SPR response to changes in the bulk refractive index with intensity modulation.

Experimental

Materials

Biotin-terminated tri(ethylene glycol) hexadecane thiol (BAT) and 1-mercapto-11-undecyl tetra(ethylene glycol) (OEG) were purchased from Asemblon (Redmond, WA). Immunopure streptavidin (SA), human IgG (Ab2), and biotin-conjugated goat anti-human IgG (Ab1) were used as received from Pierce (Rockford, IL). Absolute ethanol was purchased from AAPER Alcohol (Shelbyville, Kentucky). Nanopure water was obtained using a Barnstead Nanopure Diamond purification system, and used to prepare phosphate buffered saline (PBS, 150 mM NaCl, pH 7.4). A solution of 0.5% sodium dodecyl sulfate (SDS) was prepared to clean the flow system and a 0.5% Tween 20 solution was flowed through the MFCA to overcome nonspecific adsorption.

SPRM-MFCA System

The SPR microscope is custom-built and is similar to a previously described system.[33] The layout of the microscope components is presented in Figure 2.2. An intensity-stabilized HeNe laser from Melles Griot (Carlsbad, California) is used as a light source. The laser beam is expanded and collimated by optics from Newport Corporation (Irvine, CA) before traveling through a SF_{14} hemispherical prism (R. Mathews Optical Works, Poulsbo, WA) and SF_{14} substrate (Refractive Index 1.7618) from Schott AG (Elmsford,

NY). The filter is an absorptive neutral density filter. L1 is a plano-concave lens (KPC025AR.14); L2 is a plano-convex lens (KPX119AR.14). These two lenses work as a beam expander. L3 and L4 are precision achromatic doublet lenses (PAC040AR.14) to focus the beam light. The substrate is coated with 2 nm of titanium or chromium and 50 nm of gold using a Denton electron-beam evaporator. The reflected light is detected by a CCD camera (IMB-3145FT) from k-Space Associates (Ann Arbor, MI). Two rotation stages from Newport Corporation (Irvine, CA) are used to control the angles of incidence and reflection of the laser beam. The whole system is mounted on a laser table. An imaging angle of 54.8º was used for the experiments described in this chapter. Software from k-Space Associates (Ann Arbor, MI) was used to acquire and process images. For real-time analysis, detection windows of specific pixels were put in the regions of interest (ROIs) in the SPRM image, and intensity signals from ROIs were collected with one-second time resolution. The MFCA was integrated into the SPRM optical system with a custom-made manifold mounted on an X-Y stage from Newport Corporation (Irvine, CA). The pressure to push the MFCA tip against the substrate was adjusted by controlling the position of the stage.

Microfluidic Flow Cell Array

MFCAs (Wasatch Microfluidics, Salt Lake City, UT) were fabricated in polydimethylsiloxane (PDMS) by adapting soft lithography methods and using injection molding to increase throughput as described previously.[30] Master molds were fabricated by micromilling the pattern in brass to the proper dimensions. A polycarbonate replica was made and used for casting the PDMS devices. Multiple layers of PDMS were bonded

through partial curing of layers or oxygen plasma bonding to form sophisticated 3D networks.[30]

Flow Control

A 24-channel peristaltic pump from Ismatec (Glattbrugg, Switzerland) was used for loading samples and driving solutions through the MFCA. The peristaltic pump contains eight rollers to minimize pulsing in the flow rate. Distinguishable pulsing was noticed at flow rates above 250 µL/min. In order to avoid pulsing issues, we used flow rates in the range of 20−100 µL/min; optimization of the flow rate will be discussed in Chapter 3. PTFE tubing (0.012" ID x 0.030" OD from Cole-Parmer) connections to the MFCA were cut to the same length to maintain the same volume across all of the channels. Platinum-Cured Silicone Tubing (3 mm long, 0.020" ID x 0.083" OD from Cole-Parmer) was used as a connector between the PTFE tubing and channels. The MFCA fluidic design ensures nearly simultaneous fluid arrival to each region on the sensor surface. Confirmation of the flow rate was achieved by injecting fluids with different refractive indices and monitoring their arrival to the surface with the SPR microscope.

Rotation Stage Control

In Figure 2.2, simultaneous control of the angles of incidence and reflectance in the SPRM is based on mounting the prism on stacked rotation stages. Both stages are driven by an ESP 300 motion controller/ driver from Newport Corporation (Irvine, CA). The top stage is used to change the light incident angle and the bottom one is to control the position of CCD camera to detect the intensity of reflected light. In order to generate the real-time SPR angle curve that is based on a plotting the reflected light intensity versus

the angle of incident light, the top stage (stage 2) is slaved to the bottom one (stage 1) and the angles are changed simultaneously. The moving angle ratio of stage 2 to stage 1 is 0.5, which means the rotation angle of stage 2 is as half that of stage 1. Detailed commands used to control the stages are listed below:

1MO; 2MO //Turn stage 1, 2 on

1OR; 2OR // Move stage 1, 2 to absolute 0

2SL-90; 2SR90 // Set moving angle rang of stage 2

2PA-45 // Move stage 2 to angle -45.00

2SS1; 2GR-0.5 // Set stage 2 slaved to stage 1 and their moving angle ratio

1TJ1; 2TJ4 // Set trajectory mode for stage 1, 2

1SL-90; 1SR90 // Set moving angle rang of stage 1

1AC1; 1VA0.1 // Set the accelerate rate and moving rate of stage 1

Detection Methods

For real-time analysis, windows with specific pixel height and width are placed in the regions of interest (ROIs) in the SPRM image. An example of the selection of ROIs is shown in Figure 2.4a. There are two detection modulations: angular and intensity modulation. With the angular modulation, the flow in the flow cell is stopped while the rotation stages are moved. Rotation stages are moved to tune the light incident angle for SPR coupling conditions and intensity of reflected light is measured at the detector as described in Chapter 1. At one specific angle, the SPR coupling reaches a maximum and the intensity of reflected light drops to a minimum. This angle is called the SPR angle, which is a characteristic of solution of this refractive index (RI) as described by Equation 1.1 and 1.2. The same equations show that higher RI solution has higher SPR angle, so

the SPR angle curves shift to larger angles with increasing value of RI in Figure 2.3b. For example, the SPR angle curves shift to larger angles when the solution in flow cell changes from water to protein because protein has larger RI value. From the SPR angle curves in Figure 2.3b, if we collected the signal at a fixed angle, the light intensity increases when the solution changes from water to protein. This is the intensity detection mode we used to measure the adsorption of protein with continuous flow and the detection curves are shown in Figure 2.4c. At a fixed angle and within a small range of RI, the intensity increases linearly with an increasing RI, so we can monitor the RI change with time by measuring the intensity change of reflected light. The intensity modulation is especially useful for biomolecular interaction analysis since the SPR curves provide information for both kinetic and quantitative analysis.

Surface Coverage Calculations

SPR sensing is based on the excitation of SPPs at a metal-dielectric interface. The propagating charge density waves create an evanescent electromagnetic wave extending several hundred nanometers above the sensor surface. Under energy and momentum matching conditions, incident light couples with the SPPs leading to a loss of reflected light at a specific wavelength or angle, depending on the instrument configuration. Binding events occurring within the evanescent wave result in local effective refractive index (η_{eff}) changes at the metal-dielectric interface leading to a shift in the wavelength or angle of coupling (i.e., SPR wavelength or SPR angle). SPR angle curves in Figure 2.5 are from theoretical calculations of SPR angle shift caused by the change of bulk refractive index adjacent to a gold surface. Within the linear regime defined in Figure 2.5, the change in reflected light intensity can be related to changes in effective refractive

index due to molecules binding to the SPR sensor surface. The linear relationship is shown in Equation 2.1.[33, 34]

$$\Delta I = s\Delta\eta = s(\eta_{eff} - \eta_s) \tag{2.1}$$

where ΔI is the shift in light intensity and $\eta_s$is the refractive index of solvent. ($\eta_{eff} - \eta_{s)}$ Is the change of local refractive index. s is the sensitivity factor, which can be experimentally determined by a calibration plot of ΔI versus the change of bulk refractive index.[33] s depends on the slope of the SPR angle curve in Figure 2.5 and the sensitivity factor of the SPR angle curves, which is also experimentally measured by plotting the SPR angle shift versus the change of local refractive index.

Effective refractive index (η_{eff}) is a properly weighted average of refractive index of the dielectric medium that consists of any adsorbed layers and the bulk solution. It is given by Equation 2.2 and proved to be accurate by Maxwell's equations.[33, 34]

$$\eta_{eff} = \left(\frac{2}{l_d}\right)\int_0^{\infty} \eta(z) e^{\frac{-2z}{l_d}}\, dz \tag{2.2}$$

where $\eta(z)$ is the refractive index at height z and l_d is the decay length of the evanescent field at the metal-dielectric interface.

For an adsorption layer of thickness of d, $\eta(z) = \eta_a$ for $0 < z < d$, η_a is the refractive index of adsorbed layer; $\eta(z) = \eta_s$ for $0 < z < \infty$. The integral of Equation 2.2 gives

$$\eta_{eff} - \eta_s = (\eta_a - \eta_s)\left(1 - e^{\frac{-2d}{l_d}}\right) \tag{2.3}$$

Combining Equation 2.1 and 2.3 gives

$$1 - \frac{\Delta I}{s(\eta_a - \eta_s)} = e^{\frac{-2d}{l_d}} \tag{2.4}$$

Taking the natural logarithm of both sides in Equation 2.4, and in the case of *d* is very small compared to l_d, the approximation gives an expression for the thickness of adsorbed layer

$$d = \left(\frac{l_d}{2}\right)\left[\frac{\Delta I}{s(\eta_a - \eta_s)}\right] \tag{2.5}$$

Multiplying the thickness *d* with the density of molecules can be used to estimate the surface coverage of adsorbed molecules.

$$Surface\ Coverage\ \left(\frac{molecules}{cm^2}\right) = d\ (cm) \times N\left(\frac{molecules}{cm^3}\right)$$

$$= \left(\frac{l_d}{2}\right)\left[\frac{\Delta I}{s(\eta_p - \eta_s)}\right]\left(\frac{\rho N_A}{M_w}\right) \tag{2.6}$$

where η_p and η_s are the refractive indices of protein and buffer, respectively. We used a value for η_p of 1.57[34] and η_s was measured using a refractometer. M_w is the molecular weight of the protein. ρ is the density of protein and typically equal to 1.37 g/cm.[3, 33, 34] N_A is Avogadro's number. l_d is the decay length of the evanescent wave, which was assumed to be 300 nm as derived from Maxwell's equation.[33] The value for *s*, the SPRM sensitivity factor, was measured as 2905% /refractive index unit (RIU) for our system.

SPR Microscope Sensitivity Measurement

The SPR microscope's response to bulk refractive index changes was characterized by preparing mixtures of ethanol and Nanopure water. The refractive indices of the solutions (ethanol/water) were measured using an Abbe-3L refractometer from Milton Roy (Rochester, NY).

Self-Assembled Monolayer (SAM) Formation

Gold-coated glass substrates were immersed in 0.1 mM mixed BAT and OEG solutions (BAT:OEG mole ratio of 1:9) for 24 h to form a mixed-SAM on the surface. Then the substrate was removed from the solution, rinsed with pure ethanol, and dried by a stream of nitrogen. Finally, the substrate was mounted on the planar face of the SPRM prism with refractive index matching liquid (Refractive Index 1.7600 ± 0.0005) from Cargille Laboratories (Cedar Grove, NJ).

Antibody-Antibody Interaction Analysis

As shown in Figure 2.5, a streptavidin (SA) layer was formed on the mixed SAM by introducing SA solutions (100 μg/mL SA in PBS) using the MFCA. Next, biotin-labeled goat anti-human antibody (Ab1, 1:100 dilutions in PBS) was introduced and adsorbed on the SA-coated surface. In the final step, human IgG (Ab2) was delivered at concentrations of 6, 12, 25, 50, 100 and 200 μg/mL. All steps of SA and Ab1 immobilization as well as Ab2 binding were monitored by SPRM. Twenty-four microfluidic channels of the MFCA were employed with one channel serving as a control. The microarray creation and antibody assay takes about one hour.

Results and Discussion

SPR Microscope Sensitivity Measurement

The response of the SPR microscope to bulk refractive index changes was characterized by preparing mixtures of ethanol and water. The refractive indices of the solutions (ethanol/water) were measured by an Abbe-3L refractometer from Milton Roy (Rochester, NY). The calibration provides characterization of SPRM sensitivity and monitoring of the MFCA flow control. In the calibration, six solutions containing different volume ratios of water/ethanol with different bulk refractive indices (RI) were loaded into the inlet wells and flowed through the microfluidic cells at the substrate/MFCA interface and into the outlet wells. Water was used to establish a baseline between introductions of each calibration solution. Figure 2.6b presents the *in situ*, real time SPRM response to the bulk RI changes monitored in ROIs in the 24 flow cells of Figure 2.6a. The good overlap of the rise and fall time points demonstrates the uniform channel flow rates which are important for minimizing variations in kinetic data because of flow rate effects. The SPR response to each solution is uniform with relative standard deviations (RSDs) of less than 10%. The major cause of signal deviations is from optical system, which will be discussed in Chapter 3. The sensitivity factor of the SPR microscope was calculated by averaging the slope of plots shown in Figure 2.6c. The sensitivity factor is used to calculate surface density of biomolecules and estimate the dynamic range of detection. The average sensitivity factor for 24 flow cells is 2905% reflectivity/RIU and the dynamic range is 0.01 RIU, which is comparable to that reported from a similar SPRM system(3576 ± 332%).[32]

Microarray Fabrication and Real-time Biomolecular Interaction Analysis

A long-term goal for the application of the integrated MFCA-SPRM system is to develop immunogenicity assays which are used to screen anti-drug antibodies from serum or blood samples of patients treated with biological drugs such as the humanized antibody drug Daclizumab. An antibody-antibody interaction that mimics an immunogenicity assay was used to demonstrate the capability of the system. The first step in this assay development is immobilization of the probe antibody on the SPR sensor surface. The integrated MFCA-SPRM system was used to control and monitor *in situ* antibody immobilization as part of the array fabrication process. We used a well-characterized, versatile immobilization strategy based on a tethered streptavidin layer formed on a mixed self-assembled monolayer (SAM).[12] The SAM-functionalized gold-coated substrate was mounted on the SPRM prism using refractive index match fluid.

Figure 2.7a shows real-time adsorption data from the *in situ* array fabrication and antibody binding assay. Adsorption on the sensor surface was tracked by measuring changes in the SPRM response in ROIs within the MFCA in the image. A baseline in SPR response plot was established with PBS buffer. Next, SA was introduced into the flow cells. The SA bound to the biotin groups on the SAM-covered substrate surface is shown in Figure 2.7b. The concentration used resulted in a saturation level of SA on the surface to create a nearly close-packed SA layer. This binding surface was used to capture biotinylated goat antihuman IgG (Ab1). The immobilization of the probe antibody Ab1 also was followed in real time as shown in Figure 2.7a. Finally, the

adsorption of the target human IgG antibody (Ab2) was monitored as the antibody was introduced at different concentrations.

The changes in percentage reflectivity from the SPRM measurements were converted to surface coverage using published methods.[9] The average SA surface coverage of (11.3 ± 2.0) × 10^{11} molecules/cm^2 is in agreement with reported values for saturation coverage of SA on the mixed BAT/OEG-containing SAM.[33] The average surface coverage of goat anti-human IgG (Ab1) was (6.2 ± 1.0) × 10^{11} molecules/cm^2. The Ab1/SA binding ratio of 0.5 is consistent with the expected Ab1 surface density based on the dimensions of the molecules. After probe Ab1 immobilization, solutions containing different concentrations of Ab2 were introduced in multiple channels simultaneously. Figure 2.7a shows the real-time Ab2 adsorption curves. Because the probe immobilization was performed *in situ* and quantified using the SPRM response, the target Ab2 adsorption for each MFCA microfluidic channel can be normalized using the Ab1 coverage for the corresponding ROI. The normalized responses for different bulk solution Ab2 concentrations are shown in Figure 2.7b. The average binding ratio of Ab2/Ab1 (Figure 2.7b) indicates that the average activity of immobilized Ab1 is greater than 60%, which is consistent with value reported by Peluso etc.[15] The RSD in the % reflectivity for Ab2 concentrations of 6, 12, 25, 50, 100, and 200 μg/mL were 1.7, 3.1, 2.7, 8.4, 5.3 and 16.5% reflectivity, respectively. Control experiments (data not shown) showed negligible non-specific Ab2 adsorption on the SA layer without Ab1 at concentrations of 250 μg/mL, so the higher RSD for 200 μg/mL is not due to non-specific adsorption. In Chapter 3, we will characterize the microfluidic behavior of the MFCA and investigating the impact of changes in microfluidic parameters (e.g., flow rate, contact time, and cycling) on

biomolecule delivery and binding which may provide insight into how to reduce the RSD values for the Ab2 adsorption measurements.

Figure 2.8 presents the concentration-dependent SPRM response to different Ab2 solution concentrations. The same SA and Ab1 immobilization process as described above was followed before the SPRM response to a series of solutions with different Ab2 concentrations was monitored. Each data point is an average of three or four measurements from a single multichannel experiment. The binding isotherm of Ab2 to surface-immobilized Ab1 shows that the Ab2 adsorption reaches a saturation level at Ab2 concentrations above 20 μg/mL. The Ab2/Ab1 binding ratio indicates this saturation occurs at 60−70% maximum occupancy of the Ab1 on the surface which is typical for the SA-immobilized Ab1. The inset in Figure 2.8 shows the linear trend in the response when the Ab2 solution concentration is plotted on the log scale. We found the limit of detection for this particular antibody pair based on a signal greater than three times the noise to be approximately 80 ng/mL which is well below the industry recommended assay detection limit of 500 ng/mL for immunogenicity assays.[35] The correlation of the minimum detectable signal with concentration of analyte in solution depends on the affinity constant for the interaction between the target analyte (e.g., Ab2) and the probe (e.g., Ab1) immobilized on the sensor surface and will need to be determined for specific biomolecules. The linear dynamic range of the SPRM is 0.01 RIU which is equivalent to approximately four close-packed layers of protein. This dynamic range allows measurement of all steps of probe immobilization and target binding without the need to adjust the SPRM imaging angle. If the change of refractive index exceeds the detection

range, the imaging angle could be adjusted between steps in an experiment which would extend the linear dynamic range.

Conclusions

The MFCA-SPRM integration represents a significant step forward in the throughput of SPR-based analysis which has been one of the major obstacles for the expansion to applications outside of kinetic analysis. The parallel performance capability of the MFCA dramatically increases the number of options available in planning experiments. Optimization of probe immobilization and microarray fabrication can be performed in a single experiment including controls and replicates. Biomolecule interactions in different buffers and flow conditions can be investigated on the same sensor chip. Concentration analysis for biomarker screening is a more realistic option with the ability to create standard curves while screening separate analytes with a statistically relevant number of replicates. The current MFCA configuration enables 48 separate flow cells in a 4 mm × 10 mm footprint. On-going development of the MFCA is focused on shrinking the overall spot size and increasing the density of flow cells within the same footprint (e.g., 96 and 192 channels). Future studies toward the development of immunogenicity assays based on the integrated SPRM-MFCA system will involve immobilizing an antibody-based drug as a probe to assay for target antidrug antibodies from patients' sera. In addition to immunogenicity assays, the integrated system also could be applied in biomarker screening and extended to array-based, label-free analysis of a wide range of molecular interactions involving proteins, nucleic acids, lipids, and carbohydrates. The flexibility of the MFCA also provides the option for application to other sensing platforms (e.g., fluorescence-based detection, MALDI MS).

References

1. Homola, J., Surface plasmon resonance sensors for detection of chemical and biological species. *Chem. Rev.* **2008**, *108*, 462-493.

2. Raether, H., *Surface Plasmons on Smooth and Rough Surfaces and on Gratings*. Springer: 1988.

3. Rothenhausler, B.; Knoll, W., Surface-plasmon microscopy. *Nature* **1988**, *332*, 615-616.

4. Yeatman, E.; Ash, E. A., Surface plasmon microscopy. *Electron.s Lett.* **1987**, *23*, 1091-1092.

5. Liedberg, B.; Nylander, C.; Lundström, I., Surface plasmon resonance for gas detection and biosensing. *Sens. Actuators* **1983**, *4*, 299-304.

6. Phillips, K.; Cheng, Q., Recent advances in surface plasmon resonance based techniques for bioanalysis. *Anal. Bioanal. Chem.* **2007**, *387*, 1831-1840.

7. Ruemmele, J. A.; Golden, M. S.; Gao, Y.; Cornelius, E. M.; Anderson, M. E.; Postelnicu, L.; Georgiadis, R. M., Quantitative surface plasmon resonance imaging: a simple approach to automated angle scanning. *Anal. Chem.* **2008**, *80*, 4752–4756.

8. Smith, E. A.; Corn, R. M., Surface plasmon resonance imaging as a tool to monitor biomolecular interactions in an array based format. *Appl. Spectrosc.* **2003**, *57*, 320A-332A.

9. Shumaker-Parry, J. S. *Quantitative Aspects of SPR Spectroscopy and SPR Microscopy: Applications in Protein Binding to Immobilized Vesicles and dsDNA Arrays.* University of Washington: 2002.

10. Knoll, W., Interfaces and thin films as seen by bound electromagnetic waves. *Annu. Rev. Phys. Chem.* **1998**, *49*, 569-638.

11. Lee, H. J.; Wark, A. W.; Corn, R. M., Creating advanced multifunctional biosensors with surface enzymatic transformations. *Langmuir* **2006**, *22*, 5241-5250.

12. Jung, L. S.; Shumaker-Parry, J. S.; Campbell, C. T.; Yee, S. S.; Gelb, M. H., Quantification of tight binding to surface-immobilized phospholipid vesicles using surface plasmon resonance: binding constant of phospholipase A2. *J. Am. Chem. Soc.* **2000**, *122*, 4177-4184.

13. Hong, M. Y.; Lee, D.; Kim, H. S., Kinetic and equilibrium binding analysis of protein-ligand interactions at poly(amidoamine) dendrimer monolayers. *Anal. Chem.* **2005**, *77*, 7326-7334.

14. Wegner, G. J.; Wark, A. W.; Lee, H. J.; Codner, E.; Saeki, T.; Fang, S.; Corn, R. M., Real-time surface plasmon resonance imaging measurements for the multiplexed determination of protein adsorption/desorption kinetics and surface enzymatic reactions on peptide microarrays. *Anal. Chem.* **2004**, *76*, 5677-5684.

15. Peluso, P.; Wilson, D. S.; Do, D.; Tran, H.; Venkatasubbaiah, M.; Quincy, D.; Heidecker, B.; Poindexter, K.; Tolani, N.; Phelan, M.; Witte, K.; Jung, L. S.; Wagner, P.; Nock, S., Optimizing antibody immobilization strategies for the construction of protein microarrays. *Anal. Biochem.* **2003**, *312*, 113-124.

16. Singh, B. K.; Hillier, A. C., Multicolor surface plasmon resonance imaging of ink jet-printed protein microarrays. *Anal. Chem.* **2007**, *79*, 5124-5132.

17. Wilkop, T.; Wang, Z.; Cheng, Q., Analysis of micro-contact printed protein patterns by SPR imaging with a LED light source. *Langmuir* **2004**, *20*, 11141-11148.

18. Glökler, J.; Angenendt, P., Protein and antibody microarray technology. *J. Chrom. B* **2003**, *797*, 229-240.

19. Barbulovic-Nad, I.; Lucente, M.; Sun, Y.; Zhang, M.; Wheeler, A. R.; Bussman, M., Bio-microarray fabrication techniques - A review. *Critical Reviews in Biotechnology* **2006**, *26*, 237-259.

20. Wu, P.; Grainger, D. W., Comparison of hydroxylated print additives on antibody microarray performance. *J. Proteome* **2006**, *5*, 2956-2965.

21. Whitesides, G. M., The origins and the future of microfluidics. *Nature* **2006**, *442*, 368-373.

22. Delamarche, E.; Bernard, A.; Schmid, H.; Bietsch, A.; Michel, B.; Biebuyck, H., Microfluidic networks for chemical patterning of substrates: Design and applications to bioassays. *J. Am. Chem. Soc.* **1998**, *120*, 500-508.

23. Myszka,D. G.; He, X.; Dembo, M.; Morton, T. A.; Goldstein, B., Extending the range of rate constants available from BIACORE: Interpreting mass transport-influenced binding data. *Biophys. J.* **1998**, *75*, 583–594.

24. Wegner, G. J.; Lee, H. J.; Corn, R. M., Characterization and optimization of peptide arrays for the study of epitope-antibody interactions using surface plasmon resonance imaging. *Anal. Chem.* **2002**, *74*, 5161-5168.

25. Kurita, R.; Yokota, Y.; Sato, Y.; Mizutani, F.; Niwa, O., On-chip enzyme immunoassay of a cardiac marker using a microfluidic device combined with a portable surface plasmon resonance system. *Anal. Chem.* **2006**, *78*, 5525-5531.

26. Foley, J. O.; Nelson, K. E.; Mashadi-Hossein, A.; Finlayson, B. A.; Yager, P., Concentration gradient immunoassay 2. Computational modeling for analysis and optimization. *Anal. Chem.* **2007**, *79*, 3549-3553.

27. Lee, H. J.; Goodrich, T. T.; Corn, R. M., Surface plasmon resonance imaging measurements of 1D and 2D microarrays created from microfluidic channels on gold thin films. *Anal. Chem.* **2001**, *73*, 5525-5531.

28. Wang, Z.; Wilkop, T.; Cheng, Q., Characterization of micropatterned lipid membranes on a gold surface by surface plasmon resonance imaging and electrochemical signaling of a pore-forming protein. *Langmuir* **2005**, *21*, 10292-10296.

29. Natarajan, S.; Miles, A.; Eckman, J.; Rich, R.; Gale, B. K.; Myszka, D., Continuous-flow microfluidic printing of proteins for array-based applications including surface plasmon resonance imaging. *Anal. Biochem.* **2008**, *373*, 141-146.

30. Chang-yen, D. A.; Myzska, D.; Gale, B. K., A novel PDMS microfluidic spotter for fabrication of protein chips and microarrays. *J. Micromech. Sys.* **2006**, *15*, 1145-1151.

31. Lee, H. J.; Nedelkov, D.; Corn, R. M., Surface plasmon resonance imaging measurements of antibody arrays for the multiplexed detection of low molecular weight protein biomarkers. *Anal. Chem.* **2006**, *78*, 6504-6510.

32. Campbell, C. T.; Kim, G., SPR microscopy and its applications to high-throughput analyses of biomolecular binding events and their kinetics. *Biomaterials* **2007**, *28*, 2380-2392.

33. Shumaker-Parry, J. S.; Campbell, C. T., Quantitative methods for spatially resolved adsorption/desorption measurements in real time by surface plasmon resonance microscopy. *Anal. Chem.* **2004**, 76, 907-917.

34. Jung, L. S.; Campbell, C. T.; Chinowsky, T. M.; Mar, M. N.; Yee, S. S., Quantitative interpretation of the response of surface plasmon resonance sensors to adsorbed films. *Langmuir* **1998**, 14, 5636-5648.

35. Liang, M.; Klakamp, S. L.; Funelas, C.; Lu, H.; Lam, B.; Herl, C.; Umble, A.; Drake, A. W.; Pak, M.; Ageyeva, N.; Pasumarthi, R.; Roskos, L. K., Detection of high- and low-affinity antibodies against a human monoclonal antibody using various technology platforms. *Assay Drug Dev. Technol.* **2007**, 5, 655-662.

Figure 2.1. SPR imaging for microarray-based analysis of biomolecule interactions. (a) Schematic of SPR microscopy (SPR imaging) setup based on a prism coupler. (b) Bimolecular microarrays created on SPR sensing surface to study various biomolecular interactions, the top row is DNA microarrays fabricated by a combination of self-assembly and UV photo patterning to study interactions of DNA, RNA and protein with immobilized DNA; and the bottom row are carbohydrate, peptide and protein surface patterns or microarrays made by 2-dimensional microchannels for the study of their interactions with protein. Reprinted with permission from {Lee et al. *Langmuir* **2006,** *22*, 5241-5250.}. Copyright {2006} American Chemical Society

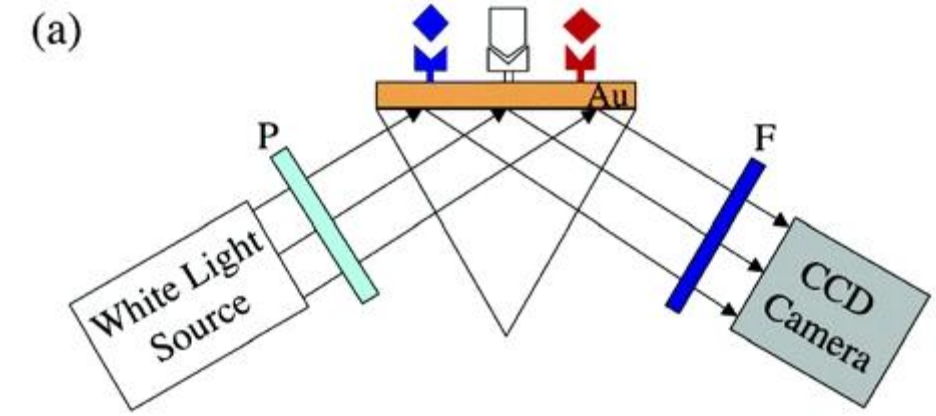
(a)
Au
P
F
White Light Source
CCD Camera

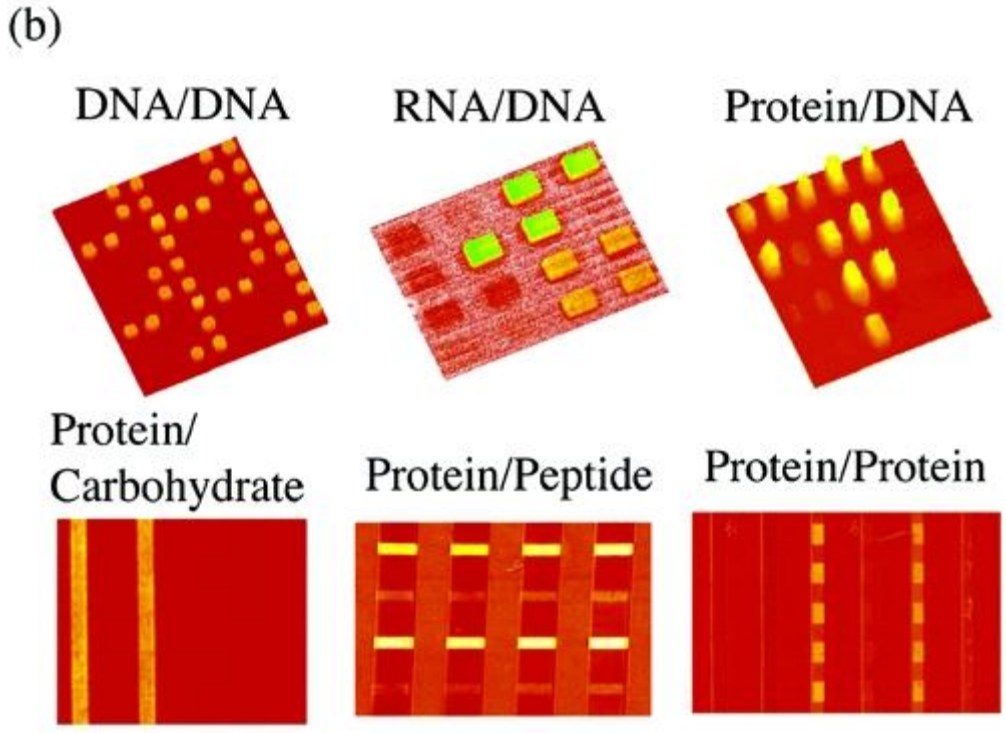
(b)
DNA/DNA
RNA/DNA
Protein/DNA
Protein/ Carbohydrate
Protein/Peptide
Protein/Protein

Figure 2.2. Schematic design of the SPR microscope based on the Kretschmann configuration with the MFCA integrated.

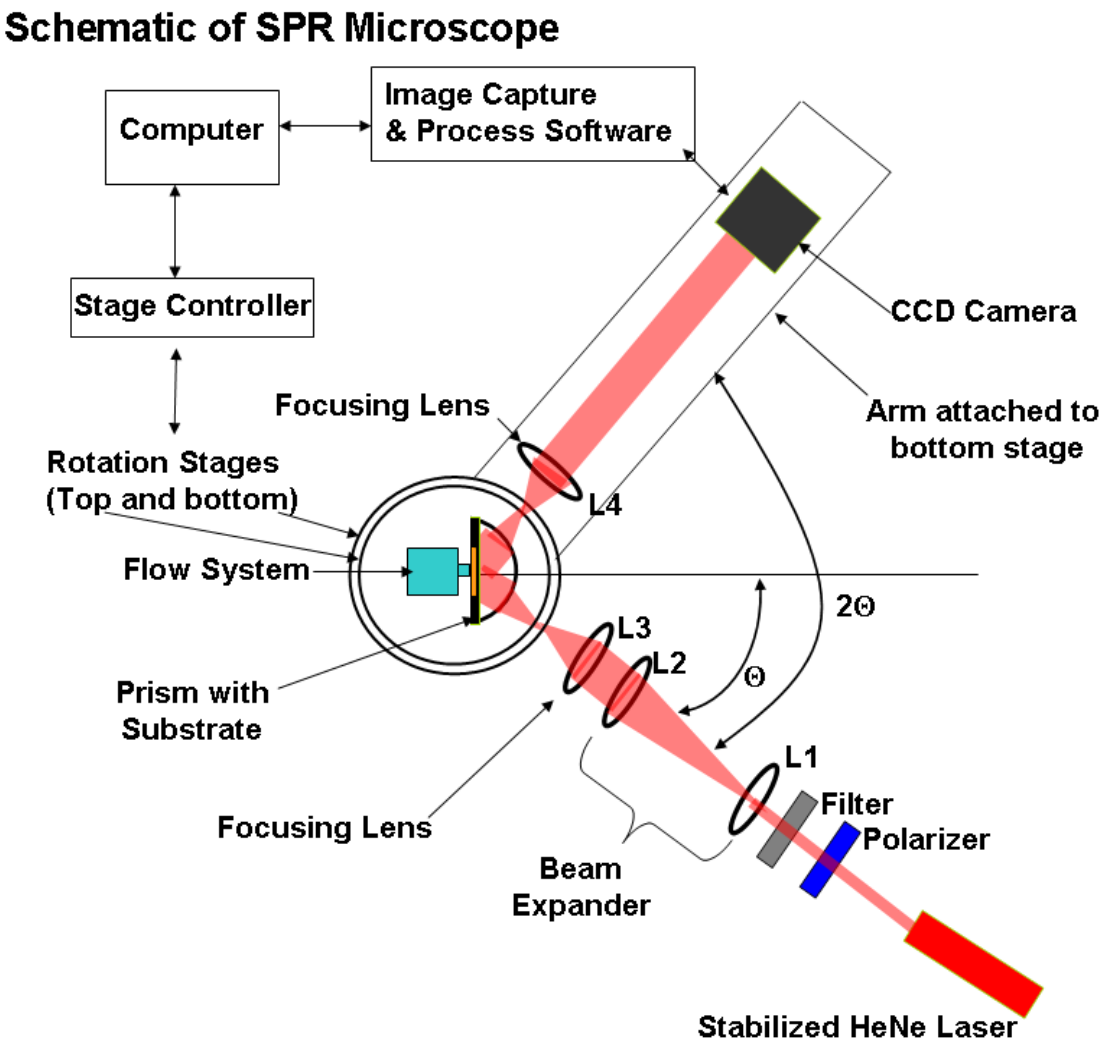
Schematic of SPR Microscope
Computer
Image Capture
& Process Software
Stage Controller
Rotation Stages
(Top and bottom)
Flow System
Prism with
Substrate
Focusing Lens
Focusing Lens
L4
L3
L2
L1
2Θ
Θ
CCD Camera
Arm attached to
bottom stage
Filter
Polarizer
Beam
Expander
Stabilized HeNe Laser

Figure 2.3. Photos and schematic structure of MFCA. (a) Photo showing top view of the MFCA. The MFCA tip extending out from the main rectangular area is shown in more detail in (b) and (c). (b) Photo of the MFCA tip face. The 48 openings comprise the 48 microfluidic cells when the face of the tip is sealed against a substrate. (c) Top view of a row of joints where the inlet and outlet microchannels meet. (d) Schematic of the layered MFCA structure and the relationship between the channels and the sample wells. (e) Cartoon of MFCA mounted at the planar face of the prism in the SPRM.

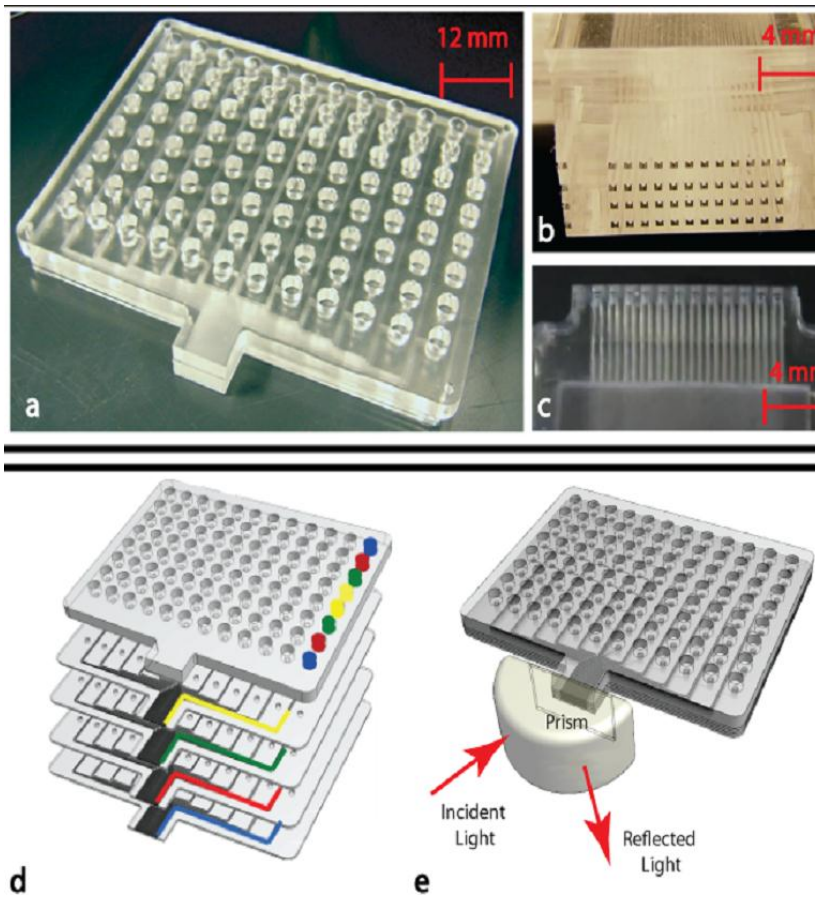
12 mm
a
b
c
d
e
Prism
Incident
Light
Reflected
Light

Figure 2.4. Detection modes of SPRM-MFCA. (a) SPRM image of 48 microfluidic cells filled with water. ROIs are selected by selecting pixels in the image. The 400 × 400 μm windows appear as rectangles rather than square in the SPRM image because of the imaging angle used. (b) SPR real-time curves with angular modulation show that the SPR angle shifts to right with increasing value of refractive index. (c) SPR real-time curves with intensity modulation show that the intensity of light increase with molecules adsorption measured at a fixed angle shows in (b).

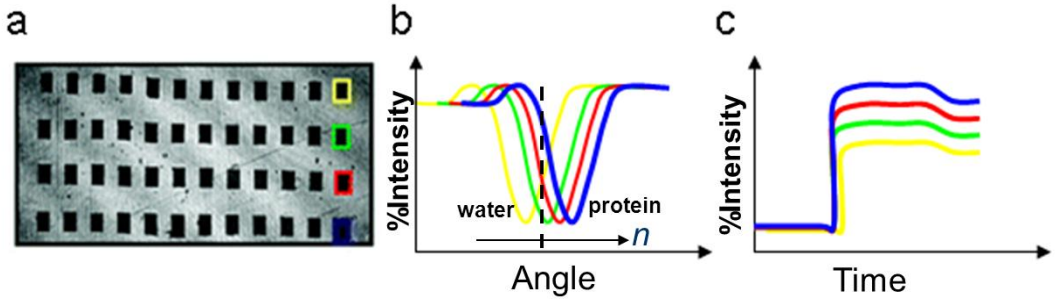
a
b
c
%Intensity
water
protein
n
Angle
%Intensity
Time

Figure 2.5. SPR reflectivity curves of infinitely thick layers of two refractive indices. Solutions of 1.3330 (black) and 1.3342 (gray) in contact with a 47.5 nm gold film on an SF14 prism illuminated by 632.8 nm wavelength light are predicted from Fresnel calculations. Reprinted with permission from {Shumaker-Parry et al. *Analytical chemistry* **2004,** *76*, 907-917.}. Copyright {2004} American Chemical Society

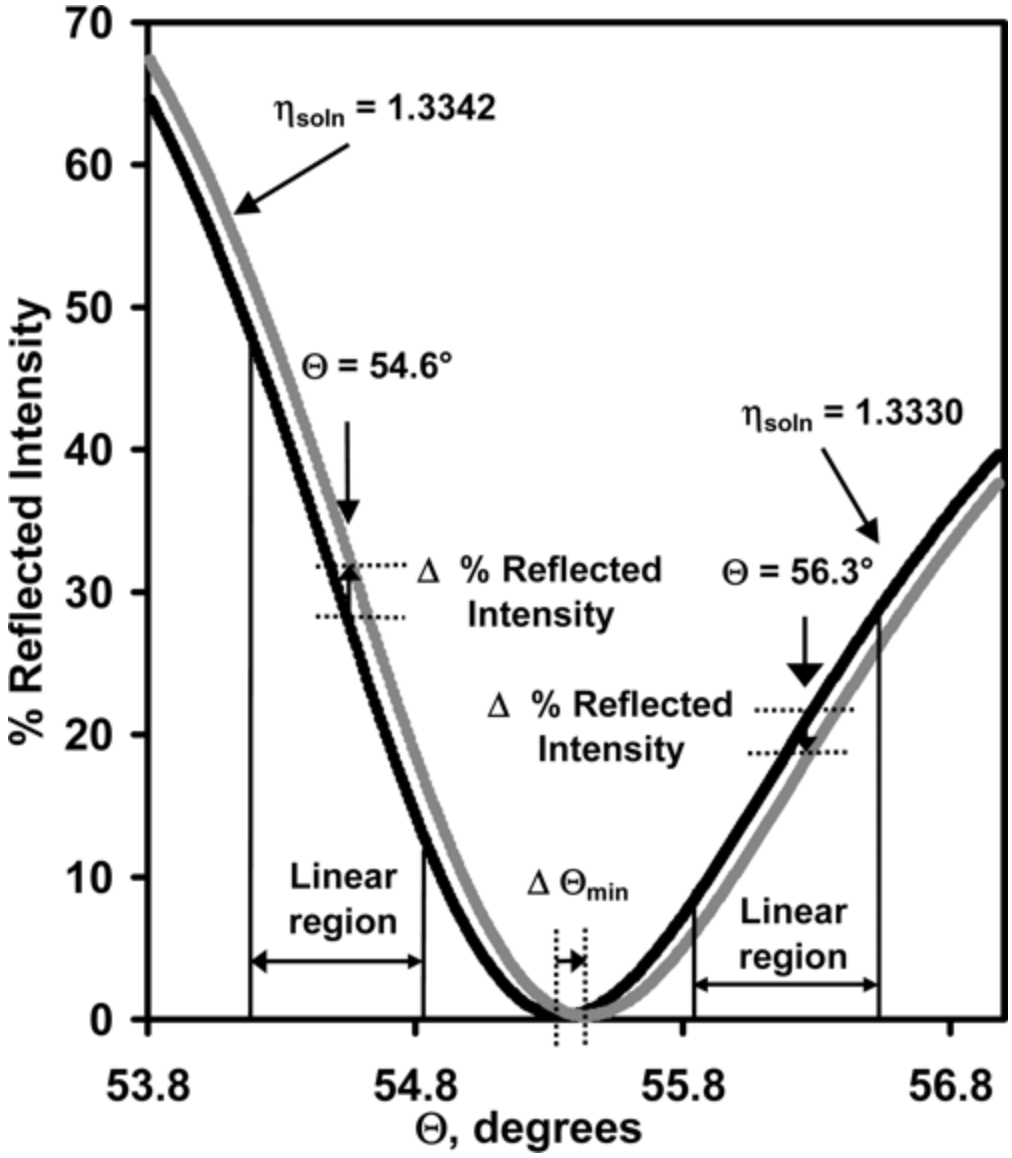
70
60
50
40
30
20
10
0
% Reflected Intensity
η_{soln} = 1.3342
Θ = 54.6°
η_{soln} = 1.3330
Θ = 56.3°
Δ % Reflected Intensity
Δ % Reflected Intensity
Linear region
Δ Θ_{min}
Linear region
53.8
54.8
55.8
56.8
Θ, degrees

Figure 2.6. SPRM calibration using 24 microfluidic cells of MFCA. (a) SPRM image of 24 microfluidic cells filled with water. The image was acquired at an incident light angle of 54.8°. (b) SPRM curves showing the system response to solutions with different refractive indices. A CCD camera with acquisition software was used to measure reflected light intensity from 20 × 20 pixel ROIs selected from the SPRM image for each microfluidic cell. The legend shows each curve and the position of the corresponding MFCA microfluidic cell in the SPRM image in (a). The refractive indices of the solutions are (baseline) 1.3320, (P1) 1.3331, (P2) 1.3340, (P3) 1.3350, (P4) 1.3370, (P5) 1.3396, and (P6) 1.3421. (c) SPRM responses from (b) are used to obtain the average SPRM sensitivity factor from the slope of the line.

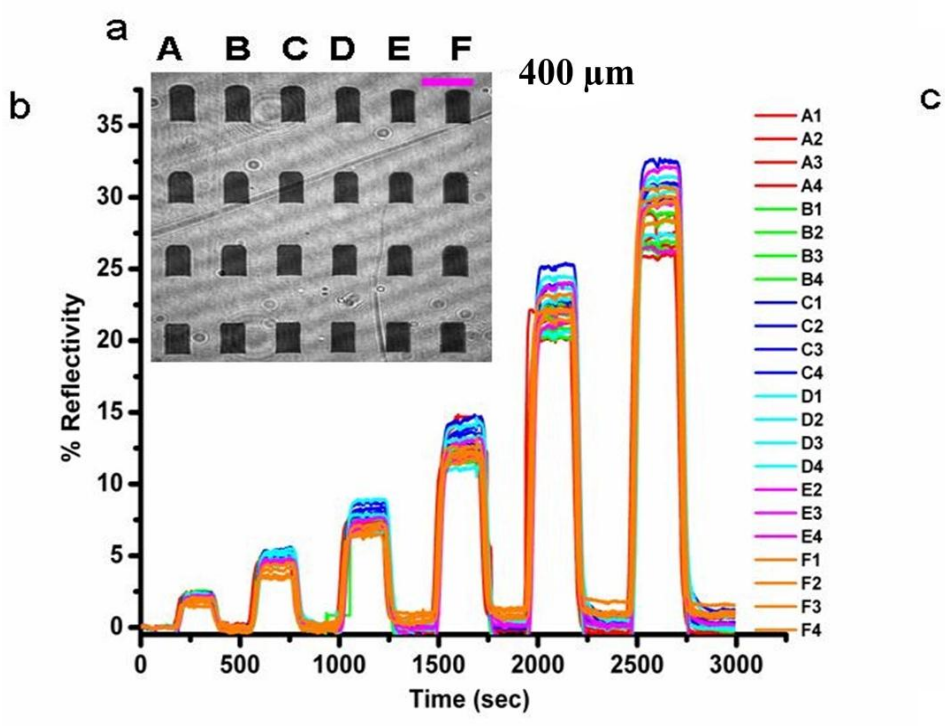
a
A B C D E F
400 µm
b
% Reflectivity
Time (sec)
A1
A2
A3
A4
B1
B2
B3
B4
C1
C2
C3
C4
D1
D2
D3
D4
E2
E3
E4
F1
F2
F3
F4

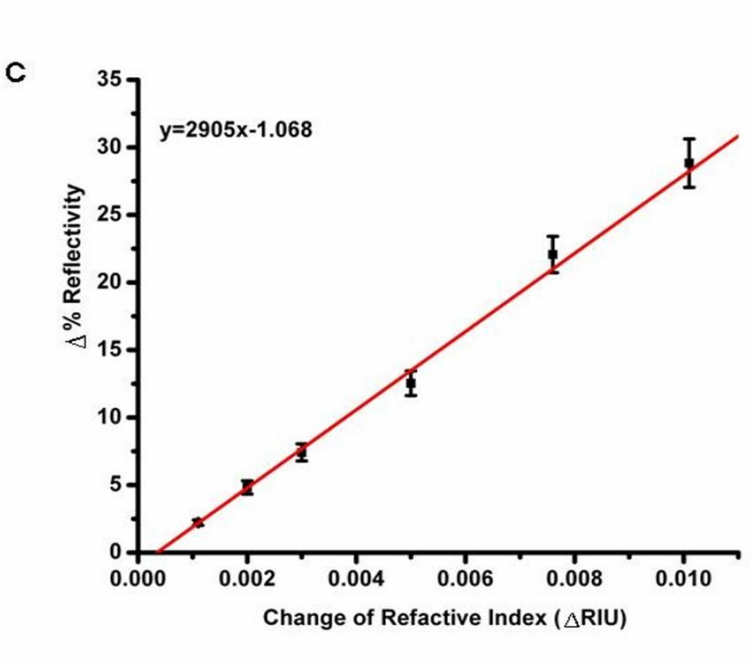
c
y=2905x-1.068
Δ % Reflectivity
Change of Refactive Index (△RIU)

Figure 2.7. *In situ* microarray fabrication and analysis with SPRM-MFCA. The data was acquired at an incident light angle of 54.8°. (a) Cartoon of adsorbed layers and real-time adsorption/desorption curves for microarray creation and antibody binding on a SAM-coated gold SPR sensor. The baseline of the plots corresponds to PBS buffer flowing through the MFCA cells. After introduction, SA binds to the biotin-containing SAM. Next, biotinylated goat antihuman IgG (Ab1) binds to the SA-coated surface. Finally, solutions with different human IgG (Ab2) concentrations were introduced to the Ab1 surface. Each letter/color represents a different Ab2 concentration, and each number signifies a different MFCA cell. The Ab2 concentrations were *A* = 6 μg/mL, *B* = 12 μg/mL, *C* = 25 μg/mL, *D* = 50 μg/mL, *E* = 100 μg/mL, *F* = 200 μg/mL. (b) Ab2 adsorption normalized to Ab1 surface coverage. The legend description is the same as (a).

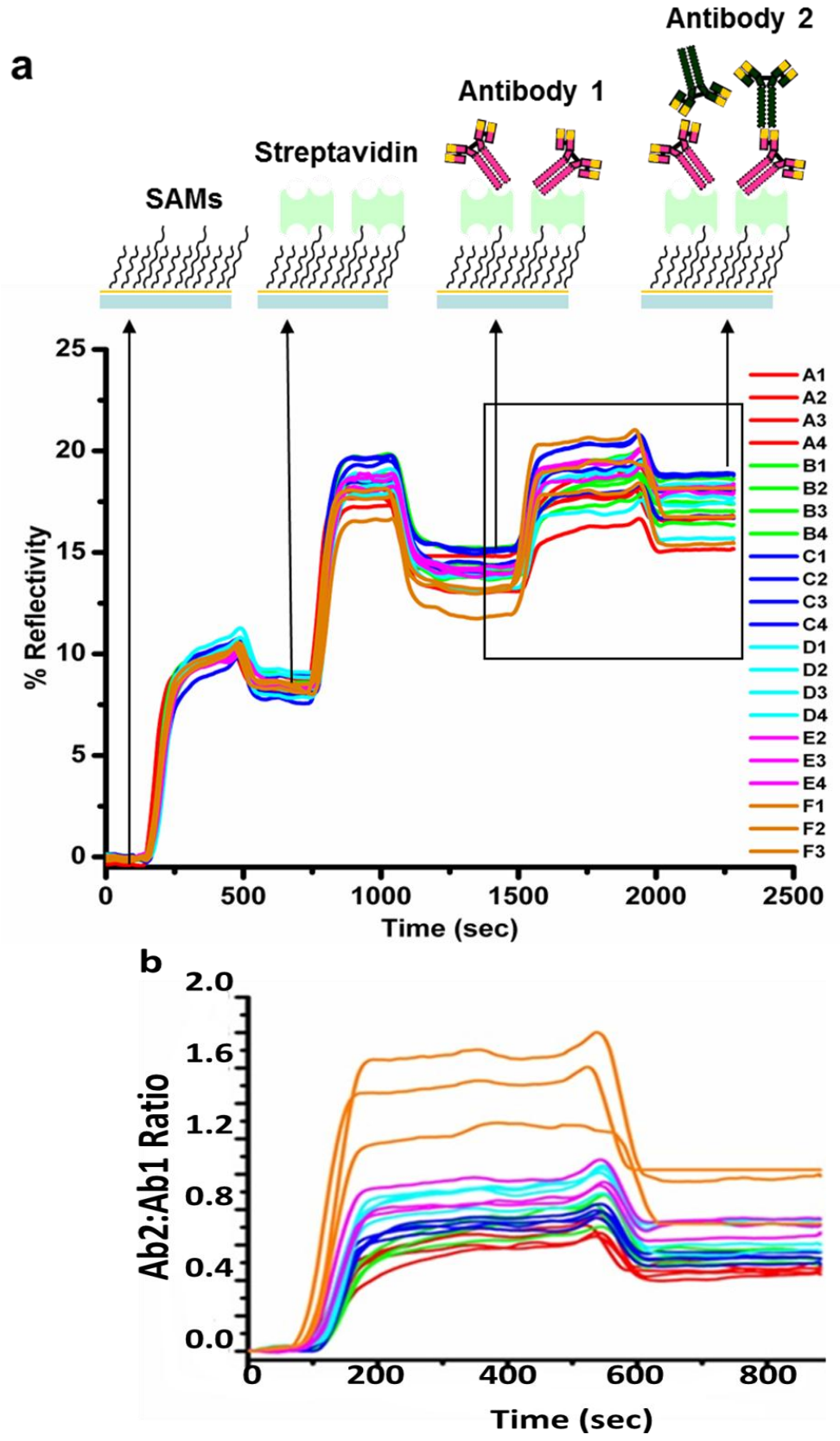
a
Antibody 2
Antibody 1
Streptavidin
SAMs
% Reflectivity
Time (sec)
A1
A2
A3
A4
B1
B2
B3
B4
C1
C2
C3
C4
D1
D2
D3
D4
E2
E3
E4
F1
F2
F3
b
Ab2:Ab1 Ratio
Time (sec)

Figure 2.8. The equilibrium SPRM signals of Ab2 adsorption versus different Ab2 solution concentrations. Each data point represents an average response calculated from at least three individual adsorption curves. All data points were measured simultaneously in a single experiment. The inset shows the linear relationship before saturation when the SPRM response is plotted versus Ab2 solution concentration on a logarithmic scale.

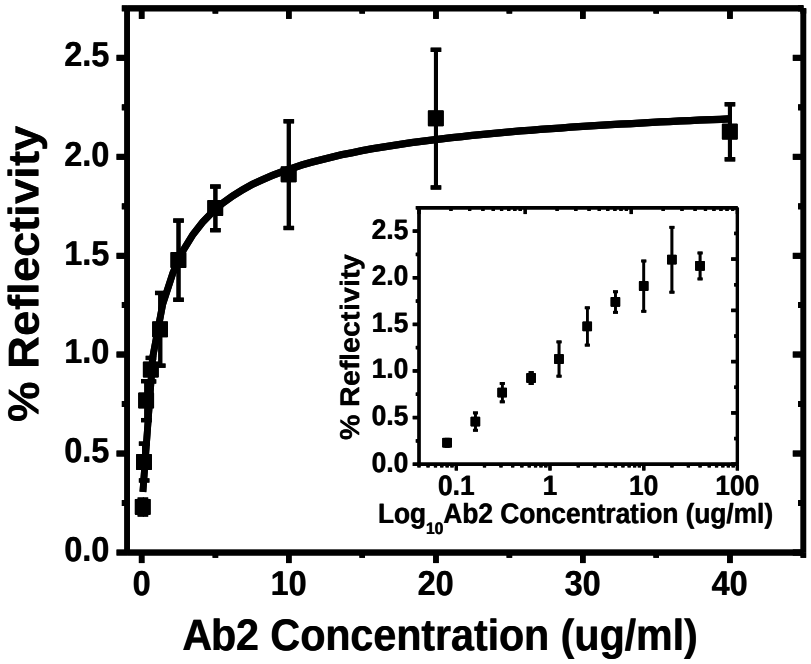
% Reflectivity
Ab2 Concentration (ug/ml)
0.0
0.5
1.0
1.5
2.0
2.5
0
10
20
30
40
% Reflectivity
Log10Ab2 Concentration (ug/ml)
0.1
1
10
100

CHAPTER 3

OPTIMIZATION OF MFCA-SPRM FOR BIOMOLECULAR INTERACTION ANALYSIS BY STUDYING MASS TRANSPORT AND SURFACE HETEROGENEITY

Introduction

As described in Chapter 2, the MFCA-SPRM is a newly developed, integrated SPR system for *in situ* microarray fabrication and multiplexed analysis of biomolecular interactions with multi-channel fluidics control. Biomolecular interactions involve multiple-step reactions between analytes in solution and ligands on the surface. Obviously, the concentration of reactants plays a key role in the reaction rate at the solid-liquid interface. The reactive analyte concentration is directly impacted by mass transport and the diffusion coefficient of the analyte. In order to improve the integrated system for rapid and sensitive microarray analysis, parameters impacting mass transport and the surface reaction, such as flow rates, concentration of reactants and rate constants, are investigated by both numerical simulation and experiments in this chapter.

Immunoassays based on microfluidics are emerging as an important technology for life science research, disease diagnostics and drug discovery because of low cost, small

sample volume and short analysis time.[1, 2] Microfluidic immunoassays can be classified as homogeneous or heterogeneous, depending on whether the reaction is in solution or interfacial. Heterogeneous immunoassays utilize probe molecules immobilized on a solid surface to capture analytes in solution. The formation of binding pairs is usually detected by fluorescence microscopy,[3] electrochemical methods[4] or label-free sensing approaches, such as surface plasmon resonance (SPR),[5, 6] quartz crystal microbalance (QCM),[7] microcantilevers[8] and nanowires.[9] Regardless of the detection method or the immunoassay format (e.g., direct, indirect or competition), kinetics of heterogeneous assays are determined by parameters that dominate mass transport of the analyte and the surface reaction.[10-12]

Generally, with a pressure-driven flow, analytes are delivered to the reaction surface by convection and diffusion described by the Navier-Stokes equations.[13] From the equations, factors that impact the interactions at the surface include the bulk concentration, flow velocity, geometry of the flow cell, diffusion constants of analytes and time. After arriving at a reaction surface, analytes react with ligands to form binding pairs, and the reaction rate depends on the surface density of binding sites and reaction constants, such as adsorption and desorption rate constants. Effects of these parameters on analyte adsorption have been extensively investigated by both simulation and experiments.[11-16]

The typical simulation approach uses finite element analysis software such as COMSOL Multiphysics to model the process of convection, diffusion and reaction simultaneously.[17-19] Generally, the model is simulated under the assumption of unidirectional 2D laminar flow where the reaction surface is parallel to the flow direction.

Theory of this type of computational model can be found in the background information below. Results from simulation predict kinetics of reaction and can inform the optimization process and selection of experimental conditions for immunoassays. For example, Parsa et al. used modeling to investigate the output of a direct binding assay in microchannels when constrained by limited sample volume and assay time.[17] Fu et al. used a 2D model to improve the sensitivity of a competitive assay based on SPR imaging.[18]

In our study, a combination of simulation and experiment was applied to optimize the conditions for immunoassays based on the MFCA-SPRM system. Physicochemical parameters, such as concentration of analytes in solution and ligands on surface, flow rate and binding affinity, and kinetics of binding reactions were investigated in the study. The simulation approach was built on a 2D model to calculate the concentration of surface binding pairs by varying a set of physicochemical constants. The 2D modeling results have shown that binding kinetics from the modeling does not fit perfectly with the experimental results.[20] The discrepancies in the modeling could be due to the experimental condition being more complex or an improper setting of parameters. However, the prediction from modeling is useful to estimate the trends caused by changes in physicochemical parameters. The experimental optimization was carried out with two model systems: (1) the binding of streptavidin to a binary biotin-terminated self-assembled monolayer (SAM) thiolate surface and (2) the binding of anti-human IgG to biotinylated-Daclizumab surface. The first model system was selected to optimize the process of creating a high-density and high-activity antibody microarray. The surface density of biotin was controlled by varying the solution mole ratio of two different thiols.

The mixed SAM surface was also characterized with XPS and AFM. Streptavidin solutions of various concentrations were flowed over SAM surfaces to find the optimal concentration, sample volume and contact time. The second model system was selected to mimic an immunogenicity assay, which was used to screen anti-drug antibodies from samples. Daclizumab is a humanized antibody drug and was immobilized on a streptavidin-covered surface via biotin-streptavidin interaction. A series of concentrations of anti-human IgG were flowed over the Daclizumab surface at various flow rates to improve the sensitivity of the assay.

Finally, in order to apply the MFCA-SPRM for parallel analyses with minimum spot-to-spot variations, a test of bulk refractive index change and protein adsorption within 24 micro flow cells is presented. Signal variations caused by the optical system and surface heterogeneity are identified and the findings will be used for future experiment design.

Background

Model System

The MFCA is a 3D flow system that consists of 48 micro flow cells. Each flow cell is connected to inlet and outlet wells via microchannels in a platform that resembles a 96-well microtiter plate.[21, 22] Sample solutions flowed over the sensing surface are driven by a peristaltic pump through microchannels and connection tubing. A 2D schematic structure of a single flow cell created when the MFCA is sealed with the SPR sensing surface for a binding reaction is shown in Figure 3.1. The inlet and outlet channels for flow entering and exiting are perpendicular to the reaction surface. In order to understand the mass transport and reaction process happening at the SPR sensing surface, Commercial CFD software, Comsol Multiphysics (Stockholm, Sweden) was used to

build a model to solve the Navier-Stokes and diffusion-convection equations.[20] Dimensions of the flow cell for numerical modeling are represented in Figure 3.2. The opening of the inlet and outlet microchannels are approximately 150 × 150 μm.[22] The height of the flow cell is approximately 100 μm; the length of the reaction surface is 650 μm and the width of the flow cell is of 400 μm, which is not shown in Figure 3.1.

Simulation

The model of the MFCA is built on coupling a 2D domain of convection-diffusion with a 1D boundary of a diffusion-reaction. The analyte in the solution is transported to the reaction surface by convection and diffusion, in which the flow rate is an important parameter. The flow velocity profile throughout the modeling domain can be evaluated with incompressible Navier-Stokes equations. For a pressure driven flow reaching steady state, the velocity and pressure at any point within the MFCA can be solved from the conservation of mass and momentum relationships described by equation 3.1 and 3.2.

$$\nabla \cdot \mathbf{u} = 0 \tag{3.1}$$

$$\rho \mathbf{u} \cdot \nabla \mathbf{u} = -\nabla p + \mu \nabla^2 \mathbf{u} \tag{3.2}$$

where $\mathbf{u}$ is the flow velocity; p is the pressure; ρ is the density; and μ is the dynamic viscosity. The nonslip boundary condition is assumed at the walls in Figure 3.2. The inlet velocity is specified as a constant and the pressure at the outlet is at atmosphere pressure.

The concentration of analyte at the inlet is set as a constant (c_0), mass transport of analyte within the MFCA is described by convection and diffusion equation as follows:

$$\frac{\partial c}{\partial t} + \mathbf{u}\cdot \nabla c = \mathrm{D}\nabla^2 c \tag{3.3}$$

where c is the bulk concentration of analyte and D the diffusion coefficient of the analyte.

For a first order reverse reaction at the reactive interface, the material balance is determined by the surface diffusion and the reaction rate expression of binding pairs (c_s),

$$\frac{\partial c_s}{\partial t} + \nabla \cdot (-D_s \nabla c_s) = k_{on} c (c_{s0} - c_s) - k_{off} c_s \tag{3.4}$$

where c_{s0} is the initial surface density of ligands, c_s is the surface concentration of binding pairs and c is the bulk concentration of analyte. k_{on} and k_{off} are the forward and reverse reaction rates. From the reaction kinetic expression above, the concentration of surface binding products can be described as:[15]

$$c_s(t) = c_s^{EQ}\left(1 - e^{\frac{-t}{\tau}}\right) \tag{3.5}$$

$$c_s^{EQ} = \frac{k_{on} c_0 c_{s0}}{k_{on} c_0 + k_{off}} \tag{3.6}$$

$$\tau = \frac{1}{k_{on} c_0 + k_{off}} \tag{3.7}$$

where c_s^{EQ} is the surface concentration of binding products when the surface reaction reaches equilibrium and τ is the equilibrium time.[10]

The boundary condition for the materials balance at the nonreactive surface is insulated meaning no adsorption occurred according to:

$$\mathbf{n} \cdot (-D_s \nabla c_s) = 0 \tag{3.8}$$

In this equation, **n** is the normal vector to the boundary.

The boundary conditions for the bulk coupled to the surface reaction with the molar flux of reactant in the bulk and the concentration of the surface reactant gives

$$\mathbf{n} \cdot (-\mathrm{D}\nabla \mathrm{c} + \mathrm{c}\mathbf{u}) = -k_{on} c(c_{s0} - c_s) + k_{off} c_s \tag{3.9}$$

The wall boundaries are set to be insulated and the inlet is set as c_0. While at the outlet, the boundary condition is set as a convective flux given by

$$\mathbf{n} \cdot (-\mathrm{D}\nabla \mathrm{c}) = 0 \tag{3.10}$$

For all of the equations, the effect of temperature is not considered.

The basic simulation process with COMSOL includes a definition of model domain, setting equations and constants used in the domain and boundary, mesh generation, computing and postprocessing.[20] As described by the equations above, the biomolecular interactions in the MFCA-SPRM depend on the flow pattern and the geometry of the flow cell. The dimensions of the flow cell are fixed in this study. The flow velocity profile was modeled previously in the 2D and 3D cases.[20] Figures 3.2 to 3.4 show a process of the modeling of a biomolecular interaction within the MFCA. Figure 3.2 is the mesh generated within the modeling region after setting domain and boundary conditions. After calculation, parameters of interest can be plotted during the step of postprocessing. Figure 3.3 is an example of the analyte bulk concentration profile in the flow cell at a

specific reaction time, and Figure 3.2c is a representative plot of the surface concentration of binding products versus reaction time.

Theoretical Analysis

Because of the diverse variables used in the equations listed above, it is useful to scale the mass transport and reaction equations without dimensions, which helps to compare results in different systems.[10, 13] The dimensionless equations are presented as follows:

$$\frac{\partial \mathrm{c}'}{\partial \mathrm{t}'} + \left(u' \frac{\partial c'}{\partial x'} + v' \frac{\partial c'}{\partial y'} \right) = \frac{1}{Pe^2} \frac{\partial^2 c'}{\partial x'^2} + \frac{\partial^2 c'}{\partial y'^2} \tag{3.11}$$

$$\frac{\partial c_s'}{\partial t'} = \varepsilon D_a [c_i'(1 - c_s') - K_D c_s'] \tag{3.12}$$

where

$$x' = \frac{x}{hPe}, \qquad y' = \frac{y}{h}, \qquad t' = \frac{Dt}{h^2}$$

$$u' = \frac{u}{u_{avg}}, \qquad v' = \frac{v}{v_{avg}}, \qquad c' = \frac{C}{C_0}, \qquad c_s' = \frac{c_s}{c_{s0}}$$

where x' and y' are dimensionless coordinates and t' is the dimensionless time. h is the height of the flow cell; u_{avg} and v_{avg} are average flow velocities in the x' and y' directions, respectively. c_0 is the inlet bulk concentration of analyte.

$$Pe = \frac{u_{avg} h}{D}, \qquad \varepsilon = \frac{c_0 h}{c_{s0}}, \qquad Da = \frac{k_{on} c_{s0} h}{D}, \qquad K_D = \frac{k_{off}}{k_{on} c_0} \tag{3.13}$$

where *Pe* and *Da* are the Peclet and Damkohler numbers, respectively. *Pe* is the ratio of convection and diffusion strength and *Da* is the strength of surface reaction compared to diffusion. ε is the relative adsorption capacity and K_D is the dimensionless equilibrium dissociation constant.

Simulation Results

Based on equation 3.6, binding rate constants (k_{on} and k_{off}), reactive bulk concentration (c), and surface density of ligands (c_{s0}) are key parameters that impact the binding reaction rate and the equilibrium concentration of binding products. Using the COMSOL model described above, effects of these parameters were investigated by varying the values applied in the model. The numbers are listed in tables below and these values cover typical SPR experimental conditions.[18, 19]

Binding Affinity

Table 3.1 presents the value of parameters used in the modeling to examine kinetic changes caused by binding rate constants at various analyte concentrations. Two sets of k_{on} and k_{off} were 10^4 $(mol \cdot s/L)^{-1}$ and 10^{-4} s^{-1}, 10^3 $(mol \cdot s/L)^{-1}$ and 10^{-3} s^{-1}, respectively. Concentrations of analyte ranging from 10^{-5} to 10^{-9} mol/L were considered. *Pe* and *Da* are numbers to compare the strength of convection/diffusion and reaction/diffusion, respectively. Under the simulation conditions, the *Pe* number is calculated to be 1000 and the *Da* number is above 10 in both cases, which represent that for both reactions, the reaction rate are limited by the diffusion of molecules.

In all reactions, the rate of change of surface concentration of binding product is proportional to the bulk concentration of analyte in solution. The higher the concentration

in solution, the more molecules diffuse to the solid surface and participate in the reaction. Figure 3.5 presents a plot of the formation of surface binding products versus time from the modeling results with constants listed in Table 3.1. A high analyte concentration of 10 μM reaches saturation within 300 s for both sets of binding rate constants, while analyte concentrations below 1 μM do not reach equilibrium within 15 min of the modeling time. The results from the modeling are useful for optimizing experimental conditions. For example, if a high affinity interaction is adopted to create high-density capture surfaces, such as biotin-streptavidin interactions, it is better to use a highly concentrated solution to functionalize the surface within a short time. In order to detect an analyte of low concentration, extended reaction time is required and the time could also be estimated from the modeling.

Flow Rate

In a flow cell of fixed geometry, the flow rate is the only variable that could be changed to affect the mass transport. The flow rate effect on the binding interactions when using the MFCA was investigated by applying two flow rates of 16.7 and 534.4 μL/min in Figure 3.6. Values of flow rates, the binding affinity and concentrations of bulk analyte used for the modeling are listed in Table 3.2. A comparison of the modeling results in Figure 3.4a and 3.4b shows that the kinetics of the binding reactions are exactly the same at two different flow rates. As discussed before, the analyte is transported to the reaction surface by convention and diffusion. The *Pe* number at the two flow rates used in the modeling are 4.6×10^4 and 1.47×10^6, respectively, which indicate that diffusion limits the transport of analyte from the bulk to the surface in both cases.

The diffusion length for mass transport from the bulk to the capture surface is determined by the height of the concentration boundary layer near the reaction surface. The boundary layer thickness is inversely proportional to the flow rate of $v^{1/3}$. However, reported modeling results shows that within the modeling range of the flow rate, the difference of boundary thickness caused by the flow rate is not significantly affected by the reaction rate.[20] Therefore, the flow rate shows little effect on the thickness of boundary layer and reaction rate from the modeling results.

Surface Density of Binding Sites

The surface density of binding sites plays a key role in determining the binding kinetics as expressed in equation 3.4. The surface density of binding sites with reference to a previous reported value (8×10^{11} molecules/cm^2) is listed in Table 3.3 and used for the simulation.[21] The modeling bulk concentration ranges from 0.1 to 20 μM and the simulated results are shown in Figure 3.7. The plot shows that the surface density of ligands determines the initial reaction rate as well as the equilibrium concentration of surface binding products. For reactions with the same binding affinity, the higher the surface density is, the faster the reaction proceeds and the more binding products are produced. The modeling is based on the assumption that evenly distributed binding sites have uniform activity on the surface. However, this assumption is also a limitation of the simulation. Under experimental conditions, the fractional activity of binding sites and the surface heterogeneity are two parameters that can cause possible different results from the theoretical study and will be discussed below.

Experimental Section

Materials

(1-Mercapto-11-undecyl) tetra (ethylene glycol) (OEG) and biotin-terminated tri (ethylene glycol) hexadecanethiol (BAT) were purchased from Asemblon (Redmond, WA). Immunopure streptavidin (Product # 21125), goat anti-human IgG (Product # 31130) and a biotinylation kit (Product # 21445) were purchased from Pierce (Rockford, IL). Daclizumab in saline (1.18 mg/mL) was provided by Dr. John Rose, Department of Neurology, School of Medicine, and University of Utah. Biotinylated-protein A (1 mg/mL) and mouse IgG (10 mg/mL) in PBS buffer was provided by Wasatch Microfluidics. Absolute ethanol was purchased from AAPER Alcohol (Shelbyville, Kentucky). Water was purified using a Barnstead Nanopure Diamond laboratory water system, and phosphate buffered saline (PBS, pH 7.4) was prepared in the laboratory.

MFCA-SPRM System

The SPR microscope is custom-built and similar to a previously described system.[23] An intensity-stabilized, HeNe laser from Melles Griot (Carlsbad, California) is used as a light source. The laser beam is expanded and collimated by optics from Newport Corporation (Irvine, CA) before traveling through a SF14 hemispherical prism (R. Mathews Optical Works, Poulsbo, WA) and SF14 substrate from Schott AG (Elmsford, NY). The substrate is coated with 2 nm of titanium and 50 nm of gold using a Denton electron-beam evaporator. The reflected light is detected by a CCD camera (IMB-3145FT) from k-Space Associates (Ann Arbor, MI). Two rotation stages from Newport Corporation (Irvine, CA) are used to control the angle of incidence and position of the

detection CCD camera. The entire system is mounted on a laser table. Software from k-Space Associates (Ann Arbor, MI) was used to acquire, record, and process images. The MFCA was integrated into the SPRM optical system with a custom-made manifold mounted on an X-Y stage from Newport Corporation (Irvine, CA). MFCAs (Wasatch Microfluidics, Salt Lake City, UT) were fabricated in poly (dimethyl siloxane) (PDMS) by adapting soft lithography methods and using injection molding to increase throughput. Master molds were fabricated by micromilling the pattern in brass to the proper dimensions. A polycarbonate replica was made and used for casting the PDMS devices. Multiple layers of PDMS were combined together to form sophisticated three-dimensional networks through partial curing of layers or oxygen plasma treatment of the surface. A 24-channel peristaltic pump from Ismatec (Glattbrugg, Switzerland) was used for loading samples and driving solutions through the MFCA. The peristaltic pump contains eight rollers to minimize pulsing in the flow rate. The minimum flow rate of the system is 16.7 μL/min.

Biotin-Streptavidin Binding Affinity Measurement

Gold-coated glass substrates were immersed in 0.1 mM mixed BAT and OEG solutions (1: 9 BAT: OEG) for 24 h to form a mixed-SAM on the surface. Then, the substrate was removed from the solution, rinsed with pure ethanol, and dried by a stream of nitrogen. Finally, the substrate was mounted on the planar face of the SPRM prism with refractive index matching liquid from Cargille Laboratories (Cedar Grove, NJ). Twenty-four (3 × 8 column × row) flow cells were used for the experiments described in this paper. Streptavidin solutions of eight concentrations (1700.0, 566.7, 188.9, 63.0, 21.0, 7.0, 2.3, and 0.8 nM) were flowed through the MFCA channels and across the SPR

sensing surface at a flow of 33.4 µL/min. The sample volume loaded into each flow cell is 300 µL. PBS buffer was loaded in to flow system right after streptavidin solution.

Daclizumab-IgG Binding Affinity Measurement

In the same way as studying the biotin-streptavidin interaction, the surface was functionalized with SAMs first. Then streptavidin solution of 1.85 µM, biotinylated Daclizumab of 0.7 µM was flowed over 24 micro flow cell sequent to make Daclizumab surface. Goat anti-human IgG solutions of eight concentrations (500, 167, 55.8, 18.6, 6.2, 2.1, 0.7, and 0.2 nM)) were flowed over the SPR sensing surface at a flow rate of 133.6 µL/min. The loading sample volume was 180 µL for each flow channel. PBS buffer was flowed over and washed off unbound IgG on the sensing surface right after the previous step.

Flow Rate Test

The flow rate effect was examined by running the biotin-streptavidin interaction at four flow rates: 33.4, 133.6, 267.2 and 534.4 µL/min, respectively. Streptavidin solutions of eight concentrations (1700.0, 566.7, 188.9, 63.0, 21.0, 7.0, 2.3, and 0.8 nM) were flowed through the MFCA channels and across the SPR sensing surface. The sample volume loaded into each flow cell is 300 µL.

SAMs Formation for XPS Analysis

Zero point one mM mixed BAT and OEG solutions with BAT mixed percentage of 0, 10, 50, 80, and 100 were prepared first. Gold-coated microscope glass slides were immersed into each solution for 24 h. Then the substrate was removed from the solution, rinsed with pure ethanol, and dried by a stream of nitrogen for XPS analysis.

XPS spectra were acquired by Dr. Brian van Denver in the microfab in University of Utah using a Kratos Axis Ultra DLD instrument (Chestnut Ridge, NY). XPS survey spectra data was collected with a pass energy of 160 e, a step increment of 1 eV and a Al Kα source power of 144 W.

In Situ SAMs Preparation for SPR Analysis

Gold-coated substrate was mounted on the prism with refractive index matching liquid and MFCA was integrated with SPRM. 0.1 mM mixed thiols solution with BAT % in the range of 0, 10, 50, 80 and 100% were loaded into 20 flow cells at a flow rate of 33.4 µL/min. 6 × 4 (column × row) flow cells were used in the test and four flow cells in a column were duplicates. Each flow cell is oval shape of size 150 × 200 µm. One column was filled with water for the control experiment. After thiol solutions filled the flow cells, the flow was stopped for an hour while thiols diffused and adsorbed on surfaces. Then 100% pure ethanol was flowed over the surface to wash off excess thiols. PBS buffer was run through each flow cell before streptavidin adsorption. Zero point one mg/mL streptavidin solution was used to test the capture ability of SAMs surfaces with various densities of biotin. The whole process was monitored and recorded at a light incident angle of 54.25° by SPRM.

Atomic Force Microscopy (AFM) Analysis of SAMs and Streptavidin Surfaces

One hour after *in situ* immobilization of SAMs and streptavidin, the glass substrate was removed from the prism and prepared for AFM measurement. AFM imaging was performed in a ScanAsyst mode with Dimension ICON-PT and Nanoscope Controller

Software (Bruker) in the Surface Analysis Laboratory at University of Utah. The ScanAsyst is a tapping mode with automatic image optimization. The scanning experiments were carried out in the air at room temperature. The ScanAsyst microcantilever was a sharp silicon nitride probe of typical radius of 2 nm. The normal spring constant is 0.4 N/m and the resonance frequency is 7 kHz. The scan rate and image resolution are one Hz and 512 × 512 pixels, respectively. The images used for roughness analyses were corrected with a second-order flatten filter in the Nanoscope software.

Protein A-IgG Interaction

Twenty-four (6 × 4 array) flow cells were used in this experiment. First the surface was functionalized with SAMs by immersed into 0.1 mM BAT solution for 24 h. A mixture of ethanol and water (Refractive Index 1.3391) was flowed through all 24 flow cells to test the change of the SPR signal to bulk refractive index changes. Biotinylated protein A solutions of five concentrations (0.66, 1.3, 2.6, 5.3 and 10.6 nM) were flowed through the MFCA channels and across the SPR sensing surface at a flow rates of 33.4 µL/min. Mouse IgG concentration of 1.33 µM was flowed over protein A surface to tests their activity. The loading sample volume of protein A and IgG are both 250 µL for each flow cell. Binding of mouse IgG and biotin-protein A was monitored at a light incident angle of 55.1° by SPRM.

Results and Discussion

SPR for biomolecular interaction analysis provides quantitative analysis of binding affinity and kinetic data of binding process. The two model systems of (1) biotin-streptavidin and (2) biotinylated Daclizumab-IgG, represent two types of interactions:

protein-ligand and protein-protein interactions. The biotin-streptavidin binding affinity is high ($K_a \sim 10^{13}$ M^{-1} in solution)[24] in solution and streptavidin has been used as a molecular linker in many applications in biosensing.[23-25] In a previous report, we demonstrated that the biotin-streptavidin interaction is a robust and efficient strategy to immobilize antibodies on an SPR sensing surface.[21] In order to create a high-density and high-activity antibody array, we further studied the interaction of biotin-streptavidin in the MFCA to optimize the conditions for antibody immobilization. Daclizumab-IgG interaction was used to mimic an immunogenicity assay of Daclizumab to screen anti-drug antibodies from serum or blood samples. Daclizumab is a humanized antibody drug with 90% structure sequence from human IgG, and goat anti-human polyclonal IgG worked as pseudo anti-drug antibodies in the binding affinity study. The binding affinity and kinetic measurement will provide information to develop immunogenicity assays based on the integrated MFCA-SPRM.

Binding Reactions and Concentrations

Before the biotin-streptavidin interaction analysis, the gold-coated SPR sensing surface was functionalized with biotin-terminated SAMs. Then streptavidin solutions of eight concentrations were flowed over 24 flow cells in MFCA at a flow rate of 33.4 μL/min; each concentration sample was run in three duplicates. The tested streptavidin concentration was in the range of 0.8 to 1700 nM and the sample volume was 300 μL for each flow cell.

Figure 3.8a is the real-time SPR signal of streptavidin adsorption collected by using the SPR microscope. Each curve represents an average of three duplicates. The detection limit of streptavidin was 7.0 nM under experimental conditions. Streptavidin samples of

concentrations above 63.3 nM can saturate the surface within a tested time of 10 min. When the adsorption reaction reaches equilibrium, the SPR signal can be converted to a surface density of streptavidin molecules by using the quantitative method reported in Chapter 2.[23] The largest surface density of streptavidin is 8.0×10^{11} molecules/cm^2, which is 57% of a reported value of 1.4×10^{12} molecules/cm.[2, 23] The lower surface density is due to the continuous-flow deposition that can wash off unbound streptavidin molecules while the reported one was deposited with microspotting. One thing that needs to be pointed out is the shape of the SPR curve for the 63.3 nM sample. The reaction rate was slower during the time from 250 to 340 s because the flow was stopped for sample loading. The decreased reaction rate shows that the reaction rate is slowed by the flow rate for the sample of concentration 63.3 nM. The reaction rate resumed after the flow was started again.

The surface concentration of streptavidin observed at equilibrium versus the bulk concentration of streptavidin was fitted into a first-order Langmuir model (equation 3.13) in Figure 3.8b. The dissociation constant (K_D) calculated from the Langmuir model is $(2.40 \pm 0.06) \times 10^{-8}$ M ($R^2 = 0.942$), which is larger than the reported value (10^{-13} M) in solution but on the same order of the reported value forat a solid-liquid interface (10^{-8} M).[26] In fact, due to the interaction among the immobilized ligands, the data of binding interaction of biotin-streptavidin fitted better with an extended Langmuir model in equation 3.14. The K_D calculated from fitting to equation 3.14 is $(2.31 \pm 0.19) \times 10^{-8}$ M ($R^2 = 0.98$). Equation 3.14 is also described as the Hill-Waud model and n is the Hill coefficient of cooperativity.[27] This model is used to find the best fit and n is found to be two in this case.

$$y = y_{max} \times \frac{c_s}{K_D + c_s} \tag{3.13}$$

$$y = y_{max} \times \frac{c_s^n}{K_D^n + c_s^n} \tag{3.14}$$

With the experimental constants listed in Table 3.4, the biotin-streptavidin interaction was modeled and the kinetics of the reaction were plotted in Figure 3.8c. The rate constants of k_{on} and k_{off} listed in Table 3.4 were calculated from the value of the dissociation constant ($K_D = k_{off}/k_{on}$) and the saturation time ($\tau = 1/(c_0 k_{on} + k_{off})$ measured from the real-time SPR curves as shown in Figure 3.8a. Comparing the surface concentration of binding products at the equilibrium time to the maximum surface concentration gives the degree of surface saturation, which is called fractional saturation or saturation fraction. A comparison of the fractional saturation from experiments and simulation results versus the streptavidin bulk concentration is presented in Figure 3.8d. The data points in Figure 3.8d show that for the same streptavidin sample concentration, the experimental fractional saturation is larger than the simulated one in all of the samples except the highest concentration. One abnormal data point in Figure 3.8d could be caused by experimental errors. The same observation was also found in Daclizumab-IgG interaction; the result of experiments was summarized in Figure 3.9a and b. Figure 3.9c was the simulation plot and a comparison of simulation and experimental results were presented in Figure 3.9d.

A higher fractional saturation indicates a higher reaction rate in the experiments compared to the modeling. This discrepancy can be attributed to the limitations of the model. Although the modeling has reflected the major physical process in the flow cell, it is far from being complete and realistic. First, the 1D model cannot fully describe the mass transport on a 3D scale. One possible explanation for a higher reaction rate in the experiment is a thinner concentration boundary layer formed in the experiment compared to the modeling. The boundary thickness plays a key role in determining the concentration gradient, concentration of reactant and diffusion time for analytes from the bulk to the reactive surface. The order of magnitude thickness of the concentration boundary layer δ is related to the shear rate (γ) as shown in the equation below:

$$\delta \propto \left(\frac{Dl}{\gamma}\right)^{\frac{1}{3}} \tag{3.15}$$

where D is the diffusion constant and *l* is the lateral length along the reaction surface. The shear rate is the rate of change of velocity at which one layer of fluid passes over an adjacent layer. In the model, only the shear rate in the direction along the 1D reactive surface was considered. While in the experiment, the shear rate on the SPR sensing surface changed in two directions, especially in the region that is perpendicular to the inlet and outlet microchannels. The higher shear rate leads to more efficient delivery of reactants and a higher concentration of reactants, so the reaction rate in a 3D flow cell is higher compared to 1D modeling.

Another possible reason is the model has an assumption of uniformly distributed and evenly active surface binding sites. Heterogeneity of the surface, steric effects, and

conformation and activity of immobilized biomolecules and their interactions could all cause the differences between experimental and simulated results. For example, the cooperative binding on the high-density biotin surface has caused different binding affinity and reaction rate.[26]

In addition, inaccurate constants being applied in the modeling could also cause may lead to different results. For example, values of surface and solution diffusion constants were set to be equal in the simulation using reported values.[19] However, according to the Einstein–Stokes equation, the solution diffusion constant depends on the temperature and the viscosity of solution. The surface diffusion constant has been reported to depend on the surface concentration of adsorbed protein. The dynamic range of the surface diffusion constant could be of one order of magnitude.[28]

Overall, the modeling could be further improved by the selection of proper constants and setting of boundary conditions. However, the prediction from the modeling is limited. Although the modeling is useful to predict the effect of analyte bulk concentration, effects of flow rate and surface density of binding sites are more complex and will be further investigated with experiments.

The Daclizumab-IgG interaction served as a model system for studying immunogenicity assay as mentioned before. The immunoasaay following the immobilization of SAMs, streptavidin and biotinylated Daclizumab was described in the methods section. IgG solutions (180 μL/ channel) of eight concentrations from 0.2 to 500 nM were flowed over a Daclizumab-functionalized surface at a flow rate of 133.6 μL/min; each concentration sample had three duplicates. Compared to streptavidin

solutions, a lower concentration range of IgG was used because this model system was used to investigate the detection limit of the immunoassay.

The experimental and simulation results were presented in Figure 3.9. Figure 3.9a shows the real-time SPR response curves of five detectable samples. The detection limit was 18.6 nM under the tested condition. The surface density of IgG was calculated and fitted to a Langmuir model in Figure 3.9b. The dissociation constant of K_D is (2.37 ± 0.01) × 10^{-7} M (R^2 = 0.988) from the model, which is higher than biotin-streptavidin interaction. Cooperative binding is not obvious because the data fits well with a simple Langmuir model. A simulation of the interaction usingconstants listed in Table 3.4 is presented in Figure 3.9c. The simulated result shows that the reaction rate increases with an increased bulk IgG concentration, which is consistent with the experimental results in Figure 3.9a. However, when comparing the saturation fraction at equilibrium time in Figure 3.9d, all of the experimental results are higher than the simulations due to limitations of the modeling as discussed before.

Effect of Flow Rate

From the previous theoretical study, the effect of flow rate on the binding kinetics the reaction in the MFCA is not significant within the flow rate range controlled by the peristaltic pump. However, the discrepancy of experimental and simulation results had shown that the effect of flow rate cannot be fully predicted from the simulation. In order to investigate the flow rate effect on surface reactions, an experiment was carried out with a fixed volume (180 µL) of streptavidin to interact with a biotin-functionalized surface at four flow rates, ranging from 33.4 to 534 µL/min. Streptavidin of eight concentrations from 0.8 to 1700 nM were used in the experiment.

SPR curves of biotin-streptavidin interactions at increasing flow rates are shown in Figure 3.10. The flow rates increased from top to bottom in the graph. The time scale is set to be equal among all four plots for the comparison of signal changes. Obviously, for samples of the same concentration, the higher the flow rate, the faster the reaction reaches equilibrium. In another words, within a limited reaction time, higher flow rates generate higher SPR signals. The same findings were also reported in an *ex situ* protein deposition with the same continuous flow system.[29]

As discussed before, if the reaction is limited by diffusion, the height of the boundary diffusion layer is critical in determining the reaction rate. The height of the diffusion layer is inversely proportional to the flow rate as shown in equation 3.12. When the flow rate increases in the MFCA, the diffusion layer decreases and the reaction rate increases. In this case, the reaction rate is proportional to the flow rate to the 1/3 power provided by the Leveque solution,[29]

$$\frac{dc_s}{dt} = 0.5384[\frac{\gamma}{Dl}]^{\frac{1}{3}} D c_0 \qquad (3.16)$$

where γ is the shear rate and proportional to the flow rate *v*. So the reaction rate is linear with the flow rate to the one-third power. To determine if the reaction in MFCA is diffusion limited, the SPR signal at reaction time t = 20 s is used to represent the reaction rate since the SPR signal is linear with the surface concentration of binding products.[23] The effect of flow rate on the reaction rate is illustrated in Figure 3.11. The plot shows that at low concentrations, the reaction is diffusion-limited at tested flow rates since the data fits well into a linear model (R^2 = 0.98~0.99). However, as the concentration

increases, the goodness of fit (R^2 = 0.88~0.96) falls because the reaction becomes more reaction-limited and less diffusion-limited at high flow rates.

Figure 3.12 presents the equilibrium isotherms of biotin-streptavidin interaction measured at four flow rates. The graphs show that the SPR signal at the lowest flow rate has the highest response signals. This can be explained by the surface concentration at equilibrium depending on the reaction rate times the contact time. As said before, the diffusion-limited reaction rate (dc_s/d_t) $\propto v^{\frac{1}{3}}$; the contact time is equal to the sample volume (Q) divided by the flow rate (Q/v), so for a fixed sample volume, the surface concentration $c_s \propto v^{(-\frac{2}{3})}$, as all the other conditions are the same. Therefore, for a low concentration sample in a diffusion-limited reaction, a lower flow rate is preferred to generate a higher signal with a limited sample volume, which is important to improve the detection limit of assays.

The data in Figure 3.12 were fitted into an extended Langmuir model (n = 2) and the calculated dissociation constants were listed in Table 3.5. The dissociation constants from the equilibrium isotherms tested at flow rates above 133.6 µL/min are very close with a fixed 180 ?l/min sample. Because as the flow rate increases, the reaction transits from diffusion-limited to reaction-limited, the effect of flow rate becomes trivial. The dissociation constant of 33.4 µL/min is slightly lower than others because the reaction is diffusion-limited, in which lower reaction rate and a longer contact time cause the variance.

Optimization of Biotin-Terminated SAMs Surface

From the previous study of biotin-streptavidin interactions, the cooperativity shows that the surface density of binding sites has an effect on the binding kinetic analysis with MFCA-SPRM. SAMs of biotin-terminated thiols on gold surface is important for immobilize streptavidin and other biomolecules. The surface density of biotin on a SAM is controlled by varying the mixed ratio of BAT and OEG in solution. The binary thiol SAMs for streptavidin immobilization is a well-studied system and has been characterized by many surface analysis techniques, such as XPS, STM and FTIR.[30-33] The optimal ratio of BAT/OEG in solution used for experiments is reported to be between 0.1 to 0.5 for the maximum the streptavidin adsorption.[30] To create an optimal biotin surface for immobilization of biomolecules using the MFCA, we apply the MFCA-SPRM for *in situ* formation of binary SAMs and compare their capacity for streptavidin adsorption.

Thiol solutions prepared with BAT mol% of 0, 10, 50, 80 and 100% were loaded into individual micro flow cells and reacted with the gold SPR surface for an hour. After that, pure ethanol was flowed over the surface to get rid of unbound molecules; PBS buffer was flowed to establish the baseline for SPR analysis of streptavidin adsorption. A concentrated streptavidin solution of 0.1 mg/mL was used to test the biotin activity of various surface densities. After the SPR analysis, the SPR substrate was removed from the prism and put into an AFM system to map the morphology of streptavidin on the surface. XPS was used to quantify the amount of biotin in the SAMs. The XPS sample was prepared with gold-coated microscope glass slides immersed into the thiol solutions mentioned above for 24 h.

Figure 3.13a presents the SPR real-time curves of streptavidin adsorption on SAMs of various surface density of biotin. Figure 3.13b shows a summary of the SPR equilibrium signals from Figure 3.13a. Non-specific adsorption of streptavidin on 100% OEG surface is very low, 0.44 ± 0.13 % reflectivity. Streptavidin adsorption on the surfaces of 10, 50, 80, and 100% BAT are saturated with little difference in SPR signals, which are 6.58 ± 1.64, 5.73 ± 0.91, 6.70 ± 1.09, and 7.12 ± 1.82% reflectivity, respectively. Compared to previous data of streptavidin adsorption, the relative standard deviation is larger than 15% because the *in situ* formation of SAMs causes surface heterogeneity. Although the thiols can absorb on the surface fast within minutes, it takes hours to form an ordered structure.[34]

The density of biotin on the surface is proportional to the BAT% in solution and was proved by XPS analysis results shown in Figure 3.14. Since the nitrogen N (1s) in XPS spectra was only attributed to BAT, we use the ratio of nitrogen N (1s) peak area in Figure 3.14a normalized to Au (4f) peak to represent the surface density of biotin. The surface density of biotin has a linear relationship with BAT% in solution shown in Figure 3.14b. Among all the surface density, from 10% to 100%, the capacity for maximum streptavidin adsorption does not vary too much. So the lower the surface density is, the higher the capture efficiency for biotin-terminated SAMs.

AFM was applied to characterize the adsorbed streptavidin layer on a SAMs surface after SPR analysis. Figures 3.15 and 3.16 are AFM images of SAMs and streptavidin surfaces obtained with a tapping mode in the air at room temperature. The RMS roughness of all SAMs and streptavidin surfaces were summarized and compared in Figure 3.17. The roughness of SAMs is below 2 nm and is about 4 nm for streptavidin

surface. The SAMs AFM image shows that the OEG and BAT thiols formed phase-separated domains because of defects of gold surface and entangling effect of long-chain OEG thiols.[35] Also the domain size and packing conformation of SAMs depend on the assembly solution conditions, such as temperature.[32] These nanoscale structure and properties could affect protein adsorption.[36] Therefore, the surface heterogeneity of mixed SAMs surfaces could affect the streptavidin adsorption.

However, AFM images in Figures 3.15 and 3.16 are dried streptavidin surface after SPR analysis. The aggregated streptavidin images could not provide enough information of the adsorption affected by the surface density of binding sites and heterogeneity.[32] But the measured roughness number could be used as a rough estimation of the amount of streptavidin bound to the surface if protein aggregation does not cause loss on the surface. The number shows the amount of streptavidin on surfaces of BAT over 50% are close and has reached saturation. The 10% BAT surface roughness is low which is inconsistent with the result of SPR analysis. This could be due to the protein on the surface was lost after drying.

Overall, mixed thiol solutions with BAT over 10% can be used for preparation of SAMs surface for streptavidin adsorption, and increasing the amount of BAT from 50% to 100% does not show significant improvement of the maximum adsorption capability of SAMs surfaces.

Surface Density and Activity of Immobilized Protein A

Protein A is a surface protein (M.W. ~ 42,000 Da) originally found in the cell wall of the bacteria *Staphylococcus aureus* that has specific binding to the Fc region of IgG from various animals.[37] It is often used for oriented immobilization of IgG on the substrate

surface.[38] Here we investigated the surface density of immobilized protein A with relations to their activity. The experiment was carried out by starting the test of SPR response to the bulk refractive index change, which is an experiment designed to test the signal variance among microspots. Then streptavidin was immobilized on a biotin-terminated SAMs surface. Biotinylated protein A solution of various concentrations from 0.66 to 10.6 nm were loaded into flow cells to create different surface density of binding sites and mouse IgG of 1.33 μM was delivered to the protein A surface to test the activity. Signal of protin A-IgG interacions will also be used in the analysis of spot-to-spot signal variations.

Figure 3.18 shows a plot of SPR real-time curves of the whole experiment process with a SPR image of 24 flow cells and their detection windows for the signal collection. The SPR signals of protein A and IgG adsorption are summarized and compared in Figure 3.19a. The plot shows that the SPR signal of IgG adsorption on all protein surfaces are almost on the same level except the lowest one created using a 0.66 nM solution. But the SPR signal of protein A adsorption increases with the bulk concentration of protein A. By converting the SPR signal to surface density, Figure 3.19b is the binding ratio of IgG to protein A on various protein A surfaces, ranging from 1:1 to 2.8:1. The binding ratio decreases with an increasedecrease in the bulk concentration of protein A, which indicatesa lower surface concentration of protein A, the higher capture effiency of protein A. It is predicted that each protein A has five binding sites to IgG from the sequence study of protein.[39] However, reported experimental data shows various binding ratio from 1:1 to 2.1:1, depending on the experimental conditions and detection methods.[39]

The protein A-IgG interaction demonstrates that the adsorption of IgG on a protein A-functionalized surface does not increase with the surface concentration of binding sites, which is due to the 3D structure of binding sites on microscopic scale not being uniformly active and evenly distributed.[40] The molecular size and orientation of immobilized protein, interactions such as steric and electrostatic forces among binding sites could cause the local surface heterogeneity and binding activity. Lower surface concentration of binding sites leads to higher activity, but higher surface concentration of binding sites capture the most absolute amount of analytes as shown in Figure 3.19.

Spot-to-Spot Signal Variations

Minimizing spot-to-spot signal variation is important for the MFCA-SPRM to develop reliable assays and generate reproducible data. In this part, data from previous experiments of protein interactions were used to investigate possible sources that cause signal variations among micro flow cells.

Table 3.5 is the SPR signal of bulk refractive index changes and protein A-IgG interactions in Figure 3.18. The positions of data in Table 3.5 correspond to the position of flow cells in Figure 3.18. The coefficient of variation (CV) of SPR signal of flow cells in a row lies in range of 3.27% to 7.33%, and the CV of SPR signal in a column is from 0.17% to 4.17%. Table 3.6 is the SPR signal of the adsorption of streptavidin in the same 24 flow cells. The CV of a row and column are in the range of 9.26% and 14.95%, 2.26% and 8.14%, respectively. In both tests, the samples were the same for all 24 flow cells.

Generally, the CV in a row is larger than the CV in a column. The larger CV in a row is caused by the shift of light incident angle at the back of SPR sensing surface in a hemi-spherical prism. Shown in Figure 3.19a, the SPR system is based on Kretschmann

configuration. Theoretically, collimated light is used to excite surface plasmon in the center of a semispherical prism. However, in order to illuminate a large sensing area, the size of light beam becomes so large that after the light traveling through the prism and being reflected at the back of sensing surface, the light incident angle varies from the beam center to both edges. Figure 3.19b shows an example of the shift of light incident angle. If the refractive index of prism (n) is 1.80, the diameter of the prism (D) is 8 cm, the diameter of light beam (d) is 1 cm, and the light incident angle of beam in the center is 55^{o}. The light incident angle is 56.3^{o} at the left edge and 53.7^{o} at the right edge, which were calculated with Snell's law. As discussed in Chapter 2, the SPR microscope sensitivity factor depends on the light incident angle and is limited within two linear ranges.[23] Both of these two linear regions are less than one degree, so the 1.3 degree shift could cause the response at the edges to exceed the linear range. This is an intrinsic property of the prism and could be overcome by using a hemi-spherical prism of larger diameter, minimizing the SPR sensing area or changing to a prism of a different shape such as a dove prism.

The overall CV of the streptavidin adsorption signal (12.0%) is larger than bulk change (5.36%). This is due to the mass transport and surface heterogeneity introducing variation in local refractive changes and corresponding SPR signals.[35] Major variables include variation of flow rate among flow cells, the nanoscale heterogeneity of SAMs surface, conformation, binding activity of immobilized proteins and interactions among binding sites etc. One possible solution to improve the mass transport is to change the geometry of flow cells based on equation 3.12.

Next the CVs for streptavidin adsorption using two types of micro flow cells were compared. One set of data is in Table 3.7 from protein A-IgG interaction, which was collected with flow cells of oval shape (250 × 150 μm). The SPR signals of streptavidin are 6.74 ± 0. 81 % reflectivity and the CV is 12.04%. The other set of data was based on an MFCA of octagon shape (650 × 400 μm) in Figure 3.21. The SPR signals of streptavidin adsorption are 4.20 ± 0. 60 % reflectivity and the CV is 14.30%. So, at least in this case, changing the geometry of flow cell does help improve the CV, however, the effect is not significant. Overall, the CV among 24 micro flow cells is below 5.36% for the test of bulk refractive index and below 15% for protein adsorption with the oval shaped MFCA.

Conclusions

We used both modeling and experimental methods to investigate factors that impact the biomolecular interaction analysis based on MFCA-SPRM. First, we used 2D modeling to demonstrate that the bulk concentration of analytes, binding affinity and surface density of binding sites are important parameters that determine the reaction rate on the sensing surface while the effect of flow rate is trivial from the modeling.

The biotin-streptavidin and Daclizumab-IgG interactions were used as two model systems to optimize the antibody immobilization and improve the detection limit of immunoassays. The parameters measured by experiments were applied in the modeling to compare the simulation and experimental data. However, the modeling results do not fit perfectly with experimental ones because mass transport and reactions in 3D flow cell are more complex than the modeling. The discrepancy between the modeling and experimental motivates further investigation of the effect of flow rate and surface density

of binding sites with experiments. The flow rate effect was examined by using fixed-volume of streptavidin that interacted with SAMs surface. The result shows the reaction rate in MFCA is proportional to the flow rate. As the flow rate increases, the reaction transits from diffusion-limited to reaction-limited. For a diffusion-limited reaction, the surface concentration of product changes linearly with time but 1/3 power of flow rate with a flow cell of fixed geometry. However, the lowest flow rate generates the highest SPR signal because of a long reaction time with the constraint of sample volume.

Finally, we identified that the major source of spot-to-spot signal variations is from the optical system and variables in the mass transport and reaction that introduce the heterogeneous local refractive changes. Changing the geometry of the flow cell shows improvements but the effect is limited.

References

1. Yager, P.; Edwards, T.; Fu, E.; Helton, K.; Nelson, K.; Tam, M. R.; Weigl, B. H., Microfluidic diagnostic technologies for global public health. *Nature* **2006**, *442*, 412-418.

2. Lion, N.; Reymond, F.; Girault, H. H.; Rossier, J. S., Why the move to microfluidics for protein analysis? *Curr. Opin.n Biotechnol.* **2004**, *15*, 31-37.

3. Kartalov, E. P., High-throughput multi-antigen microfluidic fluorescence immunoassays. *Biotechniques* **2006**, *40*, 85-90.

4. Limoges, B.; Marchal, D.; Mavra F.; Saveant, J.-M.; Schollhorn, B., Theory and practice of enzyme bioaffinity electrodes. Direct electrochemical product detection. *J. Am. Chem. Soc.* **2008**, *130*, 7259-7275.

5. Mullett, W. M.; Lai, E. P. C.; Yeung, J. M., Surface plasmon resonance-based immunoassays. *Methods* **2000**, *22*, 77-91.

6. Smith, E. A.; Corn, R. M., Surface plasmon resonance imaging as a tool to monitor biomolecular interactions in an array based format. *Appl. Spectrosc.* **2003**, *57*, 320A.

7. Michalzik, M.; Wilke, R.; Buttgenbach, S., Miniaturized QCM-based flow system for immunosensor application in liquid. *Sens. Actuators B Chem.* **2005**, *111-112*, 410-415.

8. Wu, G., Bioassay of prostate-specific antigen (PSA) using microcantilevers. *Nat. Biotechnol.* **2001**, *19*, 856-860.

9. Cui, Y.; Wei, Q. Q.; Park, H. K.; Lieber, C. M., Nanowire nanosensors for highly sensitive and selective detection of biological and chemical species. *Science* **2001**, *293*, 1289-1292.

10. Gervais, T.; Jensen, K. F., Mass transport and surface reactions in microfluidic systems. *Chem. Eng. Sci.* **2006**, *61*, 1102-1121.

11. Squires, T. M.; Messinger, R. J.; Manalis, S. R., Making it stick: Convection, reaction and diffusion in surface-based biosensors. *Nat. Biotechnol.* **2008**, *26*, 417-426.

12. Myszka, D. G.; He, X.; Dembo, M.; Morton, T. A.; Goldstein, B., Extending the range of rate constants available from BIACORE: Interpreting mass transport-influenced binding data. *Biophys. J.* **1998**, *75*, 583-594.

13. Jomeh, S.; Hoorfar, M., Numerical modeling of mass transport in microfluidic biomolecule-capturing devices equipped with reactive surfaces. *Chemical Engineering Journal* **2010**, *165*, 668-677.

14. Jenkins, J.; Prabhakarpandian, B.; Lenghaus, K.; Hickman, J.; Sundaram, S., Fluidics-resolved estimation of protein adsorption kinetics in a biomicrofluidic system. *Anal. Biochem.* **2004**, *331*, 207-215.

15. Escobedo, C.; Brolo, A. G.; Gordon, R.; Sinton, D., Flow-through vs flow-over: analysis of transport and binding in nanohole array plasmonic biosensors. *Anal. Chem.* **2010**, *82*, 10015-10020.

16. Friedrich, D.; Please, C.; Melvin, T., Optimisation of analyte transport in integrated microfluidic affinity sensors for the quantification of low levels of analyte. *Sens. Actuators B Chem.* **2008**, *131*, 323-332.

17. Parsa, H.; Chin, C. D.; Mongkolwisetwara, P.; Lee, B. W.; Wang, J. J.; Sia, S. K., Effect of volume- and time-based constraints on capture of analytes in microfluidic heterogeneous immunoassays. *Lab on a Chip* **2008**, *8*, 2062-2070.

18. Fu, E.; Nelson, K. E.; Ramsey, S. A.; Foley, J. O.; Helton, K.; Yager, P., Modeling of a competitive microfluidic heterogeneous immunoassay: Sensitivity of the assay response to varying system parameters. *Anal. Chem.* **2009**, *81*, 3407-3413.

19. Yang, C.-K.; Chang, J.-S.; Chao, S. D.; Wu, K.-C., Effects of diffusion boundary layer on reaction kinetics of immunoassay in a biosensor. *J. Appl. Phys.* **2008**, *103*, 084702.

20. Eddings, M. A. *Expanding the Capabilities of Surface Plasmon Resonance microscopy Using Three-Dimensional Microfluidic Platforms.* University of Utah: 2009.

21. Liu, J.; Eddings, M. A.; Miles, A. R.; Bukasov, R.; Gale, B. K.; Shumaker-Parry, J. S., In situ microarray fabrication and analysis using a microfluidic flow cell array integrated with surface plasmon resonance microscopy. *Anal. Chem.* **2009**, *81*, 4296-4301.

22. Eddings, M. A.; Miles, A. R.; Eckman, J. W.; Kim, J.; Rich, R. L.; Gale, B. K.; Myszka, D. G., Improved continuous-flow print head for micro-array deposition. *Anal. Biochem.* **2008**, *382*, 55-59.

23. Shumaker-Parry, J. S.; Campbell, C. T., Quantitative methods for spatially resolved adsorption/desorption measurements in real time by surface plasmon resonance microscopy. *Anal. Chem.* **2004**, *76*, 907-917.

24. Jung, L. S.; Nelson, K. E.; Stayton, P. S.; Campbell, C. T., Binding and dissociation kinetics of wild-type and mutant streptavidins on mixed biotin-containing alkylthiolate monolayers. *Langmuir* **2000**, *16*, 9421-9432.

25. Larsson, C.; Rodahl, M.; Hook, F., Characterization of DNA immobilization and subsequent hybridization on a 2D arrangement of streptavidin on a biotin-modified lipid bilayer supported on SiO2. *Anal. Chem.* **2003**, *75*, 5080-5087.

26. Zhao, S.; Walker, D. S.; Reichert, W. M., Cooperativity in the binding of avidin to biotin-lipid-doped Langmuir-Blodgett films. *Langmuir* **1993**, *9*, 3166-3173.

27. Moran-Mirabal, J. M.; Edel, J. B.; Meyer, G. D.; Throckmorton, D.; Singh, A. K.; Craighead, H. G., Micrometer-sized supported lipid bilayer arrays for bacterial toxin binding studies through total internal reflection fluorescence microscopy. *Biophys. J.* **2005**, *89*, 296-305.

28. Tilton, R. D.; Gast, A. P.; Robertson, C. R., Surface diffusion of interacting proteins. Effect of concentration on the lateral mobility of adsorbed bovine serum albumin. *Biophys. J.* **1990**, *58*, 1321-1326.

29. Natarajan, S.; Hatch, A.; Myszka, D. G.; Gale, B. K., Optimal conditions for protein array deposition using continuous flow. *Anal. Chem.* **2008**, *80*, 8561.

30. Nelson, K. E.; Gamble, L.; Jung, L. S.; Boeckl, M. S.; Naeemi, E.; Golledge, S. L.; Sasaki, T.; Castner, D. G.; Campbell, C. T.; Stayton, P. S., Surface characterization of

mixed self-assembled monolayers designed for streptavidin immobilization. *Langmuir* **2001**, *17*, 2807-2816.

31. Tokuhisa, H.; Liu, J. A.; Omori, K.; Kanesato, M.; Hiratani, K.; Baker, L. A., Efficient biosensor interfaces based on space-controlled self-assembled monolayers. *Langmuir* **2008**, *25*, 1633-1637.

32. Kim, H.; Noh, J.; Hara, M.; Lee, H., Characterization of mixed self-assembled monolayers for immobilization of streptavidin using chemical force microscopy. *Ultramicroscopy* **2008**, *108*, 1140-1143.

33. Seifert, M.; Rinke, M. T.; Galla, H.-J., Characterization of streptavidin binding to biotinylated, binary self-assembled thiol monolayers - Influence of component ratio and solvent. *Langmuir* **2010**, *26*, 6386-6393.

34. Schwartz, D. K., Mechanisms and kinetics of self-assembled monolayer formation. *Annu. Rev. Phys. Chem.* **2001**, *52*, 107-137.

35. Li, L.; Chen, S.; Jiang, S., Protein adsorption on alkanethiolate self-assembled monolayers: Nanoscale surface structural and chemical effects. *Langmuir* **2003**, *19*, 2974-2982.

36. Rabe, M.; Verdes, D.; Seeger, S., Understanding protein adsorption phenomena at solid surfaces. *Adv. Colloid Interface Sci.* **2011**, *162*, 87-106.

37. Owaku, K.; Goto, M.; Ikariyama, Y.; Aizawa, M., Protein A langmuir-blodgett film for antibody immobilization and its use in optical immunosensing. *Anal. Chem.* **1995,** *67*, 1613-1616.

38. Babacan, S.; Pivarnik, P.; Letcher, S.; Rand, A. G., Evaluation of antibody immobilization methods for piezoelectric biosensor application. *Biosens. Bioelectron.* **2000,** *15*, 615-621.

39. Yang, L.; Biswas, M. E.; Chen, P., Study of binding between protein A and immunoglobulin G using a surface tension probe. *Biophys. J.* **2003,** *84*, 509-522.

40. Nico J. de Mol, M. J. E. F., *Surface Plasmon Resonance Methods and Protocols*. Humana Press: 2010.

Figure 3.1. 2D schematic representation of a single micro flow cell in the MFCA-SPRM system. The dimensions of the flow cell and prism are not shown to scale.

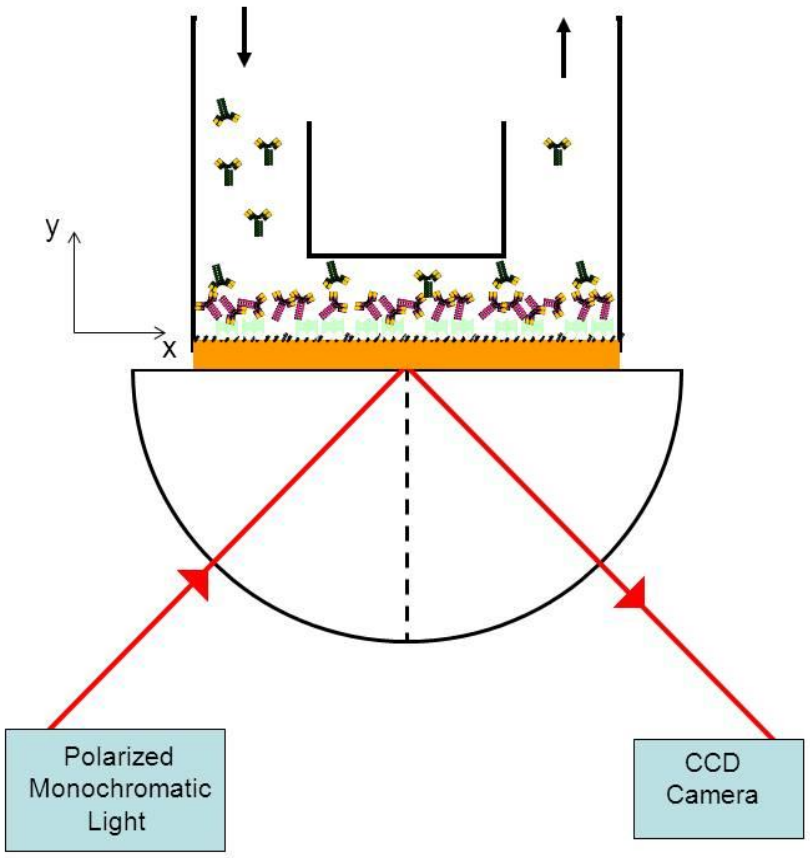
y
x
Polarized
Monochromatic
Light
CCD
Camera

Figure 3.2. 2D mesh of MFCA modeling region. The length of the reaction surface at the bottom is 650 μm; the widths of the inlet and the outlet are 150 μm, and the height in the center of the flow cell is 100 μm.

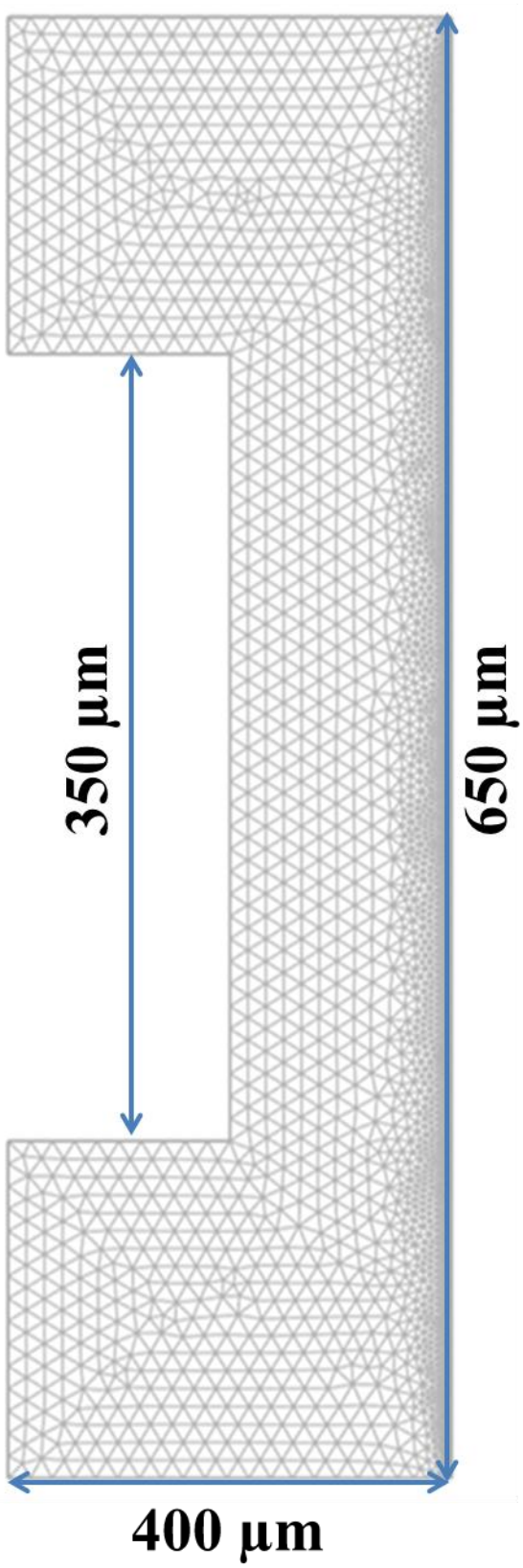
350 µm
650 µm
400 µm

Figure 3.3. Profile of the analyte bulk concentration within the MFCA at time of t = 5 s.

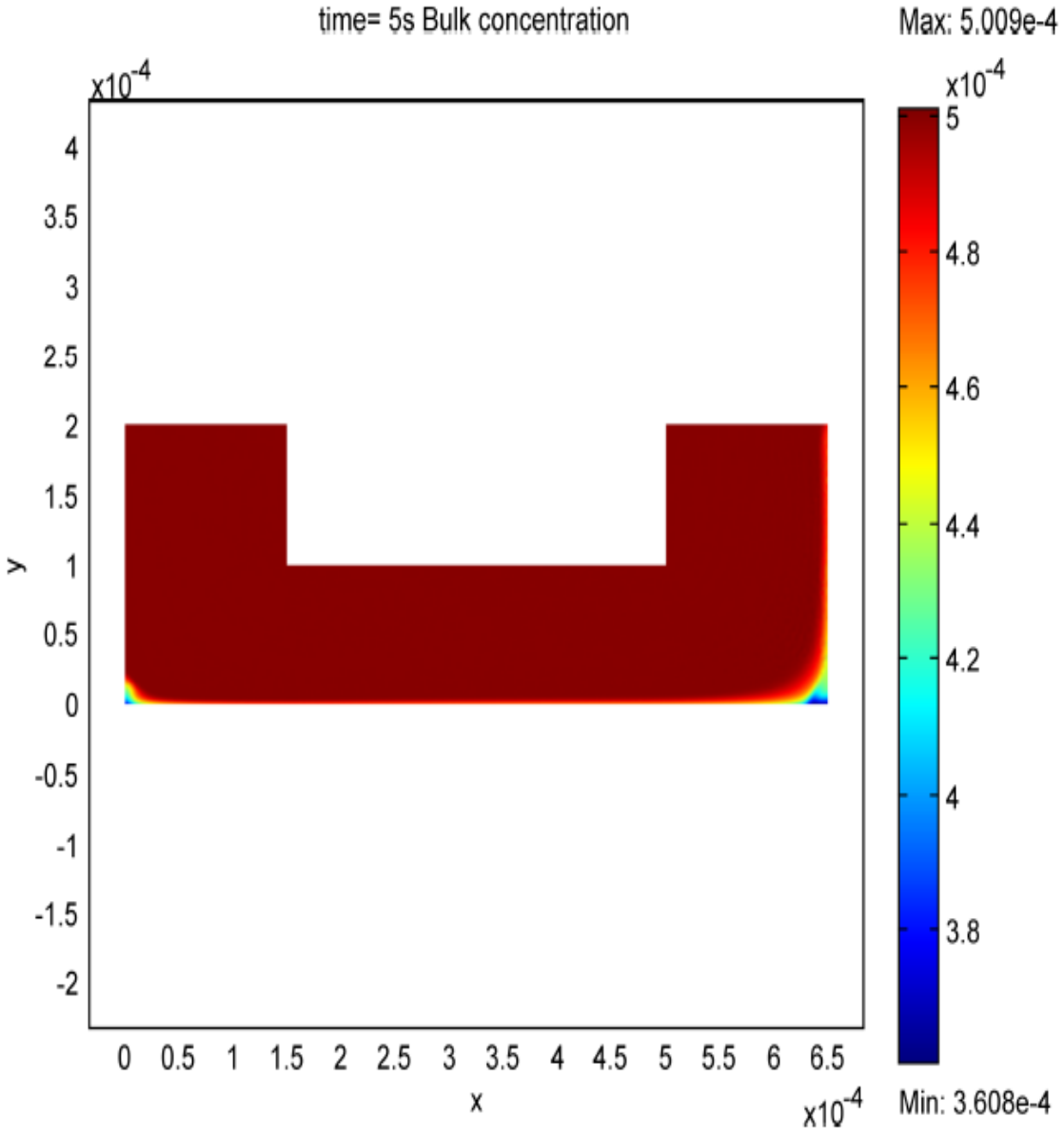
time= 5s Bulk concentration
Max: 5.009e-4
x10^-4
4
3.5
3
2.5
2
1.5
1
0.5
0
-0.5
-1
-1.5
-2
y
0 0.5 1 1.5 2 2.5 3 3.5 4 4.5 5 5.5 6 6.5
x
x10^-4
x10^-4
5
4.8
4.6
4.4
4.2
4
3.8
Min: 3.608e-4

Figure 3.4. A representative plot of surface concentration of binding products (c_s) versus reaction time.

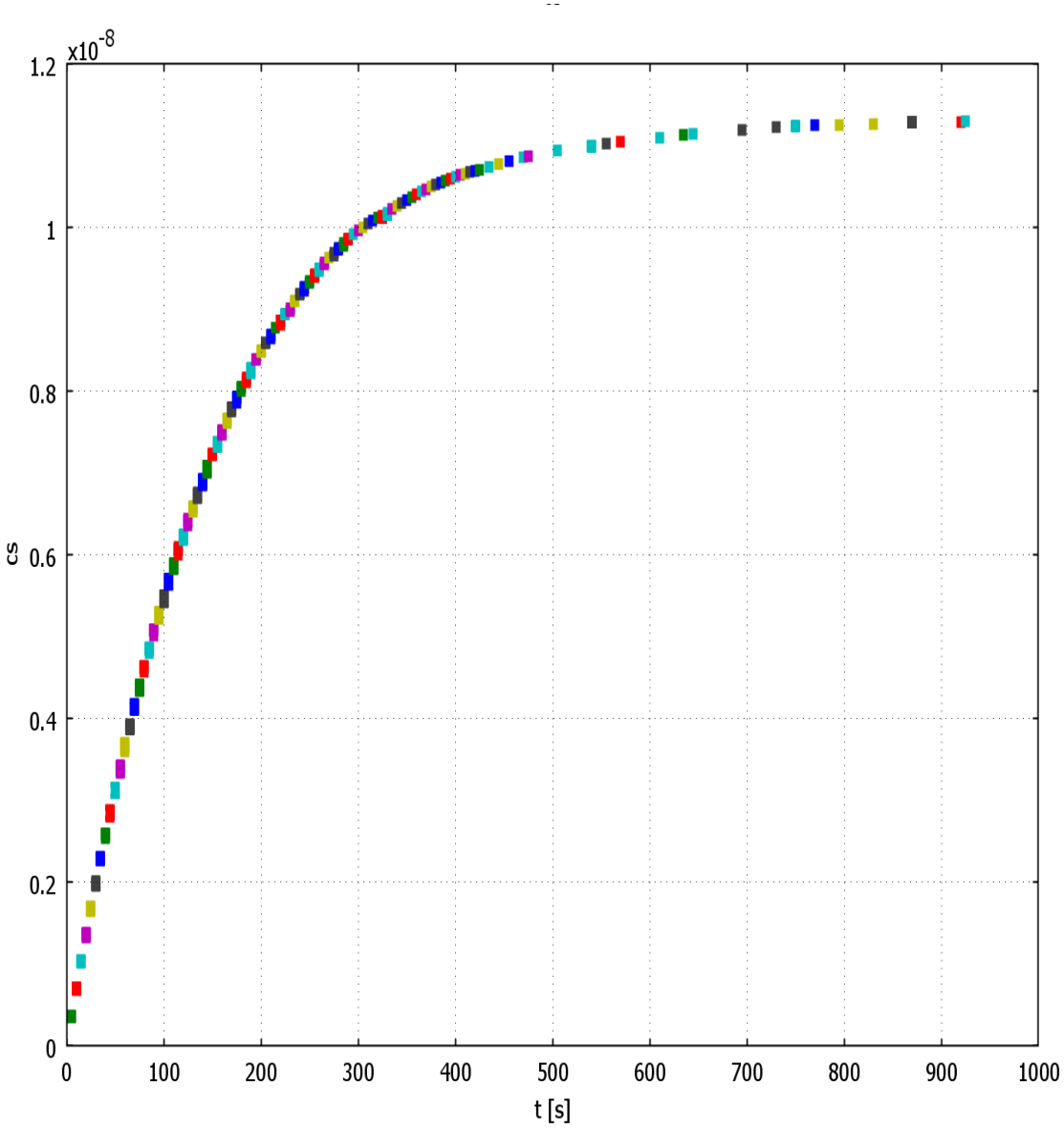
x10^-8
1.2
1
0.8
0.6
0.4
0.2
0
cs
0
100
200
300
400
500
600
700
800
900
1000
t [s]

Figure 3.5. Kinetics of surface binding products simulated by using two sets of binding affinity constants and various bulk concentrations of analytes. The parameters are listed in Table 3.1.The solid lines represent high binding affinity (k_{on} and k_{off} are 10^4 $(mol \cdot s/L)^{-1}$ and 10^{-4} s^{-1}) dashed lines are lower binding affinity (k_{on} and k_{off} are 10^3 $(mol \cdot s/L)^{-1}$ and 10^{-3} s^{-1}).

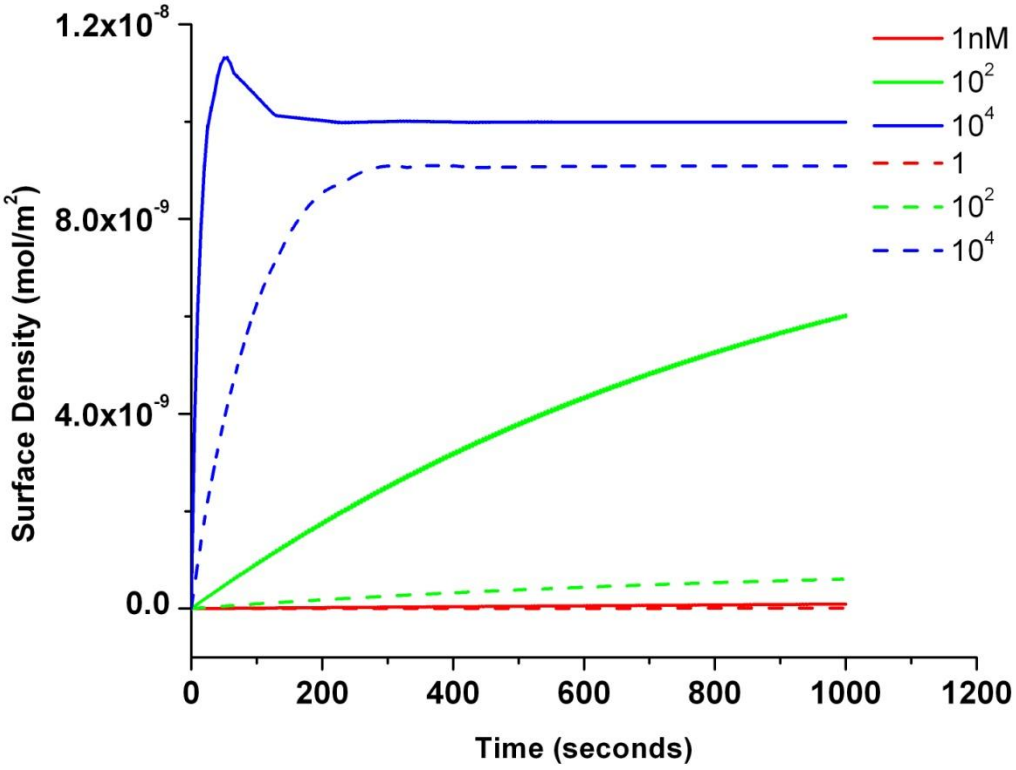
1.2x10-8
8.0x10-9
4.0x10-9
0.0
Surface Density (mol/m2)
0
200
400
600
800
1000
1200
Time (seconds)
1nM
10^2
10^4
1
10^2
10^4

Figure 3.6. Kinetics of surface binding products simulated by using two flow rates. (a) 1.47×10^{-1} m/s (534.4 µL/min), (b) 4.6×10^{-3}m/s (16.7 µL/min). The bulk concentration of analyte ranges between 0.1 nM to 1 µM. The binding affinities are k_{on} and k_{off} are 1.1×10^{4} $(\text{mol}\bullet\text{s/L})^{-1}$ and 10^{-4} s^{-1}, respectively.

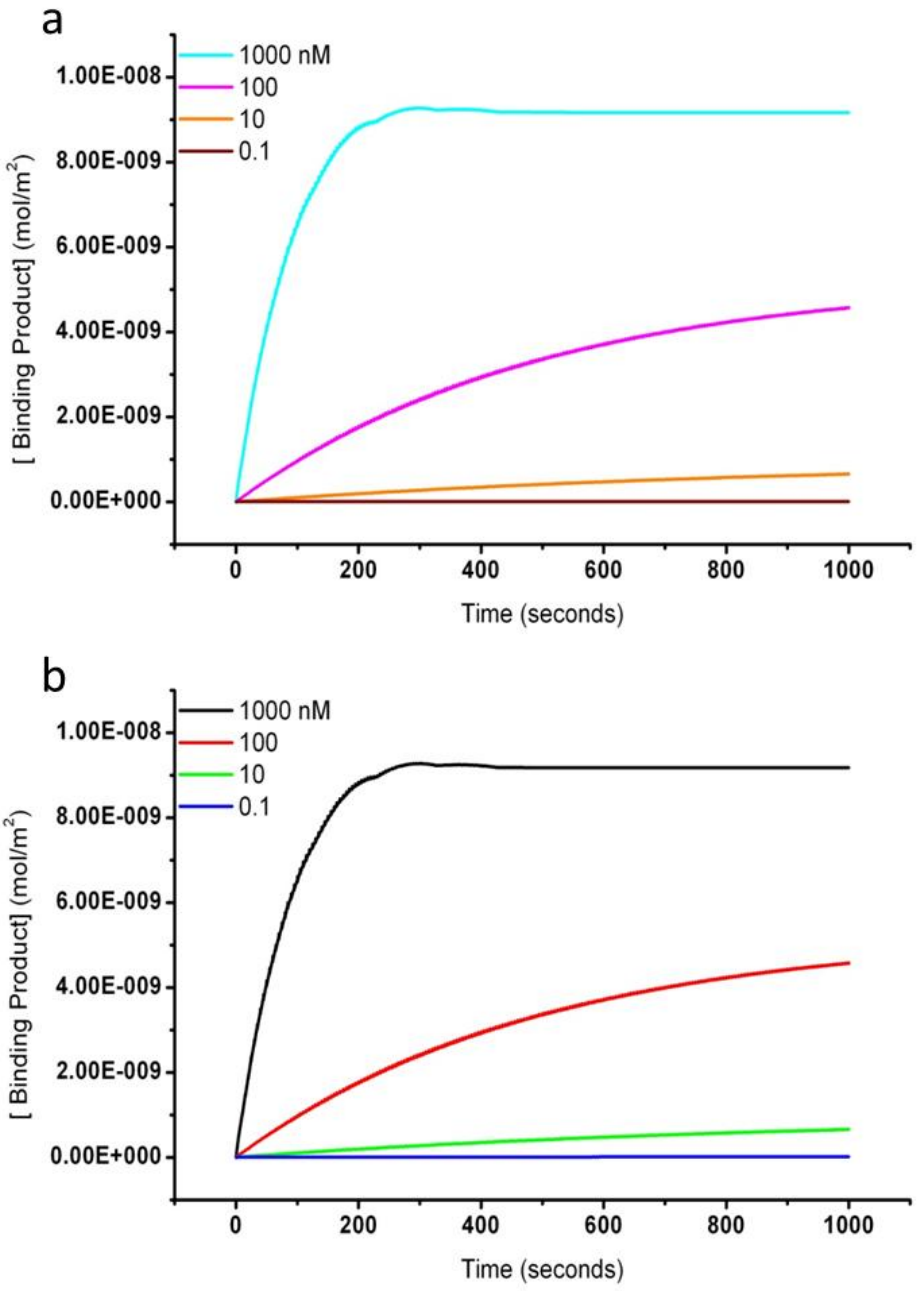
a
1000 nM
100
10
0.1
1.00E-008
8.00E-009
6.00E-009
4.00E-009
2.00E-009
0.00E+000
[Binding Product] (mol/m2)
0
200
400
600
800
1000
Time (seconds)
b
1000 nM
100
10
0.1
1.00E-008
8.00E-009
6.00E-009
4.00E-009
2.00E-009
0.00E+000
[Binding Product] (mol/m2)
0
200
400
600
800
1000
Time (seconds)

Figure 3.7. Kinetics of the formation of surface binding products simulated by using two values of surface density. The values are 1.33×10^{-8} and 2.66×10^{-8} mol/m^2. The concentration of analyte is in the range of 0.11 to 18.5 μM. The dashed lines represent a high density of binding sites (2.66×10^{-8} mol/m^2) and the solid lines are for a lower density (1.33×10^{-8} mol/m^2).

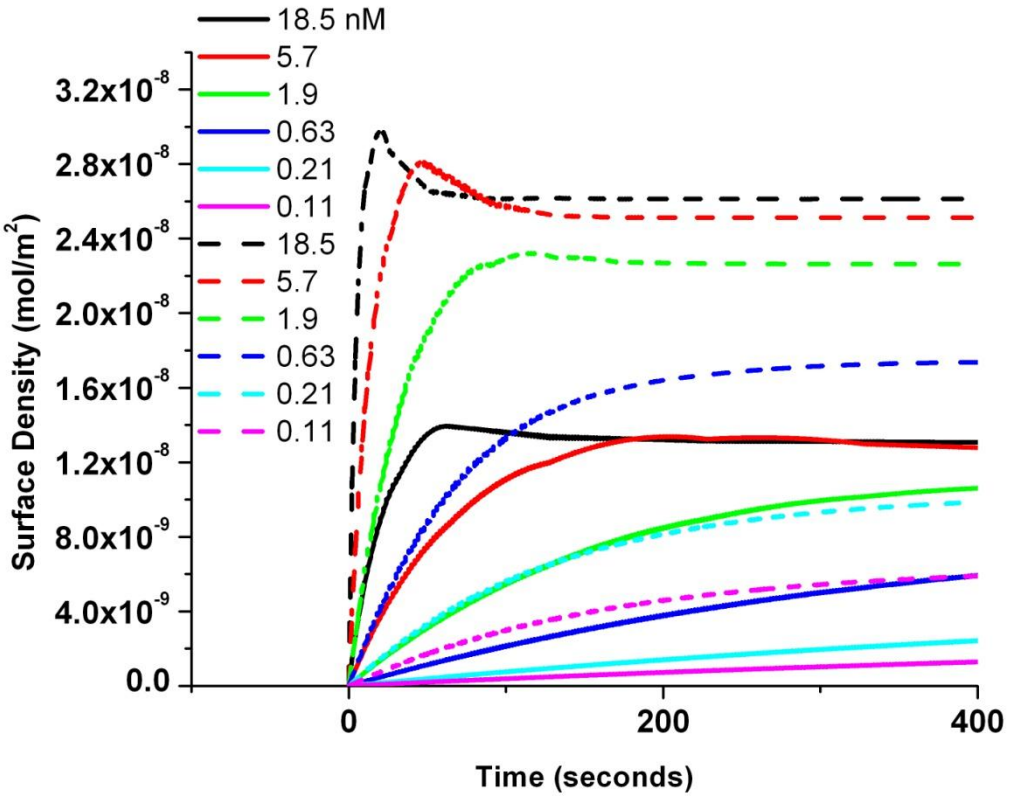
18.5 nM
5.7
1.9
0.63
0.21
0.11
18.5
5.7
1.9
0.63
0.21
0.11
Surface Density (mol/m2)
3.2x10-8
2.8x10-8
2.4x10-8
2.0x10-8
1.6x10-8
1.2x10-8
8.0x10-9
4.0x10-9
0.0
0
200
400
Time (seconds)

Figure 3.8. Results from experiments and simulations of biotin-streptavidin binding interactions based on the SPRM-MFCA. (a) Real-time SPR response of streptavidin adsorption on a biotin SAM surface measured at flow rate of 33.4 μL/min. (b) Equilibrium isotherm of biotin-streptavidin interaction summarized from the SPR curves in (a). (c) Kinetics of streptavidin adsorption calculated by simulation with parameters listed in Table 3.4. (d) A comparison of the average fractional saturation of the reaction surface measured by SPR and simulations when streptavidin adsorption reached equilibrium at time t = 500 s.

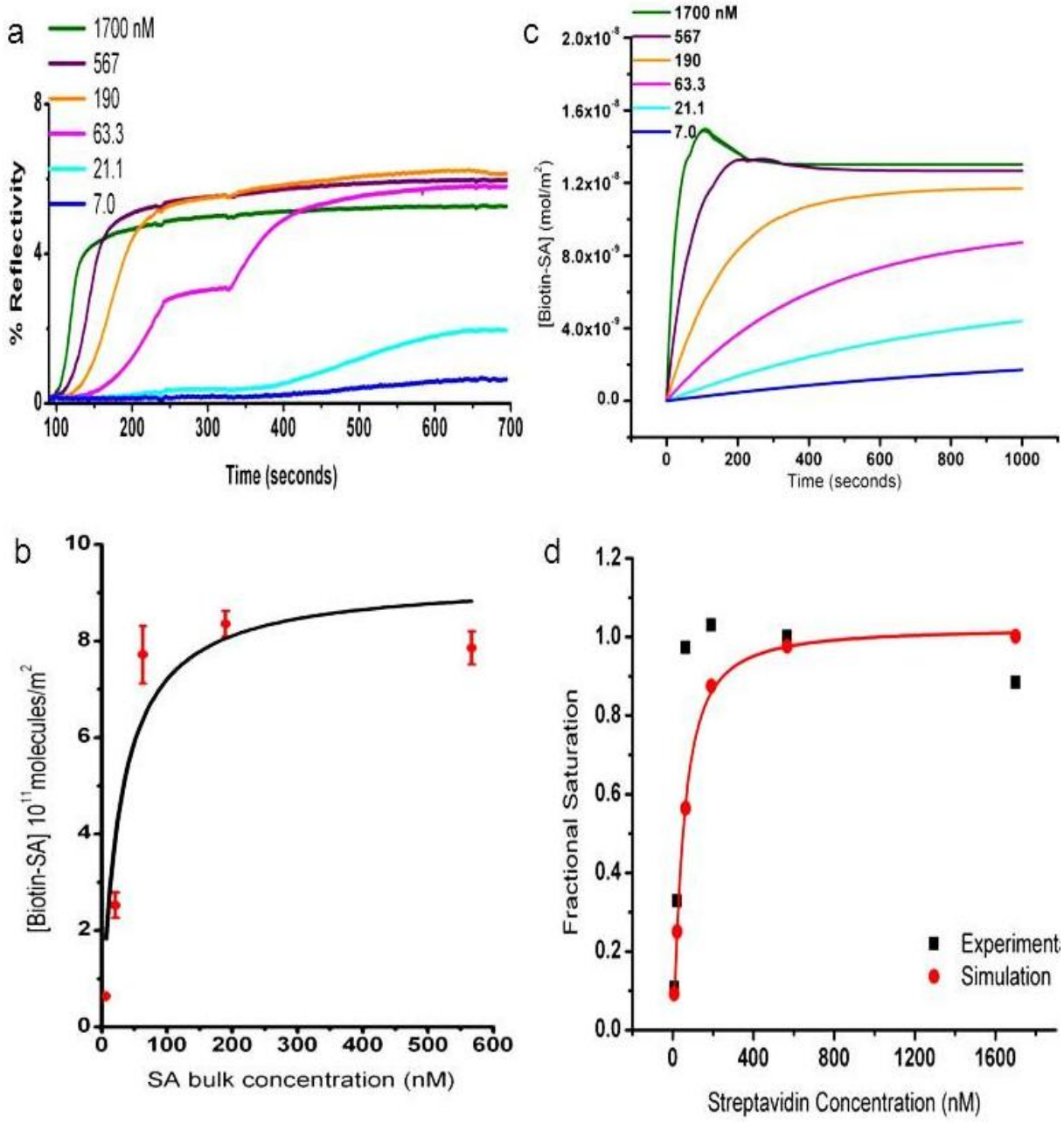
a
1700 nM
567
190
63.3
21.1
7.0
% Reflectivity
Time (seconds)
c
1700 nM
567
190
63.3
21.1
7.0
[Biotin-SA] (mol/m²)
Time (seconds)
b
[Biotin-SA] 10¹¹ molecules/m²
SA bulk concentration (nM)
d
Fractional Saturation
Experiment
Simulation
Streptavidin Concentration (nM)

Figure 3.9. Results from experiments and simulations of Dac-IgG binding interaction based on the SPRM-MFCA. (a) Real-time SPR response of IgG adsorption on a Daclizumab surface at a flow rate of 133.6 µL/min. (b) Equilibrium isotherm of Dac-IgG interaction summarized from the SPR curves in (a). (c) Kinetics of IgG adsorption calculated by simulation with parameters listed in Table 3.4. (d) A comparison of the fractional saturation of reaction surface measured by SPR and simulations when IgG adsorption reached equilibrium at time t = 80 s.

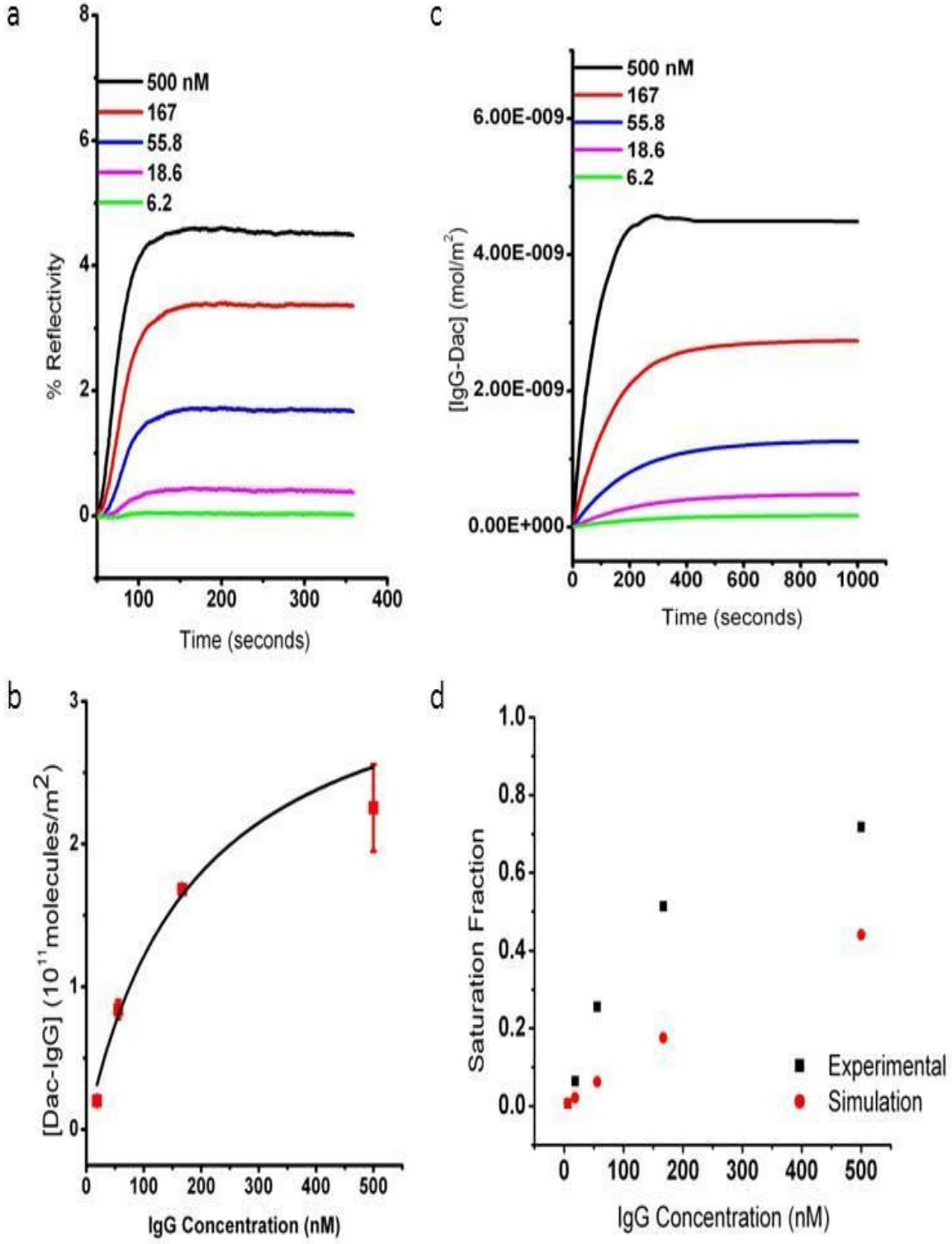
a
% Reflectivity
Time (seconds)
500 nM
167
55.8
18.6
6.2
c
[IgG-Dac] (mol/m^2)
Time (seconds)
6.00E-009
4.00E-009
2.00E-009
0.00E+000
b
[Dac-IgG] (10^{11}molecules/m^2)
IgG Concentration (nM)
d
Saturation Fraction
IgG Concentration (nM)
Experimental
Simulation

Figure 3.10. SPR real-time curves of various biotin-streptavidin interactions. Six streptavidin concentrations of 7.0, 21.1, 63.3, 190, 567 and 1700 nM were tested at four flow rates of 33.4, 133.6, 267.2 and 534.4 µL/min with a fixed sample volume of 180 µL.

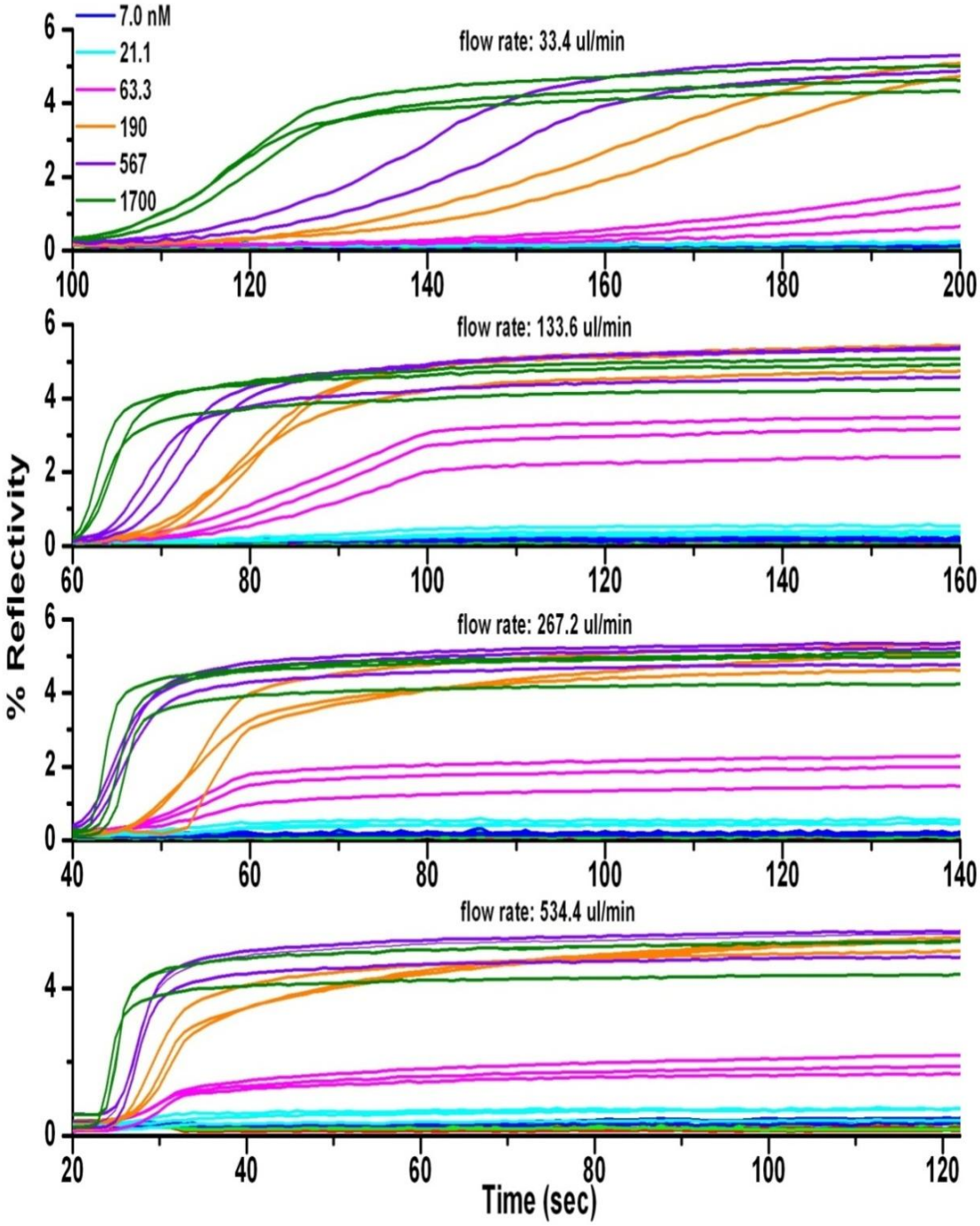
7.0 nM
21.1
63.3
190
567
1700
flow rate: 33.4 ul/min
flow rate: 133.6 ul/min
flow rate: 267.2 ul/min
flow rate: 534.4 ul/min
% Reflectivity
Time (sec)

Figure 3.11. SPR signal of biotin-streptavidin interaction at reaction time t = 20 s versus the flow rate to the one-third power. The data were fitted into a straight line for streptavidin concentration of 6.3, 190, 567 and 1700 nM.

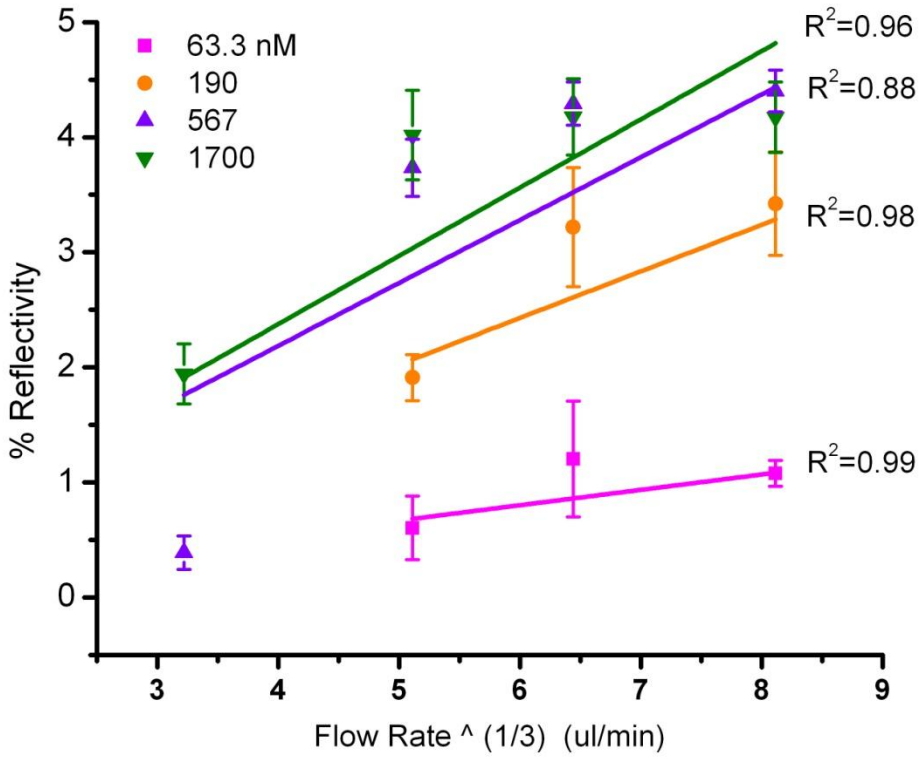
63.3 nM
190
567
1700
R2=0.96
R2=0.88
R2=0.98
R2=0.99
% Reflectivity
Flow Rate ^ (1/3) (ul/min)
0
1
2
3
4
5
3
4
5
6
7
8
9

Figure 3.12. Equilibrium isotherms of biotin-streptavidin interactions at flow rates of 33.4, 133.6, 267.2 and 534.4 µL/min. The solid lines are fits of the data using an extended Langmuir model (n = 2).

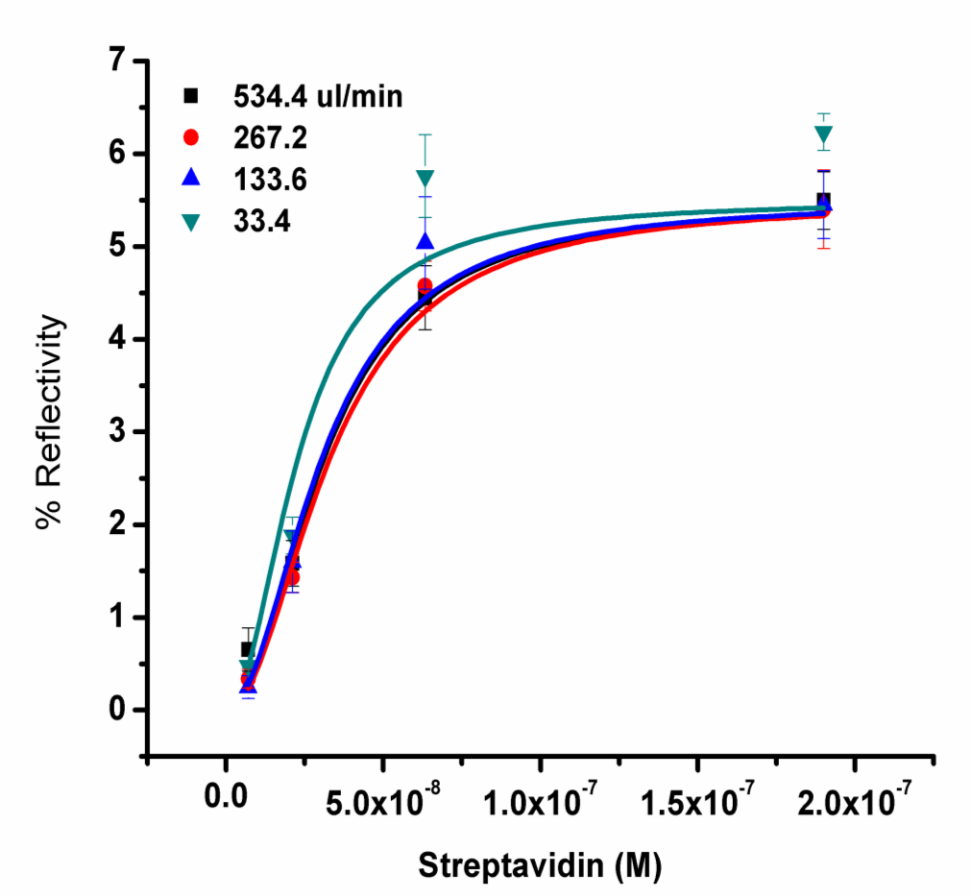
534.4 ul/min
267.2
133.6
33.4
% Reflectivity
0
1
2
3
4
5
6
7
0.0
5.0x10-8
1.0x10-7
1.5x10-7
2.0x10-7
Streptavidin (M)

Figure 3.13. Experimental results of streptavidin adsorption on various SAMs surfaces of *in situ* functionalized by the SPRM-MFCA. (a) Real-time SPR response of streptavidin adsorption on a Daclizumab surface at a flow rate of 16.7 μL/min. (b) The SPR signal of streptavidin adsorption versus BAT percentage in thiol solutions used in the corresponding SAMs surface.

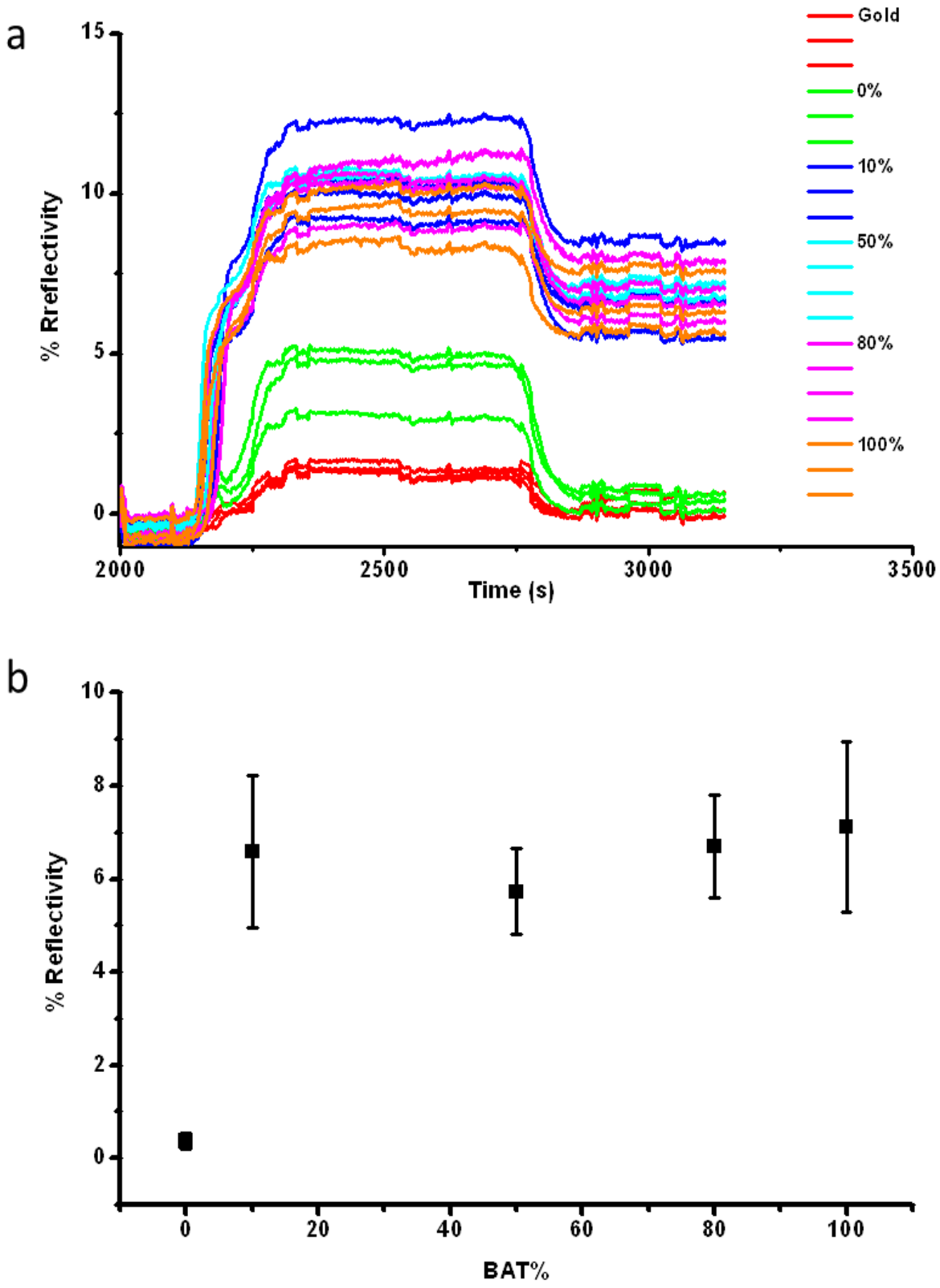
a
% Rreflectivity
Time (s)
Gold
0%
10%
50%
80%
100%
b
% Reflectivity
BAT%

Figure 3.14. XPS spectra of the N (1s) region for all of the mixed SAM surfaces. (a) XPS spectra of the N (1s) region for all of the mixed SAM surfaces. (b) The peak area ratios of the N (1s) to the Au (4f).

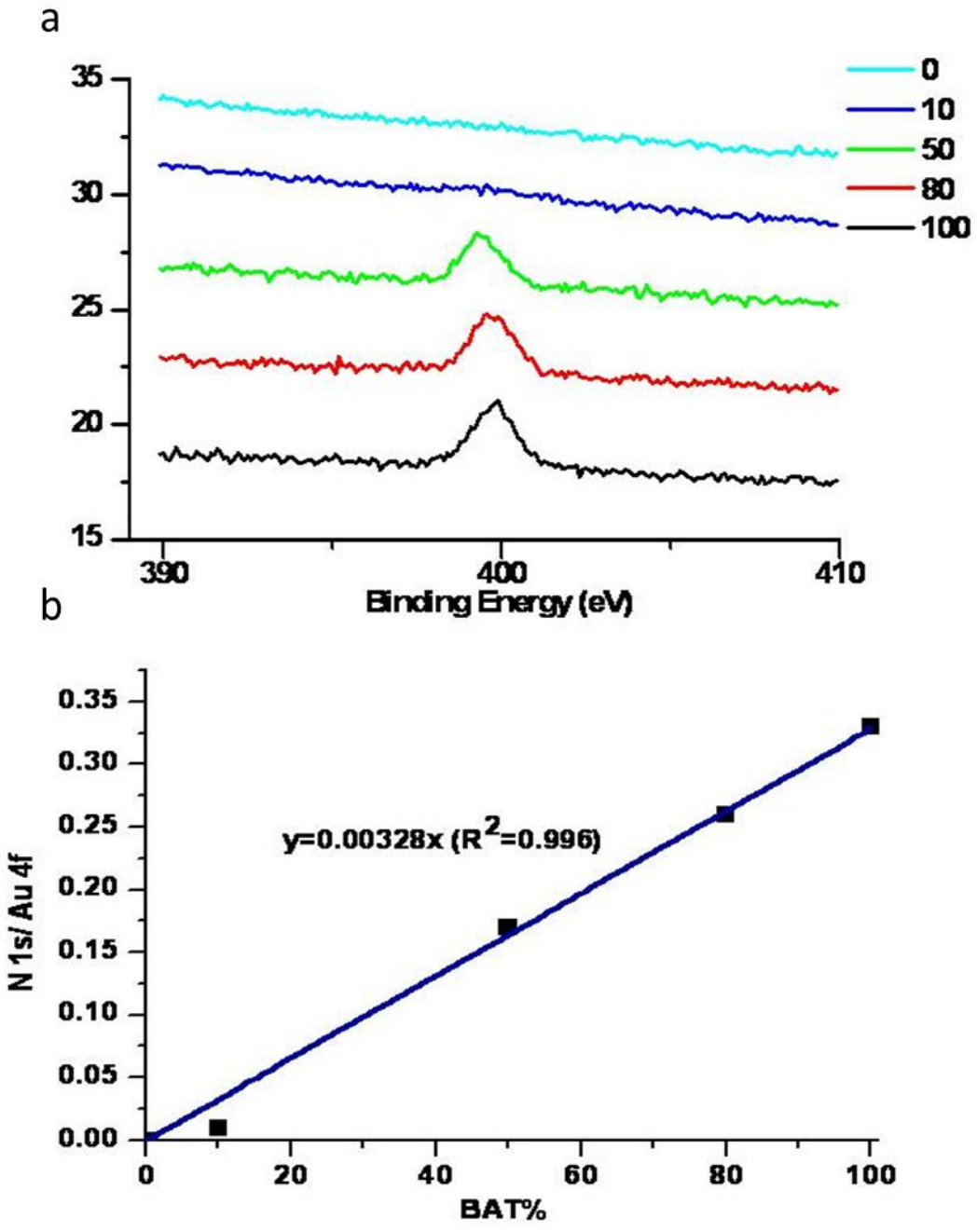
a
35
30
25
20
15
390
400
410
Binding Energy (eV)
0
10
50
80
100
b
0.35
0.30
0.25
0.20
0.15
0.10
0.05
0.00
N 1s/ Au 4f
y=0.00328x (R2=0.996)
0
20
40
60
80
100
BAT%

Figure 3.15. AFM images of gold surface deposited by electron-beam deposition and functionalized SAMs surfaces. (a) gold surface (b) SAMs surface deposited by 100% OEG. (c) SAMs surface deposited by 50% OEG and 50% BAT. (d) SAMs surface deposited by 100% BAT. The RMS roughness of (a)-(d) surfaces are 1.38, 1.43, 1.61 and 1.22 nm, respectively.

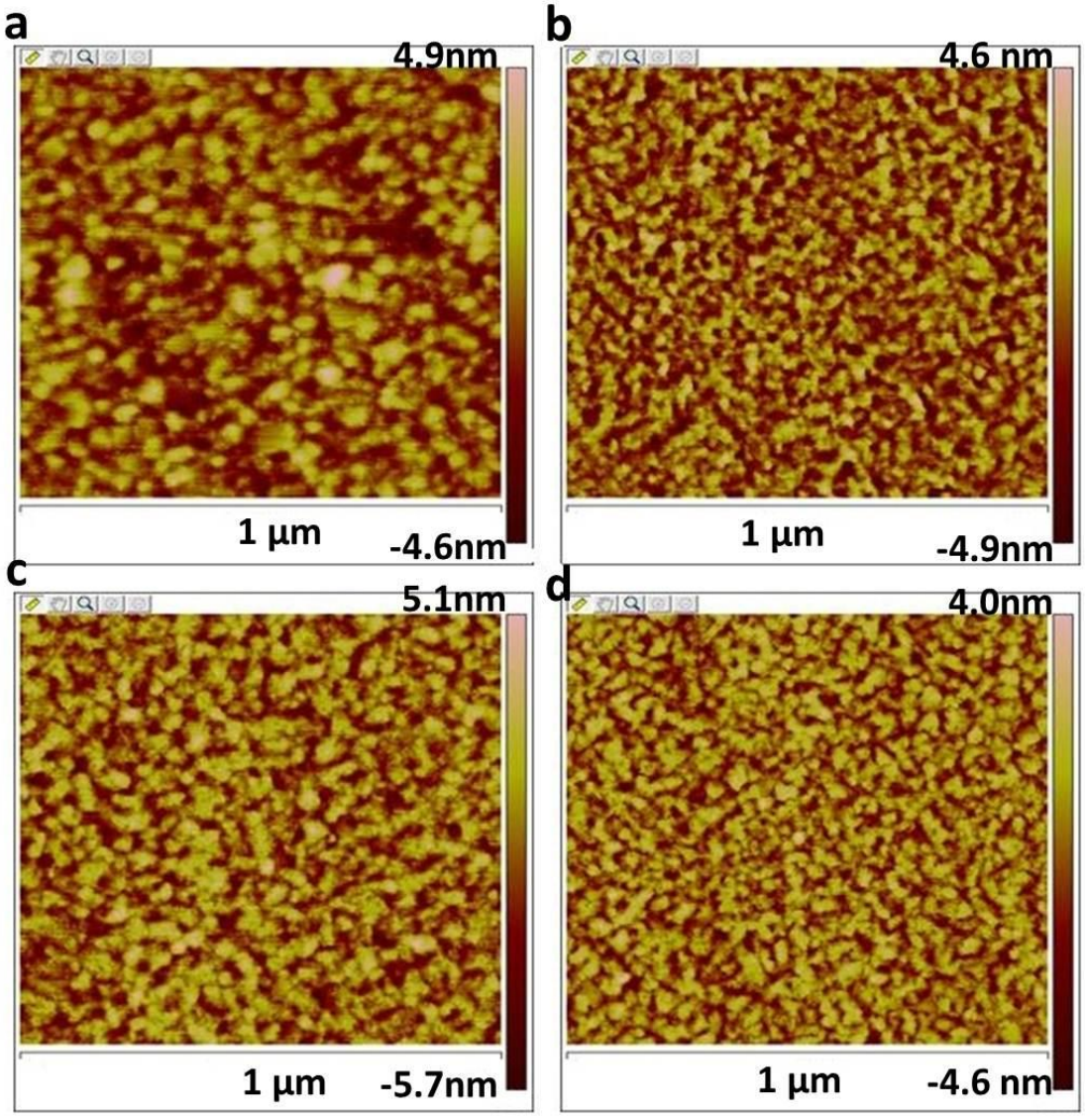
a
4.9nm
1 µm
-4.6nm
b
4.6 nm
1 µm
-4.9nm
c
5.1nm
1 µm
-5.7nm
d
4.0nm
1 µm
-4.6 nm

Figure 3.16. AFM morphology images streptavidin adsorbed on various SAMs surfaces. (a) SA on SAMs surface made by thiol solution of 10% BAT. (b) SA on SAMs surface made by thiol solution of 50% BAT. (c) SA on SAMs surface made by thiol solution of 90% BAT. (d) SA on SAMs surface made by thiol solution of 100% BAT. The RMS roughness of (a)-(d) surfaces are 1.51, 4.08, 4.05 and 4.76 nm, respectively.

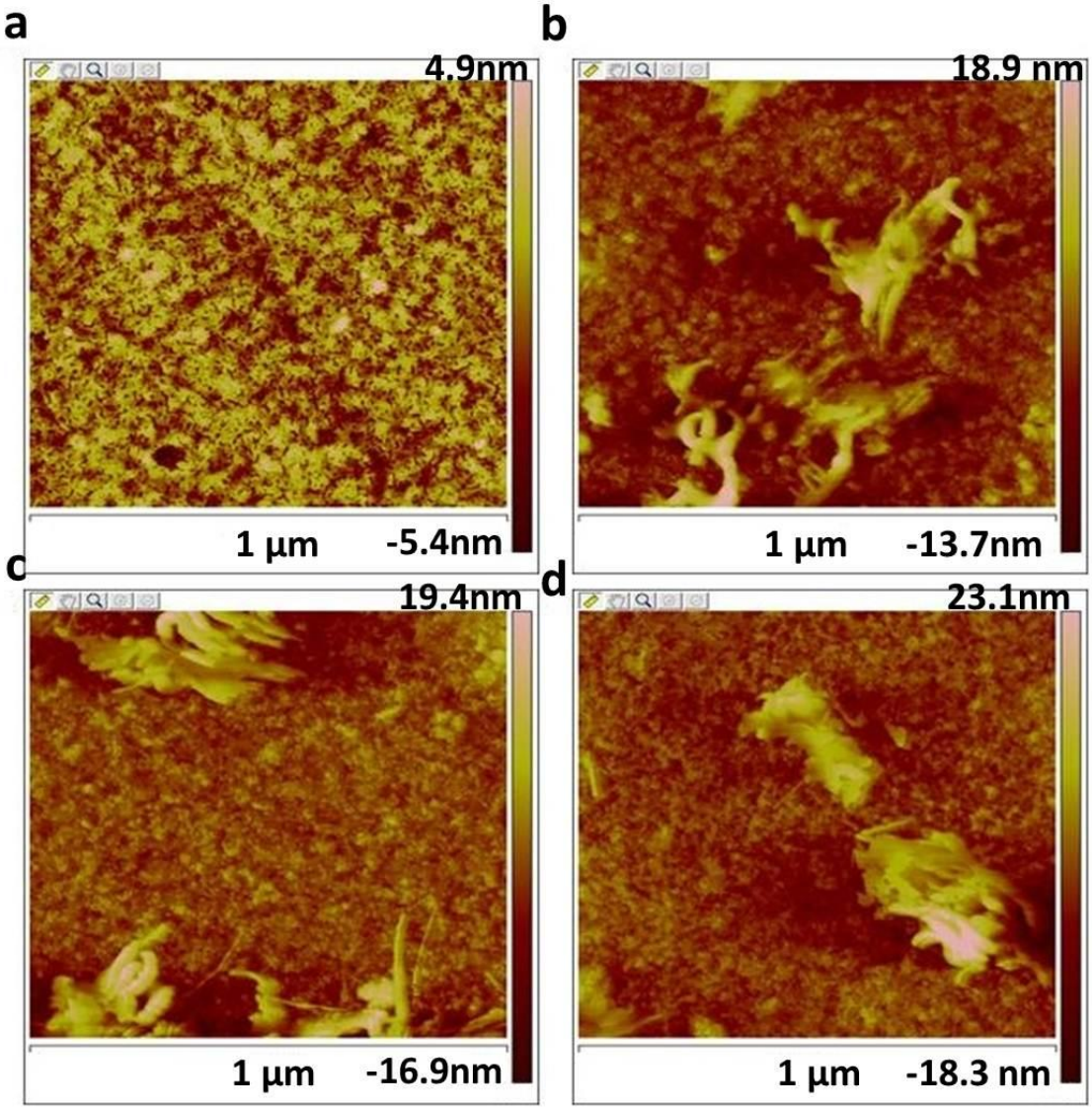
a
4.9nm
1 µm
-5.4nm
b
18.9 nm
1 µm
-13.7nm
c
19.4nm
1 µm
-16.9nm
d
23.1nm
1 µm
-18.3 nm

Figure 3.17. Results from AFM analysis of RMS roughness of SAMs surfaces and streptavidin surfaces on corresponding SAMs. The yellow bar represents surface roughness of gold and SAMs; the red one is streptavidin surface after SPR analysis.

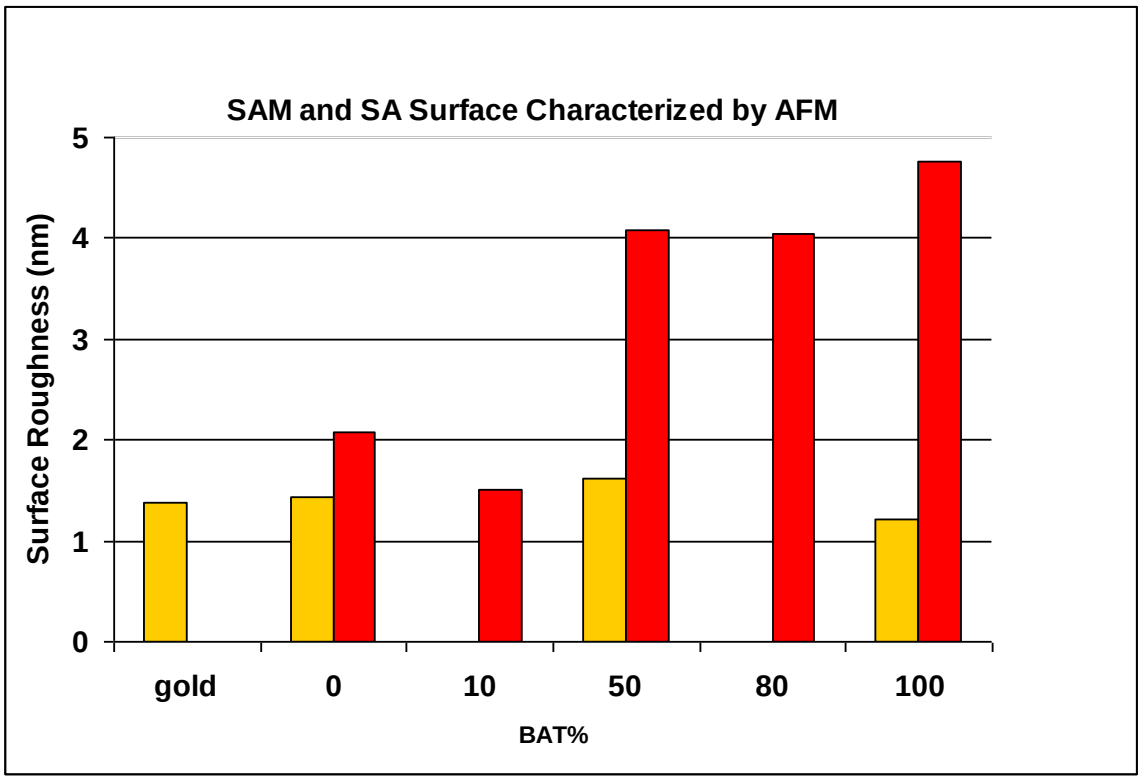
SAM and SA Surface Characterized by AFM
Surface Roughness (nm)
5
4
3
2
1
0
gold
0
10
50
80
100
BAT%

Figure 3.18. Results from experiments of protein A- IgG binding interaction based on the SPRM-MFCA. (a) SPR image of 24 flow cells filled with solutions (b) SPR real-time curves of the process of bulk refractive index change, streptavidin, protein A and IgG immobilization. Concentrations of five protein A solutions are 0.66, 1.3, 2.6, 5.3 and 10.6 nM, respectively. The concentration of IgG is 1.33 μM.

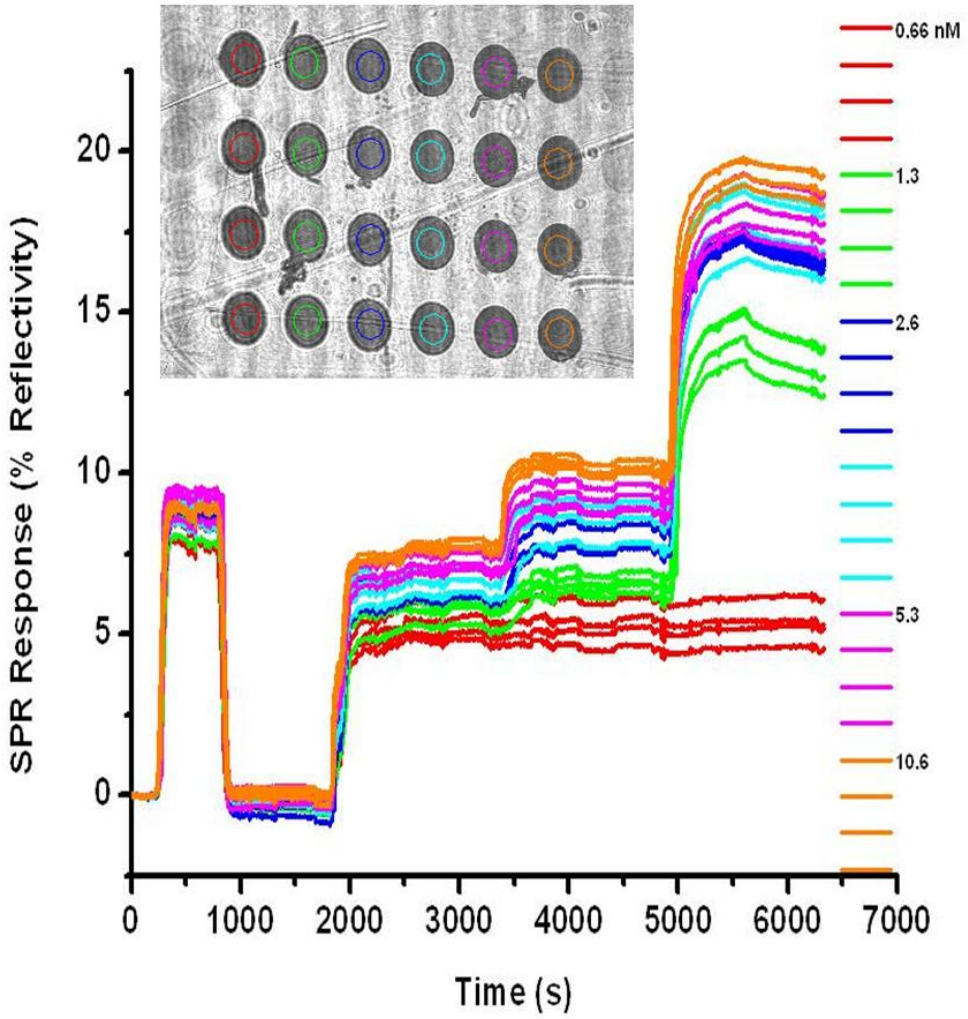
SPR Response (% Reflectivity)
Time (s)
0
5
10
15
20
0
1000
2000
3000
4000
5000
6000
7000
0.66 nM
1.3
2.6
5.3
10.6

Figure 3.19. SPR signals of IgG adsorption on protein A surface and signal ratios. (a) SPR response signal of IgG adsorption on protein A surface and the corresponding SPR signal of protein A adsorption. (b) Binding ratio of IgG/protein A versus the bulk concentration of protein A solution that creates the surface.

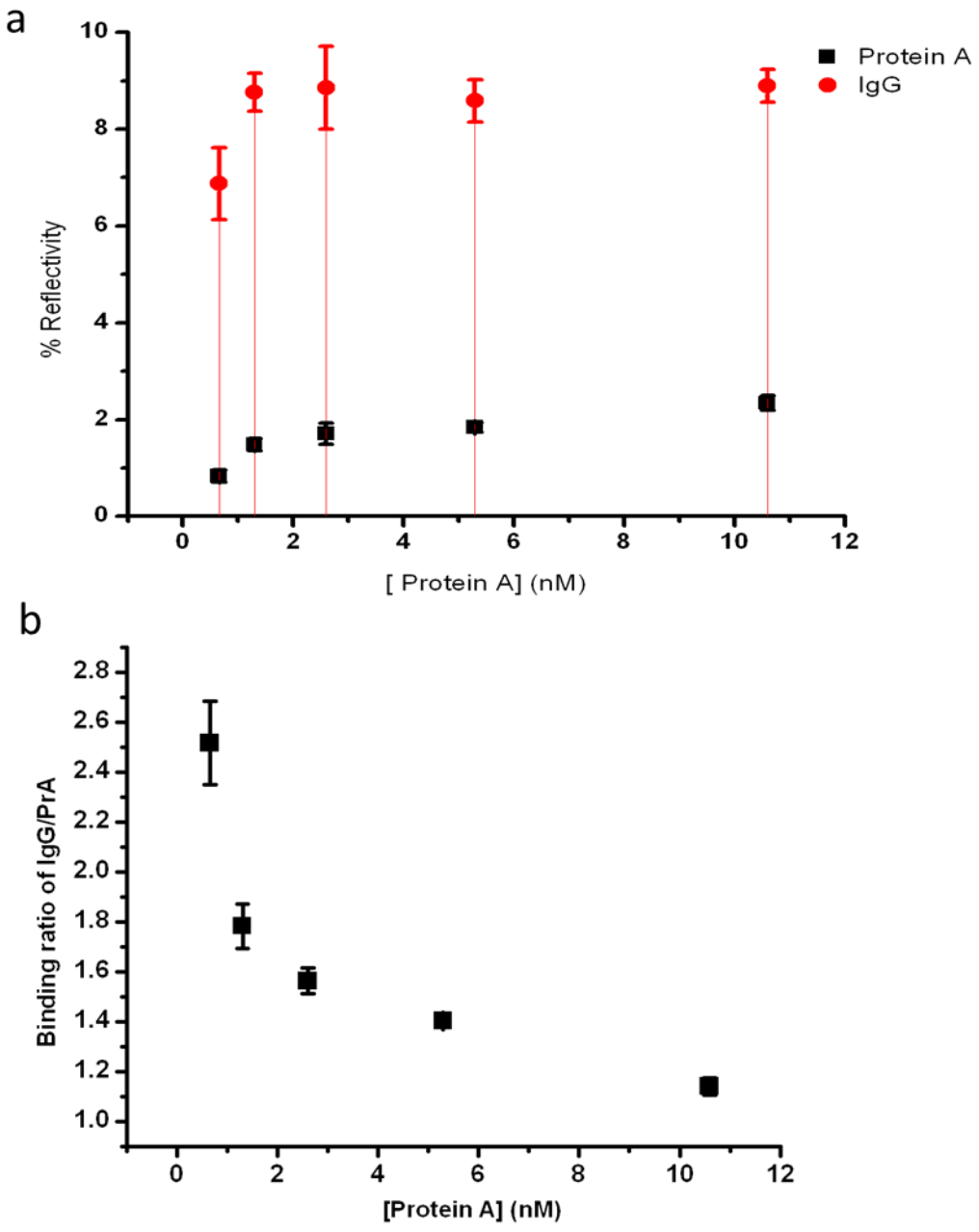
a
% Reflectivity
[Protein A] (nM)
Protein A
IgG
b
Binding ratio of IgG/PrA
[Protein A] (nM)

Figure 3.20. Schematic of the light path in the SPRM and the shift of light incident angles. (a) Schematic of the light path in the SPRM system. (b) Shift of light incident angles at the back of SPR sensing surface after light traveling through the hemi-spherical prism. For example, if the refractive index of prism (n) is 1.80, the diameter of the prism (D) is 8 cm, the diameter of light beam (d) is 1 cm, and the light incident angle of beam in the center is 55^{o}, the angles of 1-7 in the figure are calculated to be 7.5, 3.72, 11.22, 6.2, 53.7, 47.5, and 56.3^{o}, respectively. The light incident angle at the left edge of the beam is 56.3^{o} while at the right edge is 53.7^{o}.

a

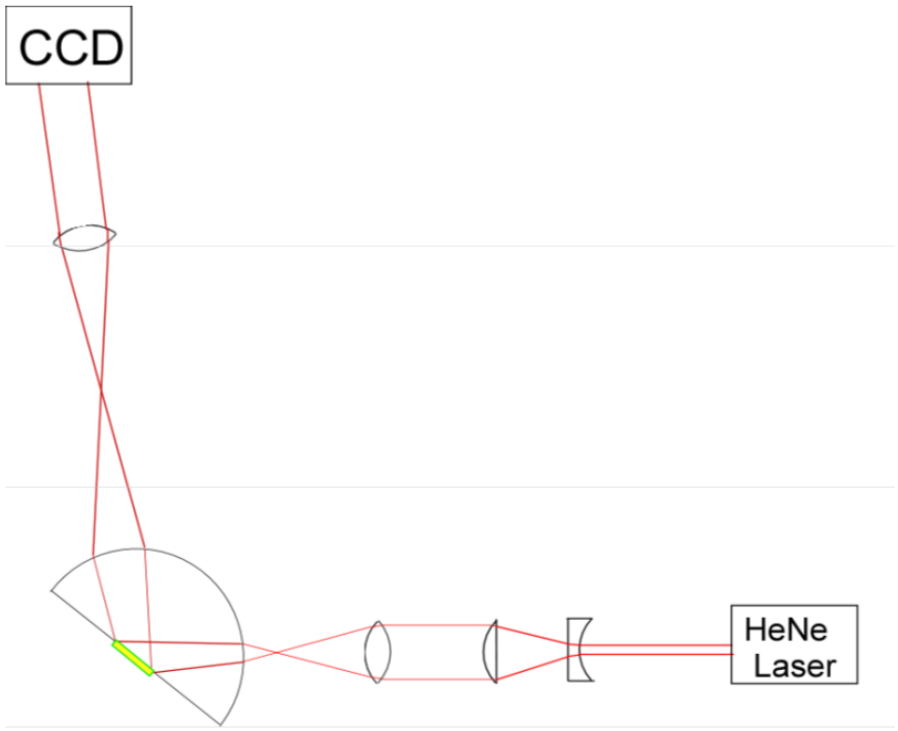

b

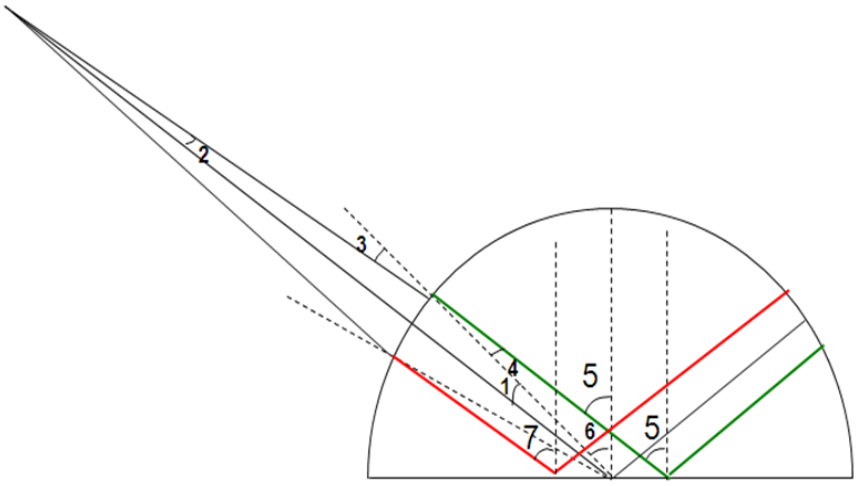

Figure 3.21. Results from experiments of streptavidin and Daclizumab adsorption in 24 flow cells of MFCA. (a) SPR image of 24 flow cells and their detection windows. (b) SPR real-time curves of the process of streptavidin and Daclizuamb immobilization. The concentration of streptavidin solution is 1.85 μM. The concentration of Daclizumab is 0.7 μM.

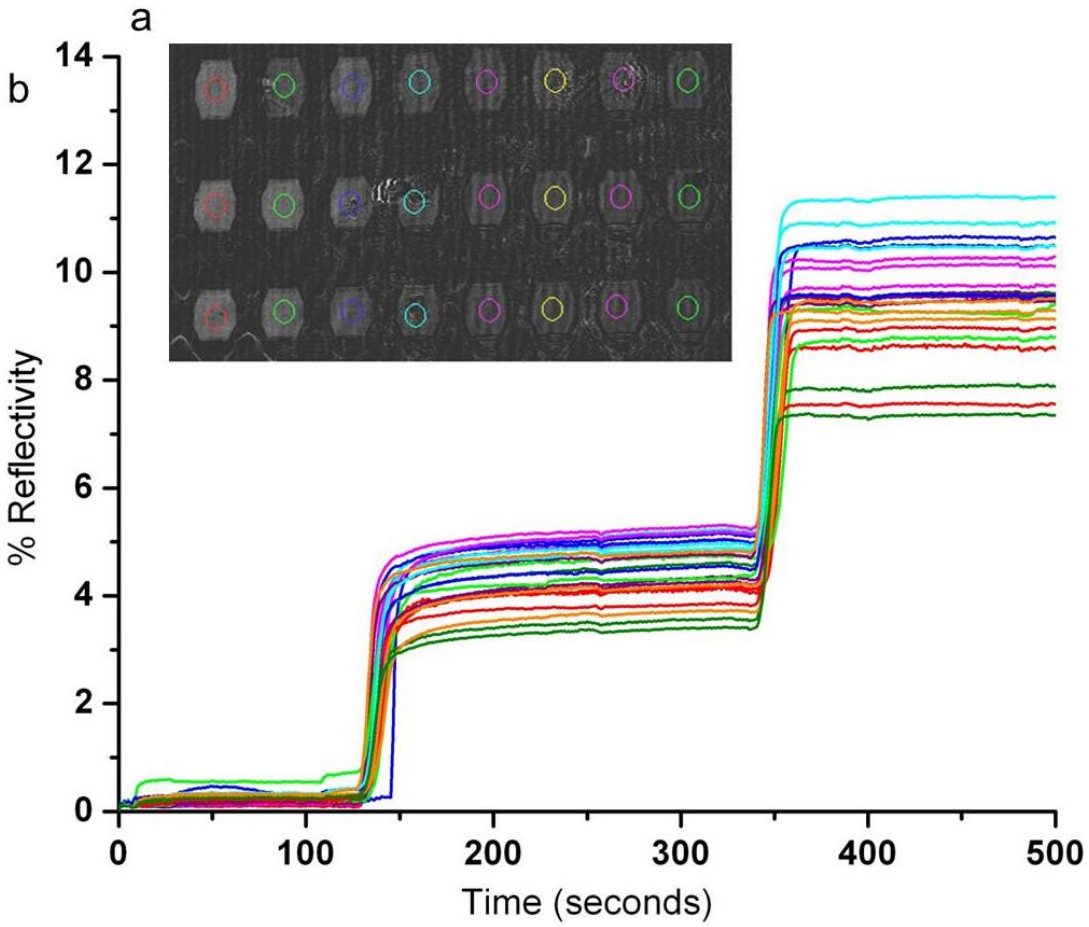
a
b
% Reflectivity
Time (seconds)
0
2
4
6
8
10
12
14
0
100
200
300
400
500

Table 3.1. Parameters used in the modeling to investigate the effect of binding affinity and bulk concentration of analyte.

parameter		unit	value					
bulk concentration	c	mol/m^3	10^{-6}	10^{-4}	10^{-2}	10^{-6}	10^{-4}	10^{-2}
forward rate constant	k_{on}	$m^3/(mol \cdot s)$		10			1	
backward rate constant	k_{off}	s^{-1}		10^{-4}			10^{-3}	
surface density	c_{s0}	mol/m^2		10^{-8}			10^{-8}	
surface diffusivity	D_s	m^2/s		10^{-11}			10^{-11}	
solution diffusivity	D	m^2/s		10^{-11}			10^{-11}	
average flow velocity	v	m/s		10^{-4}			10^{-4}	
channel height	h	m		10^{-4}			10^{-4}	
Pe	vh/D			1000			1000	
Da	$k_{on}ch/D$		100	10^4	10^6	10	1000	10^5
E	ch/c_{s0}		0.01	1	100	0.01	1	100
K_D	$k_{off}/(k_{on}c)$		10	0.1	0.001	1000	10	0.1
T	$1/(k_{on}c+k_{off})$		9091	909	10	999	909	91

Table 3.2. Parameters used in the modeling to investigate the effect of flow rate.

Parameter		unit	Value
bulk concentration	c	mol/m^3	$[1\times10^{-7},1\times10^{-3}]$
forward rate constant	k_{on}	$m^3/(mol\cdot s)$	11
backward rate constant	k_{off}	s^{-1}	10^{-3}
surface density	c_{s0}	mol/m^2	10^{-8}
surface diffusivity	D_s	m^2/s	10^{-11}
solution diffusivity	D	m^2/s	10^{-11}
average flow velocity	v	m/s	$(1.47\times10^{-1}, 4.6\times10^{-3})$
channel height	h	m	10^{-4}

Table 3.3. Parameters used in the modeling to investigate the effect of surface density of binding sites at various bulk concentrations of analyte.

Parameter		unit	Value
bulk concentration	c	mol/m^3	$[1\times10^{-4}, 2\times10^{-2}]$
forward rate constant	k_{on}	$m^3/(mol\bullet s)$	30
backward rate constant	k_{off}	s^{-1}	10^{-4}
surface density	c_{s0}	mol/m^2	$(1.33\times10^{-8}, 2.66\times10^{-8})$
surface diffusivity	D_s	m^2/s	5×10^{-11}
solution diffusivity	D	m^2/s	5×10^{-11}
average flow velocity	v	m/s	9.2×10^{-3}
channel height	h	m	10^{-4}

Table 3.4. Parameters used in the simulation of biotin-streptavidin and Daclizumab-IgG interactions.

Parameter		unit	Bio-SA	Dac-IgG
bulk concentration	c	mol/m^3	5.7×10^{-4}	5×10^{-4}
forward rate constant	k_{on}	$m^3/(mol\bullet s)$	28	17
backward rate constant	k_{off}	s^{-1}	6.7×10^{-4}	4.0×10^{-3}
surface density of binding sites	c_{s0}	mol/m^2	1.32×10^{-8}	6.6×10^{-9}
surface diffusivity	D_s	m^2/s	10^{-10}	5×10^{-11}
solution diffusivity	D	m^2/s	10^{-10}	5×10^{-11}
average flow velocity	v	m/s	1.8×10^{-2}	3.68×10^{-2}
channel height	h	m	10^{-4}	10^{-4}
dissociation constant K_D	k_{off}/k_{on}	M	2.4×10^{-8}	2.4×10^{-7}
saturation time τ	$1/(k_{on}c+k_{off})$	s	~ 60	~ 80

Table 3.5. Dissociation constants of biotin-streptavidin interactions at four flow rates from fitting of experimental results into an extended Langmuir model.

Flow rate (μL/min)	K_D (M)	Error (M)	R^2
534.4	3.16×10^{-8}	1.90×10^{-8}	0.97
267.2	3.34×10^{-8}	1.00×10^{-8}	0.99
133.6	3.09×10^{-8}	1.80×10^{-8}	0.99
33.4	2.31×10^{-8}	1.90×10^{-8}	0.98

Table 3.6. SPR signal of 24 flow cells to the bulk refractive index change caused by a diluted ethanol solution of refractive index (1.3391).

	1	2	3	4	5	6	AVR	STD	RSD
A	8.37	8.54	9.07	8.41	8.53	8.89	8.63	0.28	3.27%
B	8.45	8.65	8.53	9.20	9.29	9.00	8.85	0.36	4.03%
C	7.84	8.72	8.70	9.35	9.51	8.92	8.84	0.59	6.70%
D	7.79	7.94	8.77	9.05	9.32	9.03	8.65	0.63	7.33%
AVR	8.11	8.46	8.77	9.00	9.16	8.96			
STD	0.35	0.36	0.23	0.42	0.43	0.06			
RSD	4.28%	4.23%	2.59%	4.61%	4.71%	0.71%			

Table 3.7. SPR signal of 24 flow cells to the adsorption of streptavidin.

	1	2	3	4	5	6	AVR	STD	RSD
A	5.63	5.82	6.96	6.31	7.01	7.79	6.59	0.82	12.39%
B	6.10	6.34	6.84	7.71	7.27	7.50	6.96	0.64	9.26%
C	5.45	6.19	6.45	7.13	7.57	7.92	6.78	0.92	13.61%
D	5.26	5.74	6.52	7.05	7.46	7.81	6.64	0.99	14.95%
AVR	5.61	6.02	6.69	7.05	7.33	7.75	6.74	0.81	
STD	0.36	0.29	0.25	0.57	0.24	0.18			
RSD	6.45%	4.79%	3.67%	8.14%	3.31%	2.26%			

CHAPTER 4

INVESTIGATION OF THE MFCA-SPRM SYSTEM FOR IMMUNOGENICITY ASSAY OF THE THERAPEUTIC ANTIBODY DACLIZUMAB

Introduction

A preliminary investigation of developing an immunogenicity assay for patients who undergo treatment with the antibody-based therapeutic Daclizumab with the MFCA-SPRM system is presented in this chapter. Daclizumab is a humanized monoclonal antibody drug that is currently being investigated in a phase II clinical trial as a therapeutic for patients with relapsing-remitting multiple sclerosis.[1] Previously, Daclizumab was developed as an immunosuppressant in organ transplantations.[2] The biological target of Daclizumab is the interleukin-2 receptor (IL-2R) alpha unit of T cells.[2] IL-2R is a heterotrimeric cytokine receptor[3] involved in T cell activation and often serves as a drug target in immunologic therapy.[4] The mechanism of the biological effect of Daclizumab is to bind to IL-2R and prevent T cell activation and further formation of antibodies produced against the transplant.

Multiple sclerosis is an autoimmune disease in which active immune cells attack the nervous system and cause damage to nerve cells. Daclizumab is a potential therapy since

it suppresses the activity of the immune system.[1] However, because of the complexity of the human immune system, when biological drugs such as Daclizumab enter the human body, these therapeutics could be accepted as self-molecules by the immune system or lead to a specific or nonspecific immune response.[5] The ability of biological drugs to induce an immune response is called immunogenicity. Characterization of immunogenicity is an important aspect of drug development.[4-6] Especially, unwanted immunogenicity is a big concern in clinical trials due to the potential safety and efficacy issues,[6-8] although there have been significant improvements in understanding and reducing immunogenicity during the initial of drug design process.[9-11]

Typically the first approach in assessing immunogenicity is the detection, measurement and characterization of anti-drug antibodies (ADAs) from patient serum samples.[12] Recommendations for the design, optimization and validation of immunoassays for detection of ADA have been made by members of the American Association of Pharmaceutical Sciences.[5, 13] However, information provided by a single analytical method usually is incomplete, and an array of methods is recommended for accurate evaluation of immunogenicity of a biological drug.

The available bioanalytical methods include radio-labeling, enzymatic, fluorescence, electrochemical luminescence detection and SPR with various assay formats, such as direct, indirect, bridging and competitive assays. Compared to all of the other labeled methods, SPR is a label-free, real-time and quantitative method for direct screening of ADAs from serum samples with minimal sample preparation. Label-free detection of ADAs is essentially important for humanized antibody drugs such as Daclizumab.

Because 90% of the Daclizumab structure sequence is from human IgG, the similar structure characterization cause it hard to find chemical label agents for specific binding and detection of ADA.

Due to the lack of labeling agent, label-free immunogenicity assays based on the Biacore, a commercial SPR system, has been developed. The advantages of disadvantages of immunogenicity assay based on Biacore include the low-throughput, nonspecific adsorption, and lower sensitivity when compared to an enzyme-linked immunosorbent assay (ELISA). In this chapter, I will investigate use of the integrated MFCA-SPRM system to overcome these drawbacks. The MFCA-SPRM system has increased throughput and will be efficient in developing screening assays. With proper immobilization strategies, nonspecific adsorption could be minimized,[14] or if necessary accounted for with control channels. The capability of MFCA-SPRM for *in situ* microarray fabrication and analysis could preserve the activity of immobilized biomolecules and improve the assay sensitivity, as demonstrated in Chapter 3. The attempted combination of SPRM with MALDI mass spectrometry in Chapter 5 will provide the potential to identify ADAs bound on SPR substrate after SPR analysis in a microarray format.

Experimental

Materials

Serum samples from healthy humans were provided by Atlanta Biologicals for control experiments to measure non-specific adsorption of serum matrix that could cause SPR signal interferences in ADA assays. Three serum samples from multiple sclerosis patients

were provided by Professor John Rose (Department of Neurology, University of Utah). Samples were labeled as 83795 (6-year treatment), 78817 (4-year treatment) and 83414 (no treatment) were selected for a preliminary assessment of the immune response related to different treatment times. One hundred µL of each sample were stored at -20 °C before being used for the SPR experiments.

Dilution of Serum Samples

The biotinylated-Daclizumab microarray was fabricated using the MFCA-SPRM to capture ADAs from serum samples. In each micro flow cell, 100 µL streptavidin (40 µg/mL) and biotinylated-Daclizumab (250 µg/mL) were flowed over biotin-terminated SAMs surface continuously. In order to get rid of the signal interference from substances other than ADAs, normal human serum samples were diluted to find the optimal dilution ratio, because dilution of whole serum samples not only minimized the interference but also lowered the concentration of ADAs for detection. PBS buffer (pH 7.4) was used to dilute serum samples to 1, 5, 10, 25 and 50%. Four percent bovine serum albumin (BSA) and 100 µg/mL Daclizumab were also analyzed in the control experiments of measuring nonspecific adsorption. One hundred fifty µL of each sample were loaded into 24 channels (3 × 8), flowed over a biotinylated-Daclizumab surface at a flow rate of 33.4 µL/min.

Screening Assay of Serum Samples

From last optimization experiments, the optimal dilution ratio was found to be 25% when SPR signal generated by the nonspecific adsorption reached equilibrium. One

hundred µL of each patient serum sample was diluted to 25% with PBS buffer. Four hundred µL of each patient sample was delivered into three micro flow cells at a flow rate of 16.7 µL/min. A biotinylated-Daclizumab antibody microarray was fabricated in the same approach as described above. After the serum samples were flowed through the MFCA and across the sensor surface, PBS buffer was used to rinse the surface.

Results and Discussion

Human serum consists of heterogeneous biological components, such as proteins, antibodies, hormones and drugs,[15] which cause potential interferences of ADA detection via specific or nonspecific binding. In the SPR screening experiment of Daclizumab, factors that affect the ADA assay results could include the physicochemical adsorption of various proteins other than ADA on the SPR sensing surface, the concentration of soluble Daclizumab, the presence of drug target (IL-2R), and the possibility of binding pairs of Daclizumab – ADA and Daclizumab – IL-2R in the serum samples.

In order to minimize non-specific adsorption from the sample matrix, dilution of serum samples is one easy and fast sample preparation method to lower the concentration of matrix.[16] However, the concentration of detectable ADAs also will be lowered by the dilution. Therefore, an optimal dilution ratio was needed. On the ADA capturing surface, nonspecific adsorption of 1, 5, 10, 25, 50 % diluted and 100% serum samples from normal human, 4% BSA and 100 µg/mL Daclizumab were tested in a microarray format and the real-time SPR curves were plotted in Figure 4.1a. The SPR curves show that the bulk refractive index of concentrated serum can produce a high SPR signal of 11% reflectivity, which decreases with dilution to less than 1% reflectivity. After serum

samples were flowed over the SPR sensing surface, PBS buffer was flowed over the surface until the SPR signal indicated that equilibrium had been reached. From the real-time SPR curves in Figure 4.1a, the average of data after 300 s minus the average of data from the initial 50 s is the signal generated by nonspecific adsorption of serum matrix. Figure 4.1b shows the plot of the SPR response signal as for different serum dilutions. The average SPR signal drops dramatically from 0.9 % reflectivity to 0.3% reflectivity when the pure serum sample is diluted to 25%. However, the SPR signals generated by the serum samples of concentration equal or less than 25% reach a stable level of 0.33 ± 0.20 % reflectivity. The 25% dilution sample shows minimal nonspecific adsorption while not diluting the ADAs too much, so it was selected as an optimal dilution ratio for future sample preparation. Although 25% also was used in reported studies of the immunogenicity of other antibody drugs with SPR,[16] the data from our investigation confirmed the optimal dilution ratio.

Three labeled serum samples were provided by Dr. John Rose for preliminary development of immunogenicity assays for Daclizumab. One sample (No. 83414) is from a multiple sclerosis patient who was not treated with Daclizumab, and two other samples were from patients who have Daclizumab treatment for 4 (No. 78817) and 6 years (No. 83795), respectively. A patient serum sample obtained from patients who did not undergo treatment is required as a negative control used in ADA detection because SPR detection cannot distinguish directly between ADAs and nonspecific adsorption on the surface. These samples were diluted to 25% and flowed over the Daclizumab surface. Each sample was run in three duplicates. The real-time SPR curves of the screening

ADA are plotted in Figure 4.2a. A summary of the observed SPR signals is presented in Figure 4.2b, which shows that the SPR response signal decreases with the treatment time of Daclizumab. The negative control sample (No. 83414) shows the highest SPR response of 0.86 ± 0.11 % reflectivity which exceeds the nonspecific adsorption response of 0.33 ± 0.20 % reflectivity. The sample from the patient after a 4-year treatment of Daclizumab shows a response of 0.49 ± 0.15 % reflectivity, which is as much as 1.5 times of the nonspecific adsorption. The sample from the patient after a 6-year treatment of Daclizumab shows the lowest response of 0.33 ± 0.23 % reflectivity which is close to the signal generated by nonspecific adsorption.

In brief, the immunogenicity of Daclizumab from the SPR result shows that the negative control sample gives the highest SPR signal. The differences in the immune responses of individual patients as well as the matrix interferences impact the assay sensitivity and specificity. In clinical study, the patients' immune response to a biological drug depends on the characteristics of drug and its usage, the disease and the physical condition of the individual patient. Bioanalytical assay is only one of many approaches to evaluate the immunogenicity of biological drugs. The limitation of immunogenicity assay is associated with the methods to detect ADAs and patient immune response. In the SPR assay of Daclizumab, the free Daclizumab in serum could bind to soluble drug target of IL-2R or ADAs, which may interfere with the detection of ADAs and lead to a false-negative result. Further investigation could monitor the concentration of free drug and drug targets in serum samples before ADA tests.

It would also be interesting to investigate why the negative control sample (No. 83414) shows an SPR signal higher than the nonspecific adsorption. The high SPR signal could be due to adsorption of soluble drug target (IL-2Rα) or other proteins in patients' serum.[17, 18] Analytical methods such as mass spectrometry can be combined with SPR to identify molecules bound on the Dacliaumab surface after SPR analysis, which provides qualitative and quantitative analysis of ADA. In the future, more samples are required for analyses to generate statistically significant data to evaluate the immunogenicity of Daclizumab.

References

1. Rose, J. W.; Burns, J. B.; Bjorklund, J.; Klein, J.; Watt, H. E.; Carlson, N. G., Daclizumab phase II trial in relapsing and remitting multiple sclerosis: MRI and clinical results. *Neurology* **2007**, *69*, 785-789.

2. Wiseman, L. R.; Faulds, D., Daclizumab: A review of its use in the prevention of acute rejection in renal transplant recipients. *Drugs* **1999**, *58*, 1029-1042.

3. Stauber, D. J.; Debler, E. W.; Horton, P. A.; Smith, K. A.; Wilson, I. A., Crystal structure of the IL-2 signaling complex: Paradigm for a heterotrimeric cytokine receptor. *PNAS* **2006**, *103*, 2788-2793.

4. Taniguchi, T.; Minami, Y., The IL-2/IL-2 receptor system: A current overview. *Cell* **1993**, *73*, 5-8.

5. Marco van de Weert, E. H. M., *Immunogenicity of Biopharmaceuticals*. Springer: 2007.

6. Koren, E.; Zuckerman, L. A.; Mire-Sluis, A. R., Immune responses to therapeutic proteins in humans - Clinical significance, assessment and prediction. *Curr. Pharm. Biotechnol.* **2002**, *3*, 349-360.

7. Barnes, H. J.; Ragnarsson, G.; Alvan, G., Quality and safety considerations for recombinant biological medicines: A regulatory perspective. *Int. J. Risk Saf. Med.* **2009**, *21*, 13-22.

8. Giezen, T. J.; Mantel-Teeuwisse, A. K.; Straus, S. M. J. M.; Schellekens, H.; Leufkens, H. G. M.; Egberts, A. C. G., Safety-related regulatory actions for biologicals approved in the United States and the European Union. *JAMA* **2008**, *300*, 1887-1896.

9. Tsurushita, N.; Hinton, P. R.; Kumar, S., Design of humanized antibodies: From anti-Tac to Zenapax. *Methods* **2005**, *36*, 69-83.

10. Beck, A.; Wurch, T.; Bailly, C.; Corvaia, N., Strategies and challenges for the next generation of therapeutic antibodies. *Nat. Rev. Immuno.***2010**, *10*, 345-352.

11. Carter, P. J., Potent antibody therapeutics by design. *Nat. Rev. Immuno.* **2006,** *6*, 343-357.

12. Kaliyaperumal, A.; Jing, S., Immunogenicity assessment of therapeutic proteins and peptides. *Curr. Pharm. Biotechnol.* **2009,** *10*, 352-358.

13. Mire-Sluis, A. R.; Barrett, Y. C.; Devanarayan, V.; Koren, E.; Liu, H.; Maia, M.; Parish, T.; Scott, G.; Shankar, G.; Shores, E.; Swanson, S. J.; Taniguchi, G.; Wierda, D.; Zuckerman, L. A., Recommendations for the design and optimization of immunoassays used in the detection of host antibodies against biotechnology products. *J. Immunol. Methods* **2004,** *289*, 1-16.

14. Nelson, K. E.; Gamble, L.; Jung, L. S.; Boeckl, M. S.; Naeemi, E.; Golledge, S. L.; Sasaki, T.; Castner, D. G.; Campbell, C. T.; Stayton, P. S., Surface characterization of mixed self-assembled monolayers designed for streptavidin immobilization. *Langmuir* **2001,** *17*, 2807-2816.

15. Marshall, J.; Jankowski, A.; Furesz, S.; Kireeva, I.; Barker, L.; Dombrovsky, M.; Zhu, W.; Jacks, K.; Ingratta, L.; Bruin, J.; Kristensen, E.; Zhang, R.; Stanton, E.; Takahashi, M.; Jackowski, G., Human serum proteins preseparated by electrophoresis or chromatography followed by tandem mass spectrometry. *J. Proteome Res.* **2004,** *3*, 364-382.

16. Klakamp, S. L.; Lu, H.; Tabrizi, M.; Funelas, C.; Roskos, L. K.; Coleman, D., Application of analytical detection concepts to immunogenicity testing. *Anal. Chem.* **2007,** *79*, 8176-8184.

17. Liparoto, S. F.; Myszka, D. G.; Wu, Z.; Goldstein, B.; Laue, T. M.; Ciardelli, T. L., Analysis of the role of the interleukin-2 receptor γ chain in ligand binding. *Biochemistry* **2002,** *41*, 2543-2551.

18. Kittur, S. D.; Kittur, D. S.; Soncrant, T. T.; Rapoport, S. I.; Tourtellotte, W. W.; Nagel, J. E.; Adler, W. H., Soluble interleukin-2 receptors in cerebrospinal fluid from individuals with various neurological disorders. *Ann. Neurol.* **1990,** *28,* 168-173.

Figure 4.1. Nonspecific adsorption of serum matrix on biotinlayted-Daclizumab surface measured by SPRM-MFCA. (a) SPR real-time curves of samples of diluted serum, 4% BSA and 100 µg/mL Daclizumab flowed through 24 micro flow cells, the legends show the percentage of serum in samples and curves of same color are replicates. (b) The adsorption SPRM signal of diluted serum samples versus dilution percentage. Each data point represents an average of three duplicate measurements.

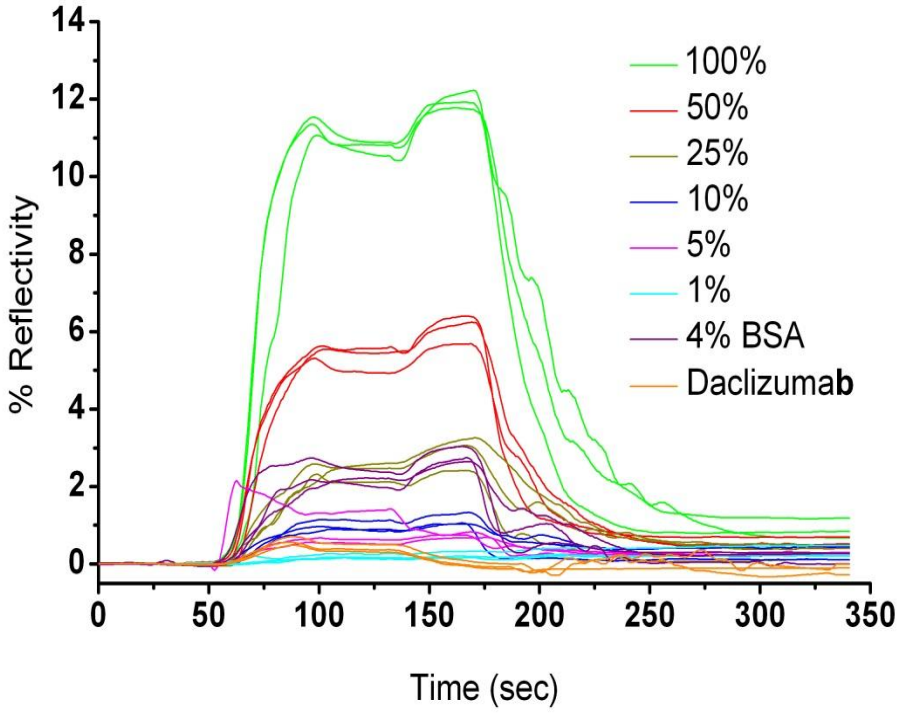
% Reflectivity
Time (sec)
100%
50%
25%
10%
5%
1%
4% BSA
Daclizumab

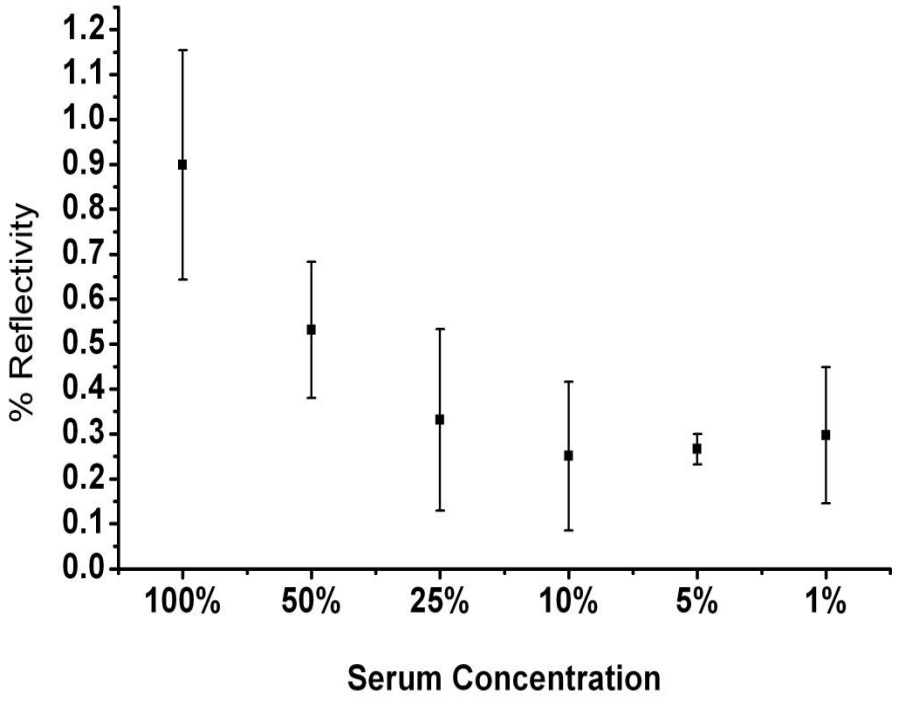
% Reflectivity
100%
50%
25%
10%
5%
1%
Serum Concentration

Figure 4.2. ADA binding assay using the SPRM-MFCA to screen ADA from samples of three multiple sclerosis patients treated with Daclizumab for different time periods. (a) SPR real-time curves of serum samples, labeled as number 83414, 78817 and 83795, from patients treated with Daclizumab for 0, 4 and 6 years, respectively. (b) The SPRM signal of patient serum samples versus the treatment time. Each data point is from an average of three duplicate measurements.

h

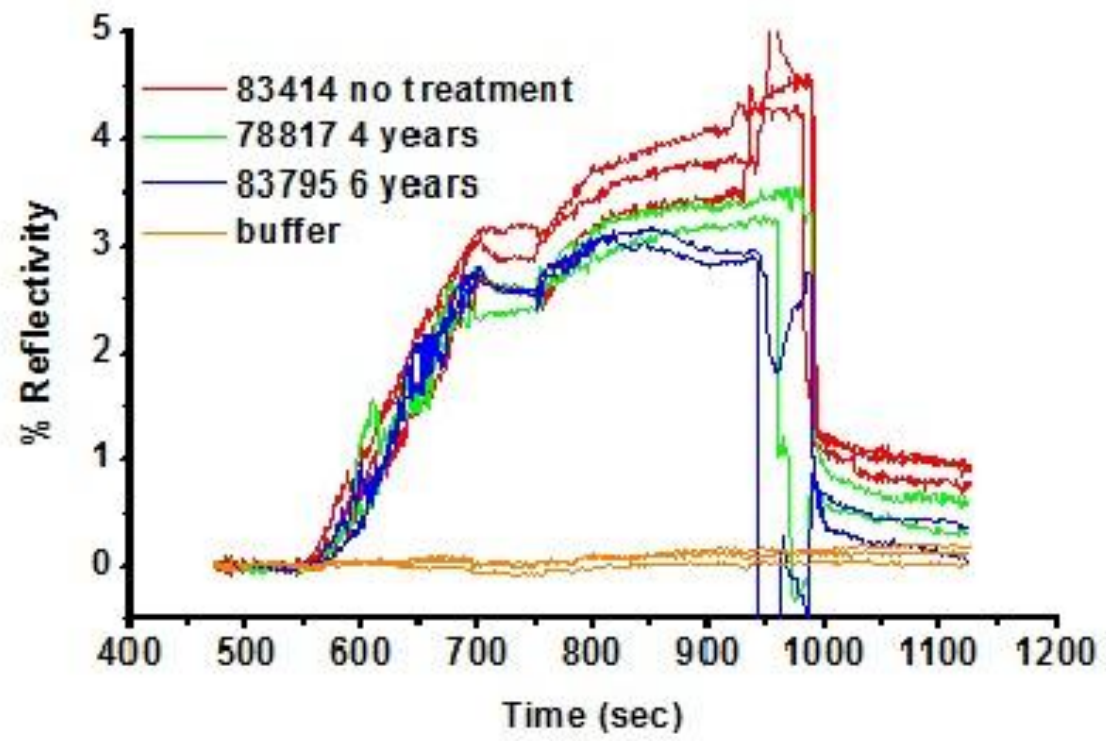
83414 no treatment
78817 4 years
83795 6 years
buffer
% Reflectivity
Time (sec)
0
1
2
3
4
5
400
500
600
700
800
900
1000
1100
1200

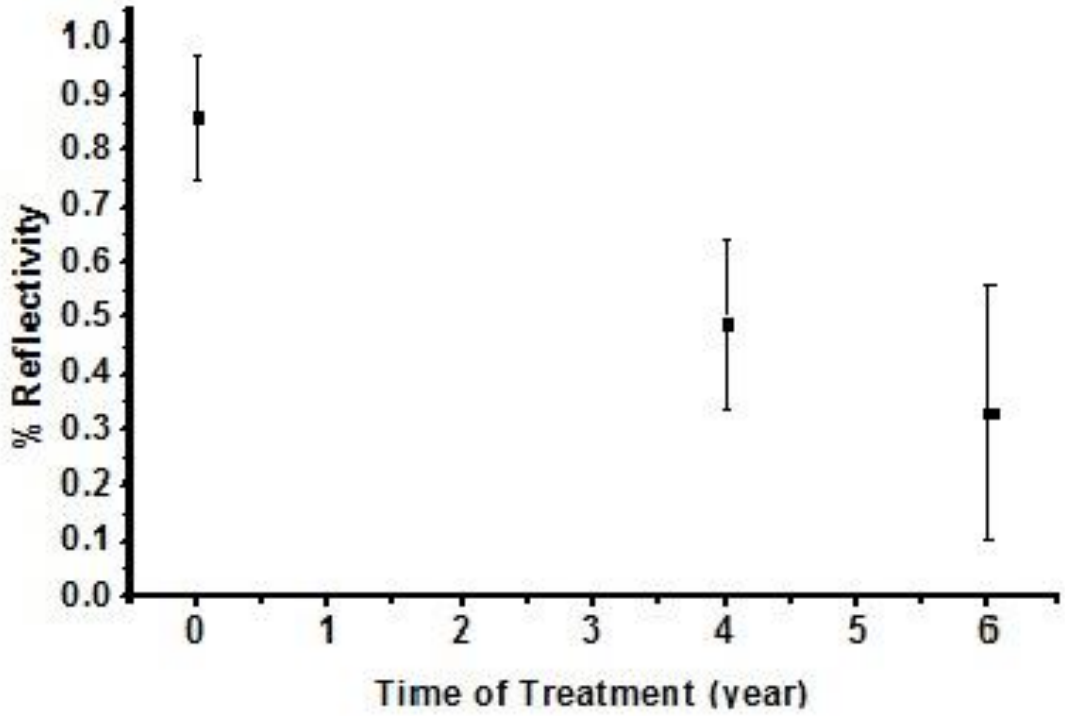
% Reflectivity
Time of Treatment (year)
0.0
0.1
0.2
0.3
0.4
0.5
0.6
0.7
0.8
0.9
1.0
0
1
2
3
4
5
6

CHAPTER 5

USING MALDI MS TO IDENTIFY CAPTURED PROTEINS ON THE SURFACE OF ANTIBODY MICROARRAYS

Introduction

This chapter describes a versatile method to use the MFCA to fabricate an antibody microarray and then identify surface-bound antibodies with a commercial matrix-assisted laser desorption/ionization (MALDI) mass spectrometry (MS). The process developed to create the microarrays and then use MALDI-TOF MS to analyze these microarrays will be useful for future work of combining the integrated MFCA-SPRM with MALDI MS for protein analysis. These experiments also demonstrate the capability of using the MFCA for fabrication of protein microarrays that may be used for MALDI MS analysis.

The primary motivation to combine SPR and MALDI MS is to identify surface bound proteins after SPR analysis of biomolecular interactions in a microarray format. As demonstrated in previous chapters, the integrated MFCA-SPRM system is useful for kinetic analysis of protein interactions and quantifying the surface coverage of an adsorbed protein layer. However, SPR analysis cannot identify the adsorbed molecules or perform structure analysis. MALDI MS is a sensitive technique to identify molecules on the surface via molecular weight and fragment patterns. As a result, a combination of these two techniques will provide both qualitative and quantitative information of protein interactions.

Basically, there are two approaches to combine SPR and MS analysis. One is to wash off the surface-bound materials in an elution step and then analyze the desorbed proteins present in the wash solution with various MS methods such as MALDI, electrospray ionization mass spectrometry (ESI-MS) or liquid chromatography-mass spectrometry (LC-MS).[1, 2] There are some drawbacks of the elution approach, such as time of analysis, loss of materials and contamination. The other approach is to use MALDI MS to directly analyze the protein bound on the SPR chip, and both SPR and MS analysis are performed on the same chip. This entire on-a-chip method overcomes the drawbacks of the elution step.[1-9] The MFCA can be used for both approaches but we focused on the on-a-chip method in this chapter.

Since 1997, there have been several reports on the combination of commercial, non-imaging SPR spectroscopy and MALDI MS for on-chip biomolecular analysis.[3-9] Most of these early SPR instruments had only a few flow cells and the throughput is low.[10] Recently, GWC technologies[11] and GenOptics[12] have introduced some commercially available SPR imaging (SPRi) systems. These SPR imaging systems can be applied for microarray-based analysis. The microarray can also be analyzed with MALDI MS, and the combination of SPRi with MALDI MS can provide a high-throughput platform for multiplex protein analysis.

Previous chapters have described the application of the MFCA-SPRM system for *in situ* microarray fabrication and analysis. Combination of MFCA-SPRM and MALDI MS would provide both qualitative and quantitative analysis of protein interactions, which would be especially useful to develop immunogenicity assays. The SPR system will screen anti-drug antibodies from complex biological samples and captured proteins on a

SPR sensing surface will be further identified with MALDI MS. The combination of the MFCA-SPRM with a commercial MALDI MS was explored and the result is presented in this chapter.

One technical problem encountered for the combination of SPR and MS was the substrate used in the SPR system did not match the thickness requirement in for the MALDI instrument. The glass substrate used in for SPRM is 2 mm thick but the normal sample thickness for MALDI is less than 0.5 mm. Because of this, we used a microscope cover glass with a thickness of less than 0.2 mm to replace the SPR substrate for MALDI MS. Although the substrate requirement makes it impossible to perform SPR and MS analyses on one chip, using the MFCA for SPR analysis and following the same procedure to create a microarray for MALDI MS can still provide useful information on protein interactions.

The antibody-antibody interaction was used as a model system to mimic an immunogenicity assay. As described before, the gold-coated surface was functionalized with biotin-terminated thiols first, and streptavidin was deposited on the SAM surface with the MFCA. The first biotinylated antibody was immobilized on the streptavidin surface via biotin-streptavidin interaction, and then the second antibody was captured to the first antibody surface. The protein microarray fabricated using the MFCA was transferred to MADLI MS for molecular identification. A method was developed to analyze antibodies on microspots in the microarray with MALDI MS.

Experimental

Materials

Micro cover glasses (22 × 22 mm, 0.16 to 0.19 mm thickness) were purchased from VWR (Product # 48366067). Biotinylated goat anti-human IgG (Product # AP112B), polyclonal human IgG (Product # AG711) and streptavidin (Product # SA101) were purchased from Millipore. Sinapinic acid (3,5-dimethoxy-4-hydroxycinnamic acid) (10 mg/mL) (Product # 186002332) was purchased from Waters Corporation. Conductive double-sided adhesive sheets (Product # 05071-AB) were purchased from SPI Supplies.

Substrate Preparation

Micro cover glasses were coated with 2 nm Ti and 50 nm Au using an electron-beam deposition system as described in Chapter 2. Then the gold-coated glass was immersed in 1 mM mixed BAT and OEG thiol (mole ratio 1:9) solution for 24 h. Finally, the SAM-functionalized surface was washed with ethanol and dried with nitrogen.

Protein Microarray Fabrication

Twenty four micro flow cells (3 row × 8 column) in MFCA were used to create a microarray. Samples in a column were replicates. Table 5.1 shows the position of flow cells and different proteins immobilized in eachlayer. The streptavidin concentration was 0.1 mg/mL and antibody solutions concentrationswere 0.4 mg/mL. The flow rate was 33.4 µL/min and the sample volume was 330 µL per flow cell for the entire experiment. After each protein deposition step, PBS buffer was flowed over the protein surface to wash off nonspecific bound protein.

MALDI MS Sample Preparation

Sinapinic acid (10 mg/mL) prepared in 50/50 (v/v) water/acetonitrile with 0.1% TFA was used as a MALDI matrix. Two methods were used to mix protein samples on the surface with the matrix. One method was to apply the matrix to the protein microarray surface as a thin mist via an aerosol-spraying device. In the other one, 1 µL of matrix solution was added on top of the entire microarray surface, and the solution was allowed to dry, leading to crystalline matrix formation.

MALDI TOF MS

The MALDI MS experiments were done with help from Dr. James Muller in the MS lab in the Chemistry Department in the University of Utah. The prepared microarray substrate was mounted on a MALDI target holder (Product # 86002324) with double-sided tape at a specific position for laser scanning and placed into a Waters micromass MALDI micro MX mass spectrometer. The MALDI mass spectrometer was equipped with a nitrogen laser (337 nm) operating at 10 Hz. The data were acquired at an accelerating potential of 12 kV in the positive and linear modes. A camera was used to locate the sample and laser firing positions. Standard instrument software MassLynx was used to acquire and analyze the mass spectra. Depending on the surface concentration of the protein sample, various numbers of shots (10 to 250) were acquired from the surface and the average data is presented as a single averaged spectrum.

MALDI MS Analysis of Protein Microarray and Sample Standards

First, a droplet of 100 µg/mL streptavidin solution was added on the gold surface and dried at room temperature. Then, 1 µL of sinapinic acid was added to the protein spot and

dried in air at room temperature. The same protocols were applied to the other antibody standard solutions. The streptavidin sample was used to optimize the instrument settings and worked as a standard to calibrate the system.

Results and Discussion

Sample Preparation for MALDI MS Analysis

In order to use MALDI MS analysis, a sample preparation method must be developed to mix the protein with MALDI-matrix on the surface. Sinapinic acid was selected as the matrix for protein ionization.[13] At first, an aerosol-spraying was used to paint a layer of the matrix on the protein surface. However, it was hard to control the amount of matrix sprayed on the surface, so samples prepared by this method did not produce reproducible results. Then the standard 'dried droplet' method in MALDI sample preparation was used, in which 1 μL matrix solution was added onto the sample surface and dried in air or with a flow of air. We did not use the standard method for the initial experiments due to a concern that the whole microarray pattern would be covered by a single droplet and each spot would not be visible. However, it was found that with the dried-droplet method, the microarray pattern still visible. Non-homogeneous matrix film distributed across the microarray surface because the surface tension inside and outside microspots were different. With the camera in the instrument, it was possible to locate the target sample spot and area for laser desorption.

MALDI MS Detection of Streptavidin Using the MFCA

Streptavidin is a model protein that has been well studied in applying MALDI and ESI MS for noncovalently bound protein complex analysis.[14, 15] It has a tetramer structure

with a molecular weight of approximate 52,800 Da.[16, 17] A droplet of 1 µL standard streptavidin solution (100 ug/mL) was added to the gold surface and formed a thin layer. Then a droplet of 1 µL sinapinic acid was added onto the protein layer as matrix for analysis. The gold-coated glass with streptavidin was affixed to a MALDI substrate by a conductive double-sided adhesive tape and loaded into the MS system.

The MALDI TOF MS spectrum of streptavidin is shown in Figure 5.1. Major ion peaks of *m/z* at 13104.0, 26221.3, 6576.9 and 39342.3 are labeled in the spectrum. The strongest peak (*m/z* = 13104.0) is from the streptavidin subunit and the peak of the streptavidin tetramer (*m/z* = 52351.8) is weak. The high intensity of the subunit is caused by a 'first-shot phenomenon' in which the data of intact protein complex can only be collected from the first laser shot.[18] The mechanism is based on when the protein co-crystalizes with the matrix, the large complex protein segregates to the exterior of the crystal and the dissociated proteins remain in the crystal interior. As the laser ablates the intact protein near the surface, more subunits were ionized and generated a higher signal.

The streptavidin was used as a standard to adjust the MS system before each sample was run. The MS spectra of the same streptavidin sample collected by the same MALDI TOF MS were not consistent from day-to-day experiments. For example, the *m/z* of streptavidin subunit peak could shift from 13115.5 to 13428.0. The variation of signal could be attributed to many factors; the major source of variation could be understood from the principles of TOF MS detection. Basically, in a TOF system, ionized molecules with charge were accelerated in a potential field and traveled freely before arriving atthe detector. The signal of *m/z* is proportional to the traveling time and the initial energy of molecules gained before traveling in a system with fixed traveling length. The initial

energy that molecules gained can be affected by factors that can impact desorption and ionization process, such as surface position in the gradient electric field and velocity of molecules extracted from their desorption plume. Therefore, the *m/z* peaks of the same ions vary and could not be used as the only standard to identify the protein; fragment ions and fragmentation pattern will also be used to identify antibodies captured on surfaces.

Identify Surface Bound Protein on an Antibody Microarray

After detection of streptavidin standard on the substrate, the same sample preparation approach was applied to an antibody array. The antibody microarray was prepared using the MFCA. Three types of protein spots were created on the SAM surface: The order of the protein surface layers and their positions on the microarray are shown in Table 5.1. The protein microarray was made using the MFCA under continuous flow. After each step of protein deposition, PBS buffer was introduced to rinse the excess unbound protein away. A big difference between protein deposited by MFCA and the dried-droplet method is specific and nonspecific binding, which could affect the surface density and homogeneity of protein surfaces. Antibody I and II solutions were also spotted on the microarray surface with the dried–droplet method to act as standards to compare with spectra acquired from spots.

Figures 5.2 and 5.3 are spectra of antibody I and II and act as standards for microarray protein identification. The characteristic peaks of antibody I are *m/z* at 33532.0, 66844.9 and 86062.7 and they are major signals generated from the subunit of the biotinylated antibody I. The whole antibody peak *m/z* at 160422.9 is weak and hardly can be seen from the spectrum. In Figure 5.3, the characteristic peaks of antibody II are *m/z* at 23685.2, 74849.4 and 149056.1. Differently from antibody I, the intact antibody

peak is higher compared to antibody I, which could be due to the fact that the concentration of antibody II standard is higher than that of antibody I from the S/N in the spectrum.

Proteins on microspots were analyzed and the results are shown in Figures 5.4 and 5.5. Microspots with a single layer of streptavidin deposited by MFCA could not be detected by MALDI MS used in this study. The reason could be the amount of streptavidin was out of the detection limit of the MS system. Another reason could be the heterogeneous streptavidin surface. The protein aggregated after being dried on surface, which is shown by the AFM images in Chapter 3. Surface heterogeneity is a problem in MALDI analysis, in which some 'sweet spots' are formed making it difficult to obtain reproducible data.[19]

Figure 5.4 is the MS spectrum collected from microspots containing three protein layers as shown in Table 5.1. The spectrum has characteristic peaks of both antibodies. The peaks at *m/z* of 23695.2, 75209.0 and 149604.2 are close to the characteristic peaks of antibody II and they are of higher intensity compared to those of antibody I of *m/z* at 33808.4, 67209.0 and 86537.9. All the characteristics peaks in Figure 5.5 shift to higher *m/z* compared to their standards. But the range of *m/z* shift (10.0 ~ 600) is not large compared to the signal (0.5%), and within the order of signal shift (Δ *m/z* ~313.0) seen from the streptavidin calibration. The reason could be the protein surfaces were prepared in different ways and surface concentrations are different.

Figure 5.5 presents a MS spectrum from spots with streptavidin and antibody I. The spectrum was collected by an average of 223 laser shots across multiple microspots and the S/N ratio was very low. The low intensity peaks which can be seen are *m/z* at 66890.3

and 86079.8, which are matched well with antibody I characteristic peaks. Optimization of the surface and improvement of the detection limit of MALDI MS method is a goal of future work.

Conclusions

Overall, a preliminary investigation of using the MFCA to prepare an antibody microarray and analyze the surface bound protein with a MALDI TOF MS was summarized in this chapter. The investigation shows that the absolute amount of protein in microspots is an important factor to determine the MALDI MS detection limit of antibody microarray prepared by MFCA. Further optimization of protocols for surface sample preparation is important to improve the detection limit of MALDI MS.

In order to develop a more accurate method to identify proteins, protein digestion on chip and tandem MS analyzers can be adopted in the future. This preliminary work also demonstrated the possibility of combing the MFCA-SPRM with MALDI MS for high-throughput, quantitative and qualitative analysis. MFCA can also be applied as a microspotter to fabricate various microarrays for MALDI MS analysis. One possible future work is to introduce nanoparticles into the combined SPR-MS system; the nanoparticles will not only enhance the SPR signal in interaction analysis, but also could work as matrix in a MALDI analysis.

References

1. Borch, J.; Roepstorff, P., SPR/MS: recovery from sensorchips for protein identification by MALDI-TOF mass spectrometry. *Methods mol. biol.* **2010**, *627*, 269-281.

2. Stigter, E. C. A.; de Jong, G. J.; van Bennekom, W. P., Development of an on-line SPR-digestion-nanoLC-MS/MS system for the quantification and identification of interferon-gamma in plasma. *Biosens. and Bioelectron.* **2009**, *24*, 2184-2190.

3. Krone, J. R.; Nelson, R. W.; Dogruel, D.; Williams, P.; Granzow, R., BIA/MS: Interfacing biomolecular interaction analysis with mass spectrometry. *Anal. Biochem.* **1997**, *244*, 124-132.

4. Nelson, R. W.; Jarvik, J. W.; Taillon, B. E.; Tubbs, K. A., BIA/MS of epitope-tagged peptides directly from E. Coli lysate: Multiplex detection and protein identification at low-femtomole to subfemtomole levels. *Anal. Chem.* **1999**, *71*, 2858-2865.

5. Nelson, R. W.; Krone, J. R., Advances in surface plasmon resonance biomolecular interaction analysis mass spectrometry (BIA/MS). *J. Mol. Recognit.* **1999**, *12*, 77-93.

6. Nedelkov, D.; Nelson, R. W., Analysis of native proteins from biological fluids by biomolecular interaction analysis mass spectrometry (BIA/MS): Exploring the limit of detection, identification of non-specific binding and detection of multi-protein complexes. *Biosens. Bioelectron.* **2001**, *16*, 1071-1078.

7. Visser, N. F. C.; Heck, A. J. R., Surface plasmon resonance mass spectrometry in proteomics. *Expert Rev. Proteomics* **2008**, *5*, 425-433.

8. Nelson, R. W., Biosensor chip mass spectrometry: A chip-based proteomics approach. *Electrophoresis* **2000**, *21*, 1155-1163.

9. Nedelkov, D.; Nelson, R. W., Practical considerations in BIA/MS: Optimizing the biosensor-mass spectrometry interface. *J. Mol. Recognit.* **2000**, *13*, 140-145.

10. Boireau, W.; Rouleau, A.; Lucchi, G.; Ducoroy, P., Revisited BIA-MS combination: Entire "on-a-chip" processing leading to the proteins identification at low femtomole to sub-femtomole levels. *Biosens. Bioelectron.* **2009**, *24*, 1121-1127.

11. Nedelkov, D., Development of surface plasmon resonance mass spectrometry array platform. *Anal. Chem.* **2007**, *79*, 5987-5990.

12. Bellon, S.; Buchmann, W.; Gonnet, F.; Jarroux, N.; Anger-Leroy, M.; Guillonneau, F.; Daniel, R., Hyphenation of surface plasmon resonance imaging to matrix-assisted laser desorption ionization mass spectrometry by on-chip mass spectrometry and tandem mass spectrometry analysis. *Anal. Chem.* **2009**, *81*, 7695-7702.

13. Franz Hillenkamp, J. P.-K., *MALDI MS A Practical Guide to Instrumentation, Methods and Applications*. WILEY-VCH: 2007.

14. Jespersen, S.; Niessen, W. M. A.; Tjaden, U. R.; Van der Greef, J., Basic matrices in the analysis of non-covalent complexes by matrix-assisted laser desorption/ionization mass spectrometry. *J. Mass Spectrom.* **1998**, *33*, 1088-1093.

15. Zehl, M.; Allmaier, G., Instrumental parameters in the MALDI-TOF mass spectrometric analysis of quaternary protein structures. *Anal. Chem.* **2005**, *77*, 103-110.

16. Loo, J. A., Electrospray ionization mass spectrometry: A technology for studying noncovalent macromolecular complexes. *Int. J. Mass Spectrom.* **2000**, *200*, 175-186.

17. Weber, P. C.; Ohlendorf, D. H.; Wendoloski, J. J.; Salemme, F. R., Structural origins of high-affinity biotin binding to streptavidin. *Science* **1989**, *243*, 85-88.

18. Wortmann, A.; Pimenova, T.; Alves, S.; Zenobi, R., Investigation of the first shot phenomenon in MALDI mass spectrometry of protein complexes. *Analyst* **2007**, *132*, 199-207.

19. Rappsilber, J.; Moniatte, M.; Nielsen, M. L.; Podtelejnikov, A. V.; Mann, M., Experiences and perspectives of MALDI MS and MS/MS in proteomic research. *Int. J. Mass Spectrom.* **2003**, *226*, 223-237.

Figure 5.1. MALDI TOF MS spectrum of streptavidin on a gold surface prepared by deposition of solution of 0.1 mg/mL with sinapinic acid as matrix with standard dried-droplet method.

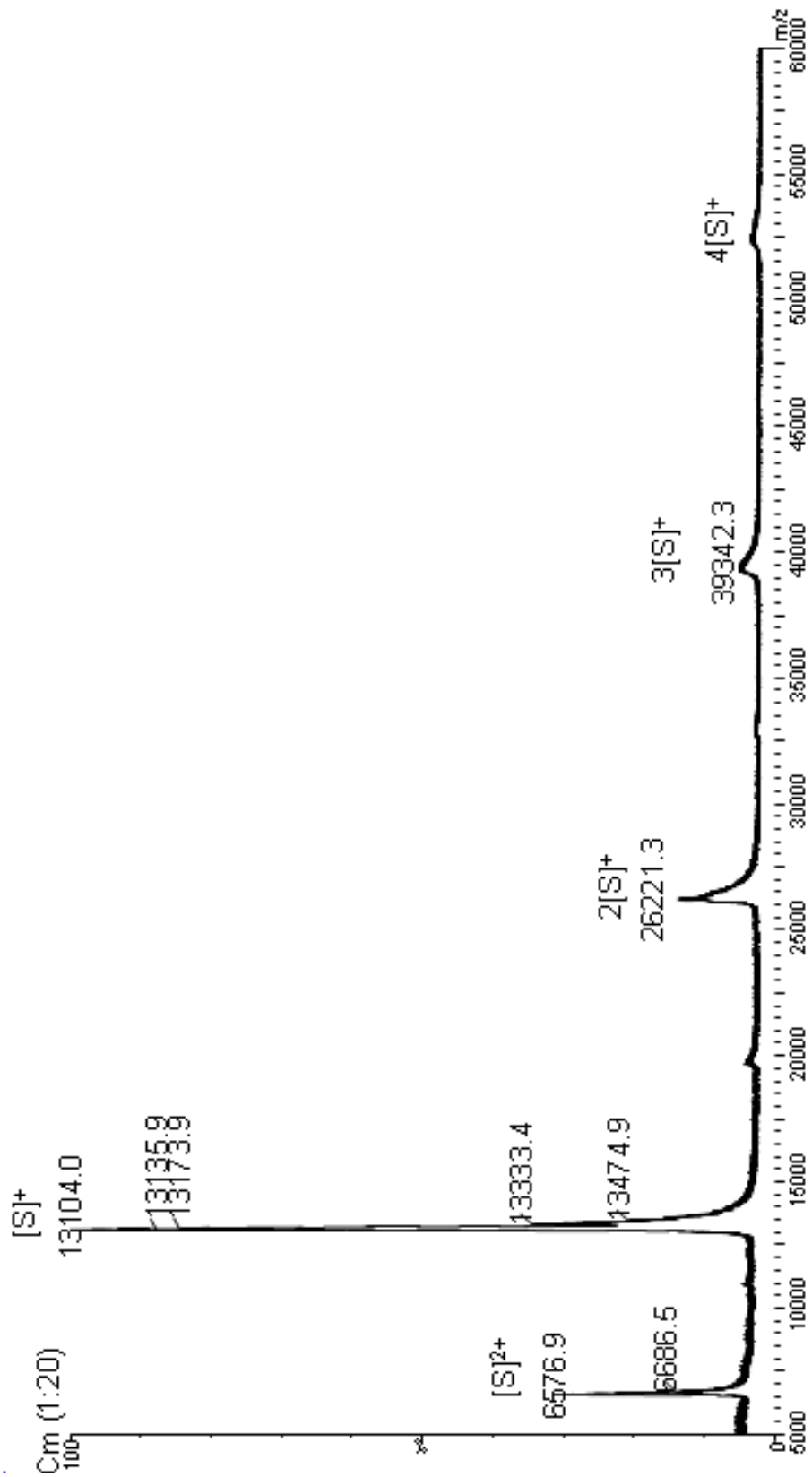
Cm (1:20)
100
%
0
5000
10000
15000
20000
25000
30000
35000
40000
45000
50000
55000
60000
m/z
[S]+
13104.0
13135.9
13173.9
[S]2+
6576.9
6686.5
13333.4
13474.9
2[S]+
26221.3
3[S]+
39342.3
4[S]+

Figure 5.2. MALDI TOF MS spectrum of biotinylated antibody I prepared with the standard dried-droplet method on the same surface with the microarray.

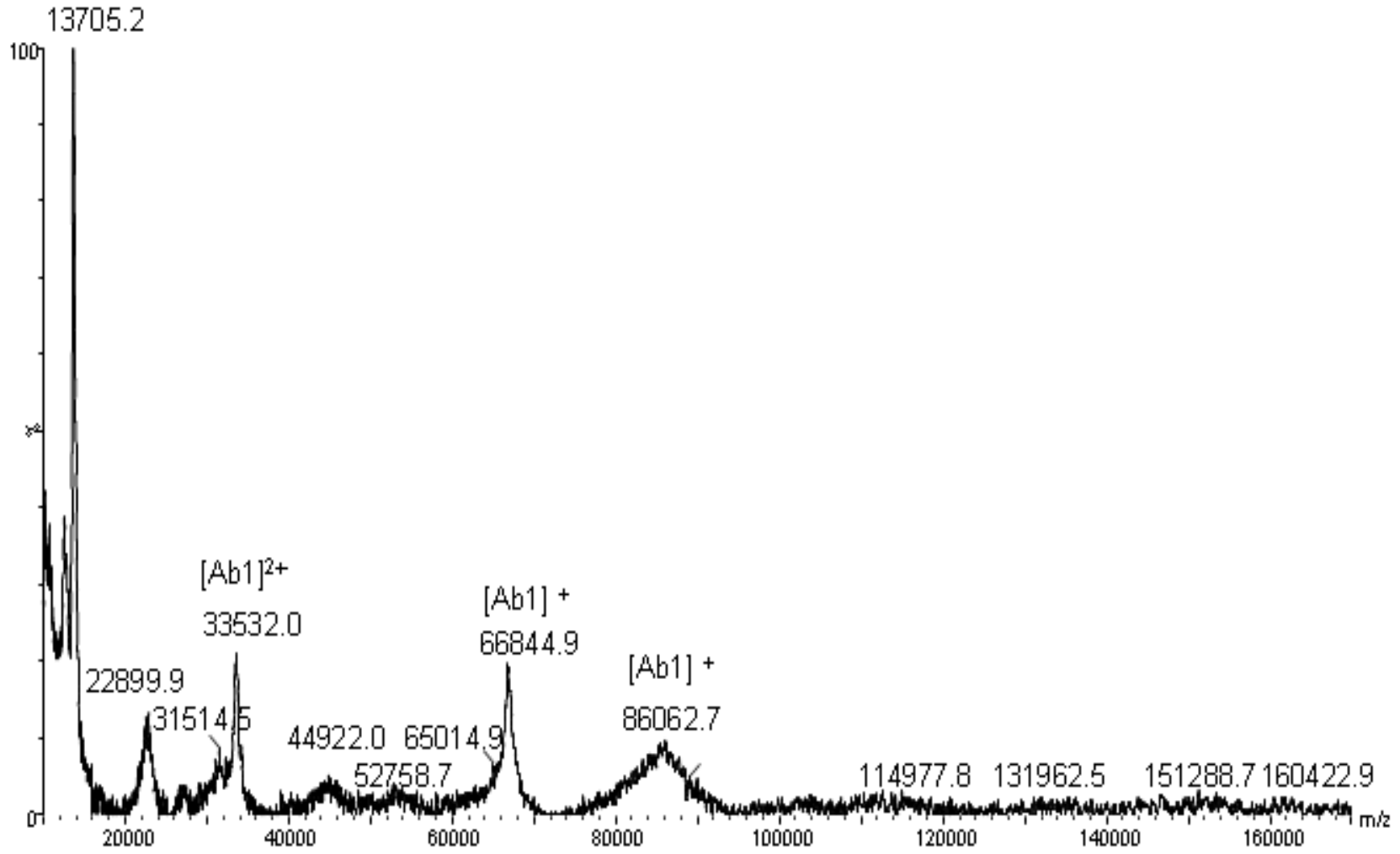
13705.2
100
%
0
[Ab1]2+
33532.0
[Ab1] +
66844.9
[Ab1] +
86062.7
22899.9
31514.5
44922.0
65014.9
52758.7
114977.8
131962.5
151288.7
160422.9
m/z
20000
40000
60000
80000
100000
120000
140000
160000

Figure 5.3. MALDI TOF MS spectrum of antibody II prepared with the standard dried-droplet method on the same surface with the microarray.

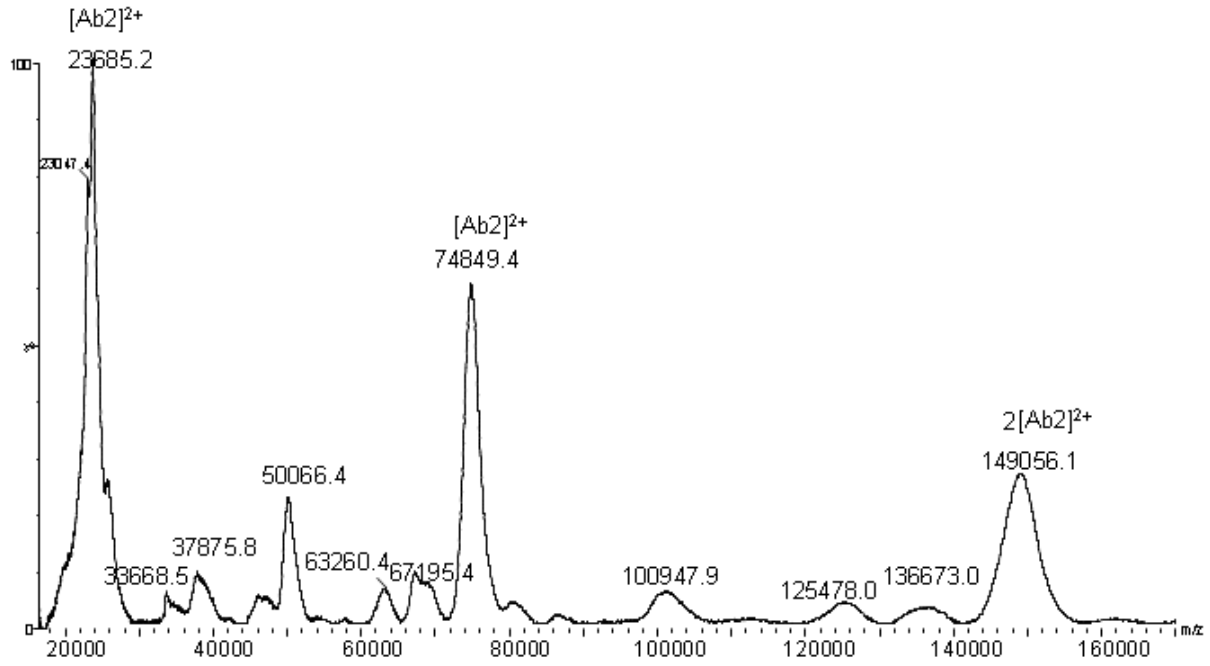
[Ab2]2+
23685.2
[Ab2]2+
74849.4
2[Ab2]2+
149056.1
50066.4
37875.8
33668.5
63260.4
67195.4
100947.9
125478.0
136673.0
%
m/z
20000
40000
60000
80000
100000
120000
140000
160000

Figure 5.4. MALDI TOF MS spectrum collected from microspots with three layers of proteins: streptavidin, antibody I and II from bottom to top.

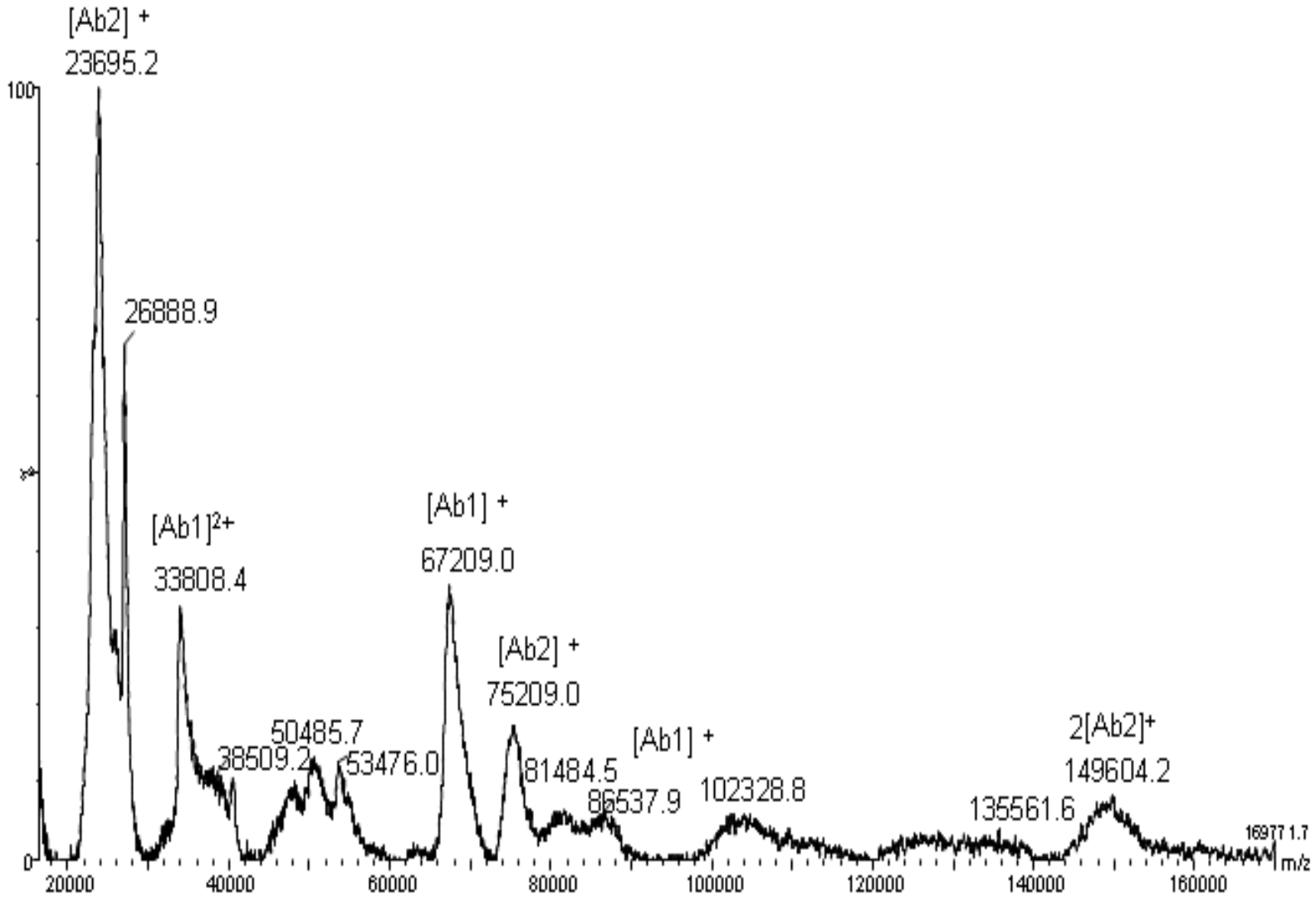
[Ab2] +
23695.2
100
%
0
26888.9
[Ab1]2+
33808.4
38509.2
50485.7
53476.0
[Ab1] +
67209.0
[Ab2] +
75209.0
81484.5
86537.9
[Ab1] +
102328.8
135561.6
2[Ab2]+
149604.2
16977 1.7
m/z
20000
40000
60000
80000
100000
120000
140000
160000

Figure 5.5. MALDI TOF MS spectrum of microspots with protein layers of streptavidin and antibody I deposited by using the MFCA.

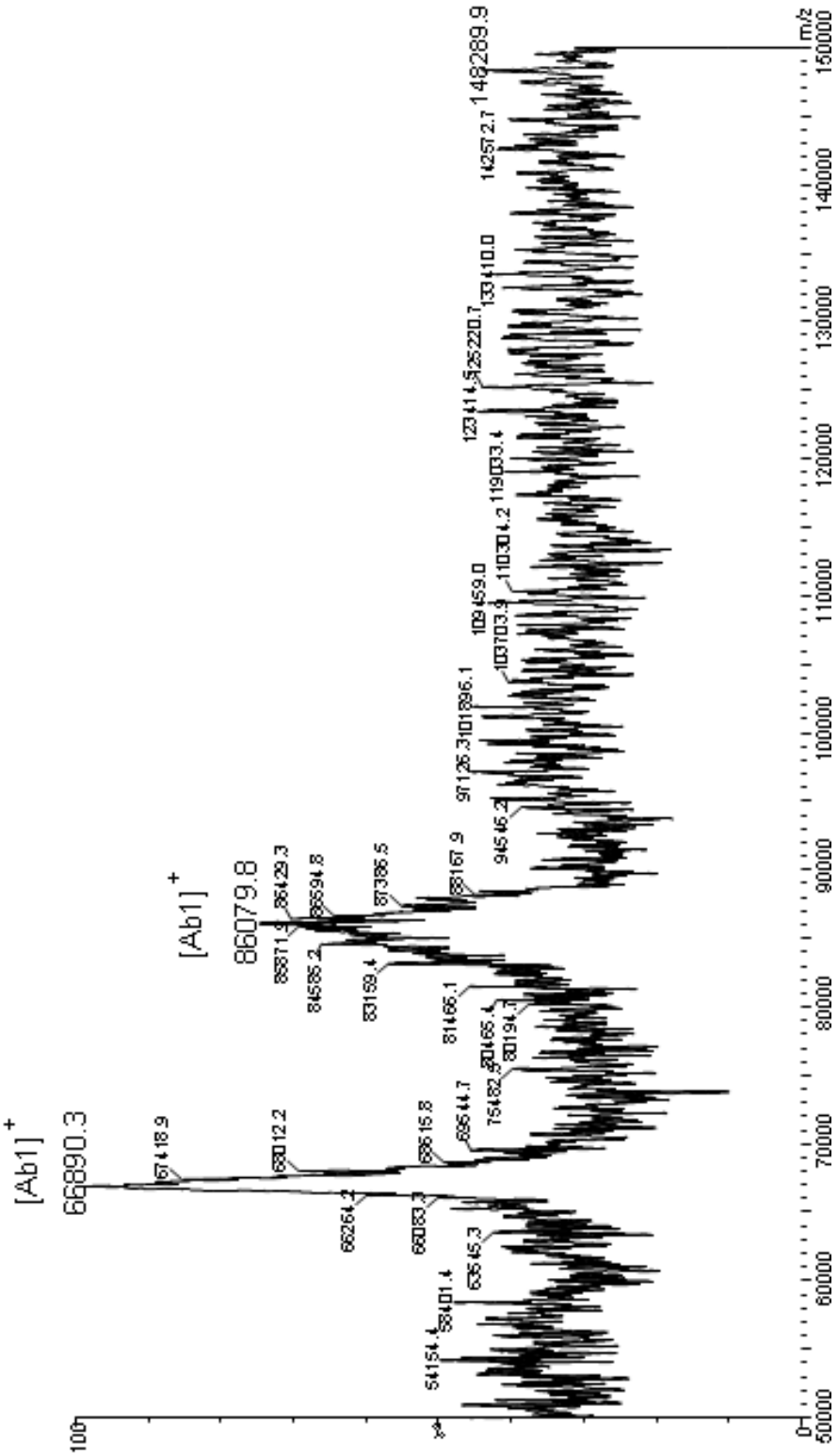
[Ab1]+
66890.3
[Ab1]+
86079.8
148289.9
m/z
100
%
0
50000
60000
70000
80000
90000
100000
110000
120000
130000
140000
150000

Table 5.1. Protein samples on microarray surface deposited by MFCA.

column	1-2	3-5	6-8
layer 3			antibody II
layer 2		antibody I	antibody I
layer 1	streptavidin	streptavidin	streptavidin

CHAPTER 6

MFCA-SPRM FOR CHARACTERIZATION OF VESICLE IMMOBILIZATION ON PLANAR SOLID SURFACES

Introduction

This chapter presents the application of the integrated MFCA-SPRM system in the study of vesicle adsorption on planar solid surfaces. The focus of the investigations is to characterize effects of vesicle preparation methods, vesicle composition, and the hydrophilicity of the binding surfaces on the structure of vesicles immobilized on a SPR sensing surface. A simple model to calculate the surface area of a lipid bilayer is proposed to correlate the SPR response with vesicle structure on the surface.

A vesicle is a useful model system of a cell membrane for basic research on the structure or function properties of cell membrane components such as receptor proteins.[1, 2] In addition to fundamental molecular biology studies, vesicles also are useful platforms in various applications such as drug delivery[3, 4] and bioanalysis.[5, 6] Depending on the application, vesicles can be immobilized intact or can form a bilayer on a sensing surface, which is a crucial step for using the surface later for molecule recognition.[7, 8] Typically, when vesicles adsorb on a hydrophilic solid surface a process of adhesion, flattening, rupture and formation of a planar single bilayer occurs.[9] Immobilization of intact vesicles is also possible by controlling the surface conditions and vesicle properties.[5]

Because of the fragile structure of vesicles, it is challenging to directly detect and measure the surface-bound vesicles. Some techniques have been used or combined to characterize vesicles on various surfaces via surface roughness, changes of mass or refractive index and fluorescence labeling,[10, 11] scanning force microscopy,[12-16] quartz crystal microbalance (QCM),[17-19] SPR,[20-23] SPR fluorescence microscopy,[24] transmission electron cryo-microscopy(TEM),[9] electrochemical impedance measurement,[25] and fluorescence microcopy and spectroscopy[5, 26] are among the widely used analytical techniques.

Several factors such as the vesicle size (depending on the preparation method),[26] the vesicle composition (lipid- and membrane-bound molecules),[27] substrate surface properties (hydrophilic or hydrophobic, flat or patterned)[28] and the environment (temperature,[29] ionic strength)[9] play key roles in influencing the adsorption mechanism of vesicles on a solid surface. These factors contribute to the interfacial force or surface tension that determines the shape or the form of vesicles on the surface.

The MFCA-SPRM with the closed flow system (no exposure of vesicles to air) is useful for high-throughput analysis of immobilization of vesicles and the factors impacting this process in a controlled manner. Previously, SPR has been used to analyze the interactions between immobilized vesicles and membrane-bound proteins.[5] In this example, the vesicles were composed of a mixture of DOPC and biotin-DOPE and immobilized on a streptavidin-coated surface. It is not clear that the vesicles bind to the streptavidin surface via biotin-streptavidin interactions or physical adsorption. In order to understand the process of vesicle immobilization, the MFCA-SPRM was used to characterize the adsorption of two types of vesicles (with and without biotin-DOPE) on

two types of surfaces: a streptavidin surface and a thiol-based SAM surface. The vesicles were prepared using two methods: extrusion and sonication. In total, eight different conditions for vesicle immobilization were investigated in this study.

Experimental

Materials

1,2-Dioleoyl-***sn***-glycero-3-phosphocholine (DOPC) (Product # 850375) and 1, 2-dioleoyl-***sn***-glycero-3-phosphoethanolamine-N-(biotinyl) (biotin-DOPE) (Product # 870282) were purchased from Avanti Polar Lipids Inc. Streptavidin (Product # 21135) was purchased from Pierce.

Preparation of Vesicles

Vesicles were prepared from DOPC and mixtures of DOPC with 0.3 mol% biotin-DOPE. Both lipids were dissolved in chloroform and dried under a stream of nitrogen and exposed to vacuum for 4 h. Then PBS buffer (pH 7.4) was added to the dried lipids to obtain 1 mM total concentration of lipids. The lipid solution was divided into two aliquots to prepare vesicles by sonication and extrusion separately.

In the sonication method, preparations of DOPC and a mixture of DOPC with 0.3 mol--% biotin-DOPE in PBS buffer were sonicated in a 30 °C water bath for 30 min before use. For the extrusion method, both samples were subjected to six freeze-thaw and vortex cycles using a dry ice/acetone mixture and a 30 °C water bath. A miniextruder (LiposoFast, Avestin) was used to push the lipid solution through polycarbonate membranes (100 nm pore, Avestin) at least 20 times. The size distribution of extruded

vesicles was measured by dynamic light scattering (DLS) (NICOMP 380 ZLS, Particle Sizing System).

MFCA- SPRM Analysis of Immobilization of Vesicles

The SAM surface was prepared as described in Chapter 2 with a mixture of BAT and OEG thiols. Four types of vesicle samples (DOPC and biotin-DOPE prepared by sonication and extrusion) were flowed through 12 flow cells, with each sample run in triplicate. The flow rate was 50 µL/min and the contact time was about 6 min. Then, PBS buffer was flowed through the flow cells after the samples.

The experiment was repeated using a surface of a streptavidin deposited on the SAM surface using the MFCA. The streptavidin concentration used to pattern the surface was 100 µg/mL. Immobilization of the streptavidin and vesicles were monitored with SPRM.

Results and Discussions

Analysis of SPR Response to Vesicle Adsorption

SPR is a label-free, surface-sensitive technique that detects biomolecular adsorption via effective local refractive index changes. In Chapter 2, we have demonstrated that the SPRM signal (changes in % reflectivity) can be converted to a biomolecule film thickness providing quantitative analysis. Figure 6.1 shows the SPR real-time curves for adsorption of streptavidin and four types of vesicles. These four types of vesicles are of two compositions: DOPC and DOPC with 0.3% biotin-DOPE prepared by sonication or extrusion.

Figure 6.2 is a comparison of four types of vesicles adsorbed on two surfaces, streptavidin and mixed SAM. The SPR signals related to the vesicle adsorption in Figure

6.2 are summarized in Table 6.1. The signals seem various and random at first. However, when the data are compared with reported results also from SPR spectroscopy, it was found that the SPR signal was related to the structure of vesicles on the surface. Jung et al.[5] reported that extruded vesicles with biotin bound to a streptavidin surface make a planar layer of intact vesicles and this was confirmed with fluorescent dye leakage experiment. In their report, the SPR spectroscopy signal of these immobilized intact vesicles was 30 nm (shift of wavelength), and the shift for the adsorption of a streptavidin layer was 10 nm. The ratio of these two signals was about three. In our experiment under the same experimental conditions, the extruded vesicles doped with biotin-labeled lipid adsorbed on a streptavidin surface to give a SPR response of 15.51 ± 0.04% reflectivity. The SPR response for streptavidin adsorption was 4.96 ± 0.61% reflectivity. The SPR signal ratio of intact vesicles to a layer of streptavidin was 3.13, which was close to the reported value of three. Equation 2.1 in Chapter 2 shows that the SPR signal is proportional to the thickness of an adsorbed layer. So if the thickness of a streptavidin layer is assumed to be close in reported and our experiment results, the thickness of vesicle layers will be the same too because of the same signal ratio. Since it is reported that the immobilized vesicles were intact,[5] the extruded vesicles will also form a layer of intact vesicles in our system.

Sonicated vesicles have been used to created lipid bilayers on a hydrophilic surface;[30] so it is assumed that sonicated DOPC vesicles formed a lipid bilayer on SAMs surface. The assumption is also reasonable by comparing the SPR signal of the sonicated DOPC vesicles (4.74 ± 0.23%) and that of a streptavidin layer (4.96 ± 0.61%). The refractive index of protein is approximated to be 1.57 and that of DOPC is estimated to be 1.49.[5]

According to Equation 2.5 in Chapter 2, the thickness of a streptavidin layer is approximately equal to that of a planar bilayer because the thickness of biomolecule layer is proportional to the SPR signal. The reported monolayer of streptavidin has a thickness of 5–7 nm, and the thickness of a surface-bound planar bilayer of DOPC is 6.0–7.5 nm.[16, 31] The reported thickness of streptavidin and bilayer also confirmed that the assumption of DOPC vesicles prepared by sonication form a bilayer structure on a hydrophilic SAM surface is reasonable.

Based on the data analysis and conclusions above, a calculation model was built to explain the SPR signal of vesicle adsorption and the corresponding structure on the SPR sensor surfaces. The SPR signal is caused by the local effective refractive index change of caused by displacement of water (buffer) by the adsorbed lipids. The SPR signal is linear to the mass of lipids within the detection region. The total mass of adsorbed DOPC can be calculated by multiplying the surface density by the surface area of a bilayer assuming the lipid bilayer is an ordered structure with uniform density. Within a fixed area (L^2), if the surface is covered by a planar lipid bilayer as shown in Figure 6.3, the surface area of the bilayer is L^2. If the surface is covered by a monolayer of vesicles with a radius of R, the surface area of the lipid bilayer is equal to $4\pi R^{2\cdot} (L/2R)^{2} = \pi L^2$. The ratio of these two values is π (3.14) and close to that of experimental data (15.51/4.74 = 3.27). A close packing could make a larger signal ratio. A planar lipid bilayer and a monolayer of intact vesicles are two ideal cases of the minimum and maximum coverage of lipid bilayer.

A simple model is shown in Figure 6.4 that explains the transformation from vesicles to planar bilayer on supported solid surface.[12] The kinetics of the transformation depends

on many factors, such as properties of the surface and vesicles and the interaction between adsorbed vesicles. In our measurement, the SPR signals between 4.74 and 15.51% reflectivity were compared with the SPR signal of a planar bilayer. The ratios are listed in Table 6.1 and can be related the transitional structure in Figure 6.4. For example, double bilayers generate a signal twice as large as that of a bilayer, which is equal to a ratio of two. The possible structures and effect of physicochemical properties of surface and vesicles will be discussed next. Conclusions from SPR experiments can be further confirmed with other analytical techniques, such as AFM imaging and QCM measurements.[16]

Effect of Vesicle Size

The difference between vesicles prepared by sonication and extrusion is the size distribution. The sizes of vesicles prepared in our experiments were consistent with reported results. With dynamic light scattering measurement, the extruded DOPC vesicles were 121.5 ± 10 nm. Published reports of the same lipids and method produced vesicles with an average size of 112 ± 6 nm.[26, 29] The sonicated vesicles were 33.4 ± 2.6 nm and a small percentage was 177.2 ± 14.4 nm. For the same DOPC vesicles, the reports also included a bimodal size distribution, with a majority of size of 28 ± 2 nm and a small percentage of vesicles with a size of 196 ± 10 nm.[26]

For the DOPC vesicles with biotin, both sonicated and extruded vesicles bound to a streptavidin surface and led to relatively high SPR signals of 15.51 ± 0.04 and 14.32 ± 0.67% reflectivity. These vesicles were intact based on our analysis of the data described above. The size of the vesicles (extruded *vs* sonicated) did not have a significant effect on

specific immobilization on the streptavidin surface. For vesicle adsorption on the SAM surface (no streptavidin layer), there was a large size effect. The SPR response measured for adsorption of the extruded DOPC vesicles (12.40 ± 0.85% reflectivity, ratio of 2.62) was nearly twice as large as the response for sonicated vesicles (6.57 ± 0.26% reflectivity, ratio of 1.39). The difference in signal can be explained by the fact that small vesicles easily break and spread on the surface to form a bilayer fast; while it takes a longer time for larger vesicles to adsorb on the surface, become flattened and ruptured into double bilayers and finally form a single bilayer. Adsorption of extruded DOPC vesicles containing biotin on a streptavidin surface produced a ratio of 2.62, which puts the signal between the signal ratio for a double bilayer of two and that for an intact vesicle of 3.14, so it is possible that most vesicles are deformed after adsorption on the SAM surface. Adsoprtion of the sonicated vesicles produced a ratio of 1.39 and likely had structures of mixed single and double bilayers.

Effect of Surface Hydrophilicity

The hydrophilicity of the surface is an important factor that determines the interfacial force and the consequent form of vesicles on the surface. DOPC vesicles tend to form a bilayer on a hydrophilic surface.[30] DOPC vesicles adsorbed on a streptavidin surface show higher signals than those adsorbed on SAMs in the experiments summarized in Table 3.1. The mixed binary SAM surface is composed of OH- and biotin-terminated functional groups and the surface is hydrophilic as confirmed by the contact angle of water droplets of over 100°.[32] The streptavidin surface has a contact angle of 26.33° and is hydrophobic compared to the SAM surface.[33] Therefore, The hydrophilicity of surfaces

also could affect the formation of bilayers. A hydrophobic surface is preferred for intact vesicle immobilization, which correlates with the observations.

Effect of Vesicle Composition

It is interesting to note that under all of the tested conditions (vesicles prepared with sonication or extrusion, adsorption on SAM or streptavidin surfaces), adsorption of vesicles of DOPC with 0.3 mol% biotin-DOPE showed a higher SPR response than DOPC vesicles without biotin as shown in Table 6.1. The change of composition of lipids could affect the molecular interactions between lipids with the surface, subsequent binding energy and the conformation of vesicles on the surfaces. How the biotin-DOPE change the vesicle immobilization can be probed by varying the concentration percentage of biotin-DOPE in the DOPC vesicles.

Nonspecific Adsorption of Intact Vesicles

The SPR responses for DOPC vesicles adsorption on a streptavidin surface when the vesicles were prepared by sonication (7.09 ± 0.48% reflectivity) and extrusion (10.26 ± 0.35% reflectivity) were 1.5 and 2.15 times that of a bilayer on a SAM surface (4.74 ± 0.23% reflectivity), respectively. The sonicated DOPC vesicles may form a mixture of double bilayer and planar bilayer on the surface; the extruded DOPC vesicles may have deformed vesicles and planar bilayer according to the calculation model. This morphology of DOPC vesicle adsorbed on a streptavidin surface could be further investigated with AFM.

Conclusions

The MFCA-SPRM is a label-free, high-throughput technique useful for characterization of the adsorption of vesicles. Adsorption of extruded and sonicated vesicles on SAMs and streptavidin surfaces was performed with the MFCA-SPRM to investigate the effect of vesicle size, lipids composition and hydrophilicity of the surface on the vesicle structure upon adsorption on solid surfaces. The results show that vesicles prepared by extrusion with specific binding are preferred for immobilization of intact vesicles on a hydrophobic protein surface. A calculation model is proposed to correlate the MFCA-SPRM signal with vesicle structure on the surface. The accuracy of the model could be further investigated with other analytical techniques such as AFM.

References

1. Lee, T. H.; Aguilar, M. I., Trends in the development and application of functional biomembrane surfaces. *Biotechnol. Annu. Rev.*, **2006**, 12, 85-136.

2. Reiss, B.; Janshoff, A.; Steinem, C.; Seebach, J.; Wegener, J., Adhesion kinetics of functionalized vesicles and mammalian cells: A comparative study. *Langmuir* **2003**, *19*, 1816-1823.

3. Vermette, P.; Meagher, L.; Gagnon, E.; Griesser, H. J.; Doillon, C. J., Immobilized liposome layers for drug delivery applications: Inhibition of angiogenesis. *J. Control. Release* **2002**, *80*, 179-195.

4. Torchilin, V. P., Recent advances with liposomes as pharmaceutical carriers. *Nat. Rev. Drug Discov.* **2005**, *4*, 145-160.

5. Jung, L. S.; Shumaker-Parry, J. S.; Campbell, C. T.; Yee, S. S.; Gelb, M. H., Quantification of tight binding to surface-immobilized phospholipid vesicles using surface plasmon resonance: Binding constant of phospholipase A_2. *J. Am. Chem. Soc.* **2000**, *122*, 4177-4184.

6. Puu, G., An approach for analysis of protein toxins based on thin films of lipid mixtures in an optical biosensor. *Anal. Chem.* **2001**, *73*, 72-79.

7. Vermette, P.; Griesser, H. J.; Kambouris, P.; Meagher, L., Characterization of surface-immobilized layers of intact liposomes. *Biomacromolecules* **2004**, *5*, 1496-1502.

8. Erb, E. M.; Chen, X.; Allen, S.; Roberts, C. J.; Tendler, S. J. B.; Davies, M. C.; Forsen, S., Characterization of the surfaces generated by liposome binding to the modified dextran matrix of a surface plasmon resonance sensor chip. *Anal. Biochem.* **2000**, *280*, 29-35.

9. Richter, R. P.; Barat, R.; Brisson, A. R., Formation of solid-supported lipid bilayers: An integrated view. *Langmuir* **2006**, *22*, 3497-3505.

10. Reimhult, E.; Zach, M.; Hook, F.; Kasemo, B., A multitechnique study of liposome adsorption on Au and lipid bilayer formation on SiO2. *Langmuir* **2006**, *22*, 3313-3319.

11. Richter, R. P.; Brisson, A. R., Following the formation of supported lipid bilayers on Mica: A study combining AFM, QCM-D, and ellipsometry. *Biophys. J.* **2005**, *88*, 3422-3433.

12. Jass, J.; Tjarnhage, T.; Puu, G., From liposomes to supported, planar bilayer structures on hydrophilic and hydrophobic surfaces: An atomic force microscopy study. *Biophys. J.* **2000**, *79*, 3153-3163.

13. Tarasova, A.; Griesser, H. J.; Meagher, L., AFM study of the stability of a dense affinity-bound liposome layer. *Langmuir* **2008**, *24*, 7371-7377.

14. Dufrane, Y. F.; Lee, G. U., Advances in the characterization of supported lipid films with the atomic force microscope. *Biochimica et Biophysica Acta - Biomembranes* **2000**, *1509*, 14-41.

15. Schunherr, H.; Johnson, J. M.; Lenz, P.; Frank, C. W.; Boxer, S. G., Vesicle adsorption and lipid bilayer formation on glass studied by atomic force microscopy. *Langmuir* **2004**, *20*, 11600-11606.

16. Pignataro, B.; Steinem, C.; Galla, H.-J.; Fuchs, H.; Janshoff, A., Specific adhesion of vesicles monitored by scanning force microscopy and quartz crystal microbalance. *Biophys. J.* **2000**, *78*, 487-498.

17. Wegener, J.; Janshoff, A.; Steinem, L., The quartz crystal microbalance as a novel means to study cell-substrate interactions in situ. *Cell Biochem. Biophys.* **2001**, *34*, 121-151.

18. Vu, T. H.; Shimanouchi, T.; Ishii, H.; Umakoshi, H.; Kuboi, R., Immobilization of intact liposomes on solid surfaces: A quartz crystal microbalance study. *J. Colloid Interface Sci.* **2009**, *336*, 902-907.

19. Luthgens, E.; Herrig, A.; Kastl, K.; Steinem, C.; Reiss, B.; Wegener, J.; Pignataro, B.; Janshoff, A., Adhesion of liposomes: A quartz crystal microbalance study. *Meas. Sci. Technol.* **2003**, *14*, 1865-1875.

20. Beseniaar, M.; Marek, P.; Lakey, J. H.; Anderluh, G., Surface plasmon resonance in protein-membrane interactions. *Chem. Phys. Lipids* **2006**, *141*, 169-178.

21. Mozsolits, H.; Aguilar, M. I., Surface plasmon resonance spectroscopy: An emerging tool for the study of peptide-membrane interactions. *Biopolymers - Peptide Science Section* **2002**, *66*, 3-18.

22. Lin, M. S.; Chiu, H. M.; Fan, F. J.; Tsai, H. T.; Wang, S. S. S.; Chang, Y.; Chen, W. Y., Kinetics and enthalpy measurements of interaction between β-amyloid and liposomes by surface plasmon resonance and isothermal titration microcalorimetry. *Colloids Surf. B Biointerfaces* **2007**, *58*, 231-236.

23. Plant, A. L.; Brigham-Burke, M.; Petrella, E. C.; O'Shannessy, D. J., Phospholipid/alkanethiol bilayers for cell-surface receptor studies by surface plasmon resonance. *Anal. Biochem.* **1995**, *226*, 342-348.

24. Tawa, K.; Morigaki, K., Substrate-supported phospholipid membranes studied by surface plasmon resonance and surface plasmon fluorescence spectroscopy. *Biophys. J.* **2005**, *89*, 2750-2758.

25. Sapper, A.; Reiss, B.; Janshoff, A.; Wegener, J., Adsorption and fluctuations of giant liposomes studied by electrochemical impedance measurements. *Langmuir* **2006**, *22*, 676-680.

26. Lapinski, M. M.; Castro-Forero, A.; Greiner, A. J.; Ofoli, R. Y.; Blanchard, G. J., Comparison of liposomes formed by sonication and extrusion: Rotational and translational diffusion of an embedded chromophore. *Langmuir* **2007**, *23*, 11677-11683.

27. Nicolini, C.; Baranski, J.; Schlummer, S.; Palomo, J.; Lumbierres-Burgues, M.; Kahms, M.; Kuhlmann, J.; Sanchez, S.; Gratton, E.; Waldmann, H.; Winter, R., Visualizing association of N-Ras in lipid microdomains: Influence of domain structure and interfacial adsorption. *J. Am. Chem. Soc.* **2006**, *128*, 192-201.

28. Tero, R.; Watanabe, H.; Urisu, T., Supported phospholipid bilayer formation on hydrophilicity-controlled silicon dioxide surfaces. *Phys. Chem. Chem. Phys.* **2006**, *8*, 3885-3894.

29. Reimhult, E.; Hook, F.; Kasemo, B., Intact vesicle adsorption and supported biomembrane formation from vesicles in solution: Influence of surface chemistry, vesicle size, temperature, and osmotic pressure. *Langmuir* **2003**, *19*, 1681-1691.

30. Smith, K. A.; Gale, B. K.; Conboy, J. C., Micropatterned fluid lipid bilayer arrays created using a continuous flow microspotter. *Anal. Chem.* **2008**, *80*, 7980-7987.

31. Wiener, M. C.; White, S. H., Structure of a fluid dioleoylphosphatidylcholine bilayer determined by joint refinement of x-ray and neutron diffraction data. III. Complete structure. *Biophys. J.* **1992**, *61*, 434-447.

32. Szori, M. n.; Tobias, D. J.; Roeselovai M., Microscopic wetting of mixed self-assembled monolayers: A molecular dynamics Study. *J. Phys. Chem. B* **2009**, *113*, 4161-4169.

33. van Oss, C. J.; Giese, R. F.; Bronson, P. M.; Docoslis, A.; Edwards, P.; Ruyechan, W. T., Macroscopic-scale surface properties of streptavidin and their influence on aspecific interactions between streptavidin and dissolved biopolymers. *Colloids Surf. B Biointerfaces* **2003**, *30*, 25-36.

Figure 6.1. SPR real-time curves of adsorption of streptavidin and four types of vesicles immobilized on of streptavidin layers on a planar surface. The DOPC (DOPC) and DOPC with 0.3 mol% biotin-DOPE (Biotin) vesicles were prepared by sonication and extrusion.

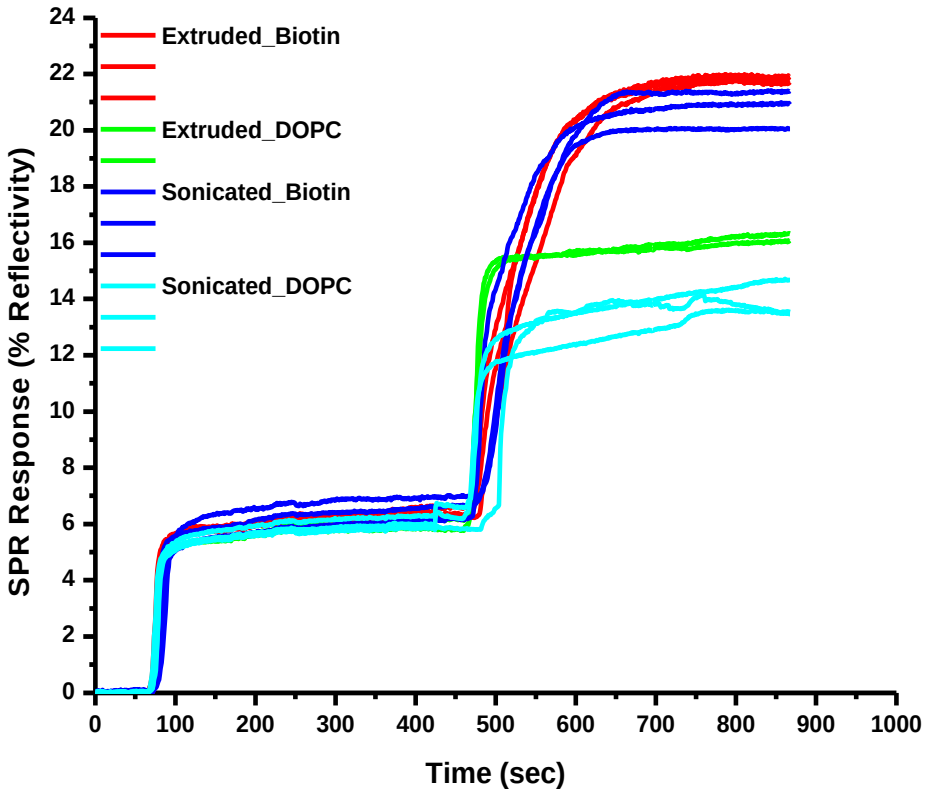
Extruded_Biotin
Extruded_DOPC
Sonicated_Biotin
Sonicated_DOPC
SPR Response (% Reflectivity)
Time (sec)
0
2
4
6
8
10
12
14
16
18
20
22
24
0
100
200
300
400
500
600
700
800
900
1000

Figure 6.2. Comparison of SPR curves of four types of vesicles adsorbed on two different surfaces. (a) Streptavidin surface and (b) amixed biotin-terminated thiol SAM surface composed of OEG and BAT.

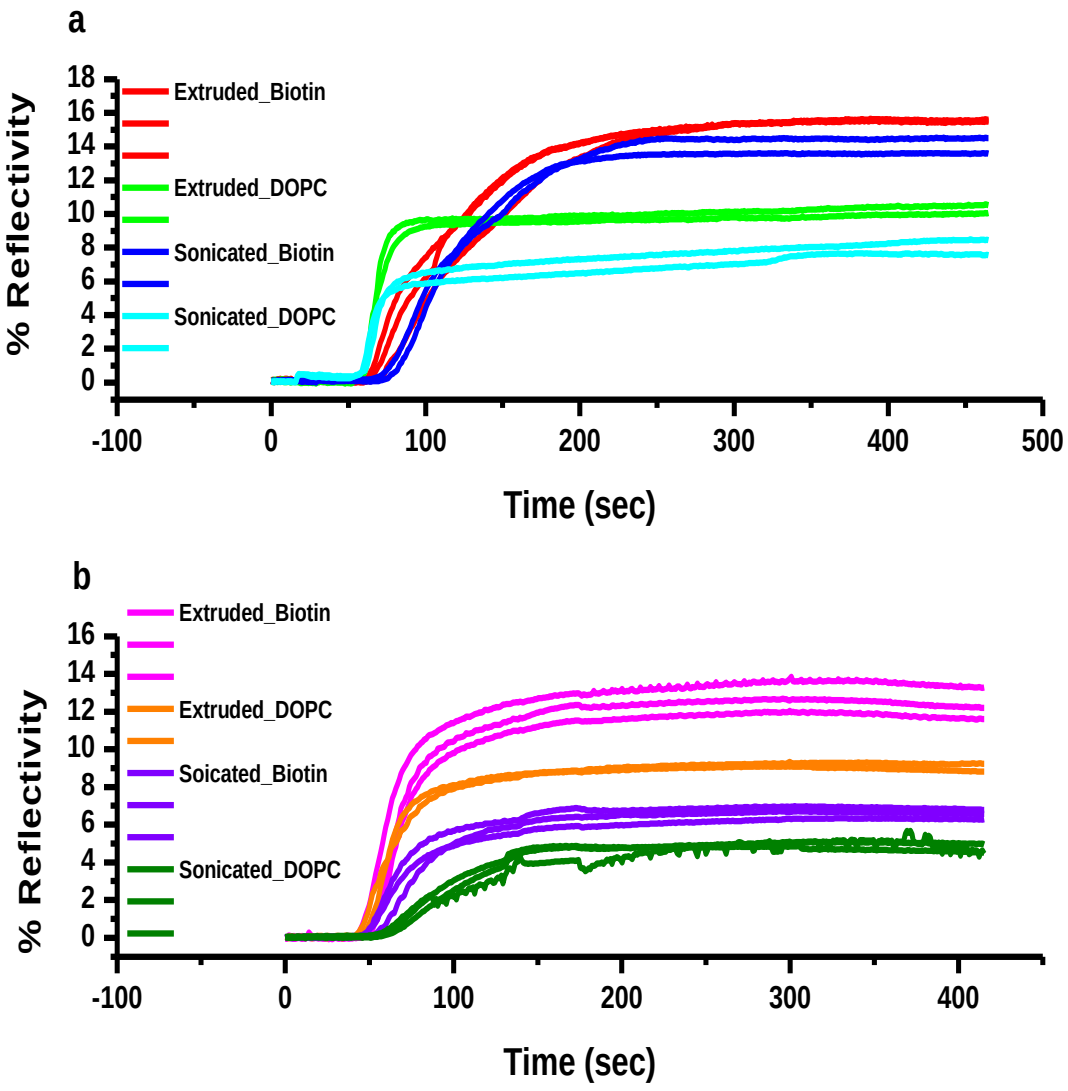
a
% Reflectivity
Extruded_Biotin
Extruded_DOPC
Sonicated_Biotin
Sonicated_DOPC
Time (sec)
b
% Reflectivity
Extruded_Biotin
Extruded_DOPC
Soicated_Biotin
Sonicated_DOPC
Time (sec)

Figure 6.3. A calculation model of the total surface area of vesicles. The model was based on the assumption that intact vesicles formed a monolayer of ordered structure on the streptavidin surface.

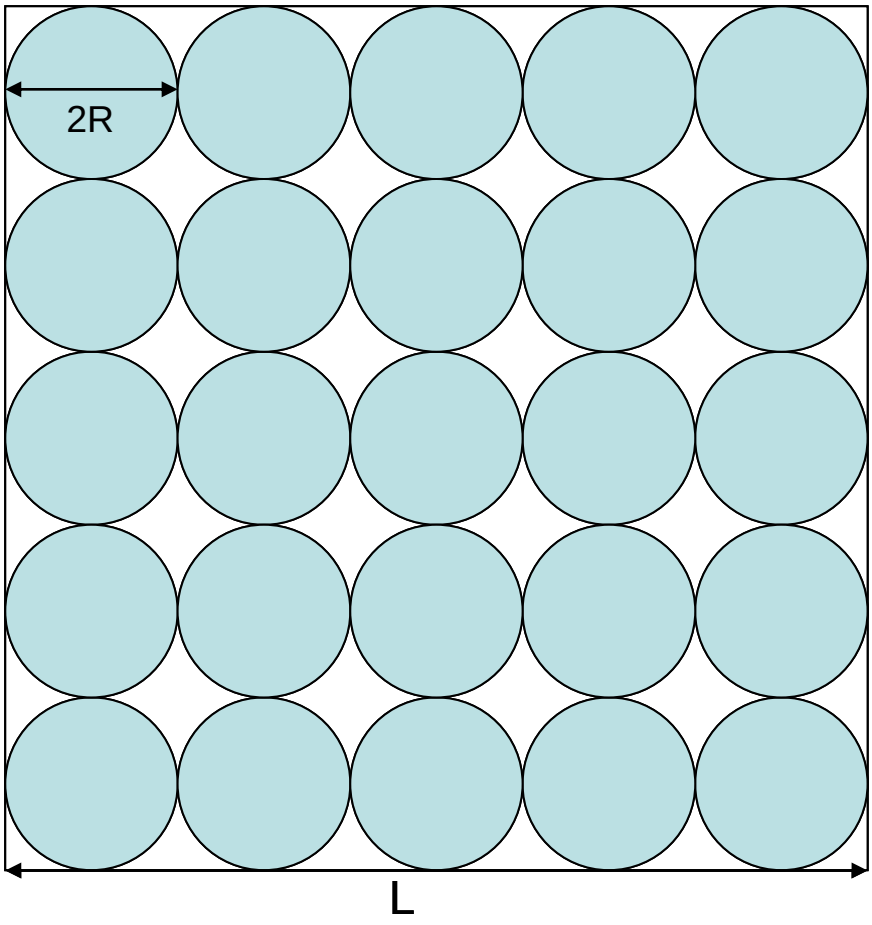
2R
L

Figure 6.4. A model to interpret the transformation from vesicles to a supported planar bilayer on a solid surface as suggested by AFM imaging. The vesicle adsorbs on the surface (A-C), becomes flattened from the edges, expands, spreads and collapses to form double bilayers (D-F). Then the vesicle either rolls (G) or slides (H) to be single bilayer (I). Reprinted from *Biophysical Journal* **2000,** *79*, Jass, J.; Tjarnhage, T.; Puu, G., From Liposomes to Supported, Planar Bilayer Structures on Hydrophilic and Hydrophobic Surfaces: An Atomic Force Microscopy Study, 3153-3163, Copyright (2000), with permission from Elsevier.

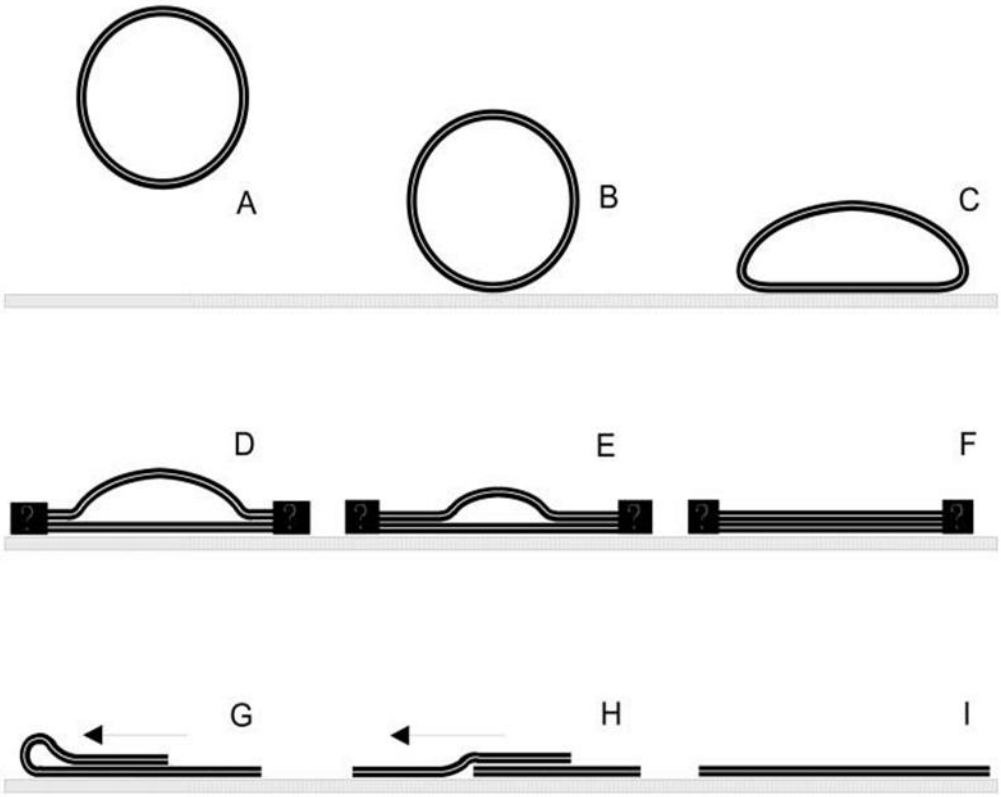
A
B
C
D
E
F
G
H
I

Table 6.1. SPR signals of the adsorption of four types of vesicles on SAM and streptavidin surfaces and their ratios with adsorption of streptavidin.

Type of Vesicles	SAMs Surface		Streptavidin Surface	
	% reflectivity	ratio	% reflectivity	ratio
Extruded-Biotin	12.40±0.85	2.62	15.51±0.04	3.27
Extruded-DOPC	9.04±0.26	1.91	10.26±0.35	2.16
Sonicated-Biotin	6.57±0.26	1.39	14.32±0.67	3.02
Sonicated-DOPC	4.74±0.23	1.00	7.09±0.48	1.50

CHAPTER 7

CONCLUSIONS

The integrated MFCA-SPRM system incorporates multichannel microfluidics with the surface sensitive technique of surface plasmon resonance microscopy. The MFCA-SPRM is useful for studying biomolecular binding events, including kinetics, at the liquid-solid interface. The multiple-step continuous-flow deposition with the MFCA enables *in situ* protein immobilization and interaction analysis in a microarray format. The procedure of integrating the MFCA with a custom-built SPRM was described in Chapter 2. Interactions between antibodies were adopted as a model to demonstrate the capability of *in situ* microarray fabrication and analysis with the MFCA-SPRM.

In Chapter 3, we used both modeling and experimental methods to investigate factors that impact the biomolecular interaction analysis based on the MFCA-SPRM. The 2D modeling results showed that the reactant concentration in solution and on surface and the binding affinity constants are important factors in binding analyses with MFCA-SPRM. However, there are some limitations of the modeling because mass transport and reactions in 3D flow cell are more complex than the 2D modeling. The biotin-streptavidin and Daclizumab-IgG interactions were used as two model systems in the experimental investigations of effects of flow rate and surface heterogeneity on analyses of

biomolecular interactions. The experimental results show the reaction rate in the MFCA is proportional to the flow rate. As the flow rate increases, the reaction transit from diffusion-limited to reaction-limited. For a diffusion-limited reaction, the surface concentration of product changes linearly with time but 1/3 power of flow rate with a flow cell of fixed geometry. The heterogeneous SAMs and protein surface create to heterogeneous local refractive changes because the 3D structure of binding sites on microscopic scale was not uniformly active and evenly distributed, which was a major source of spot-to-spot signal variations in the measurements. The activity of immobilized proteins did not increase linearly with their surface concentration. A lower surface concentration of binding sites demonstrated higher activity, but higher surface concentration of binding sites captured the most absolute amount of analysts. Changing the geometry of flow cell could improve the mass transport but the effect is limited as shown by initial investigations. Finally, we identified that another major source of signal variations among microspots was the shift of the light incident angles from the center to edges of the laser beam after the light was refracted by a hemi-spherical prism. Using a hemi-spherical prism of a larger diameter could minimize the SPR sensing area or changing to prism of other shapes such as dove prisms that can eliminate issues due to the angle shift.

The optimized MFCA-SPRM system was applied in multiple projects of bimolecular interaction analysis. A preliminary investigation of developing an immunogenicity assay of Daclizumab with MFCA-SPRM was reported in Chapter 4. Three serum samples of multiple sclerosis patients treated with Daclizumab for different durations (0, 4, and 6 years) were screened with a Daclizumab-coated SPR surface to detect ADAs. The sample

from the patient without treatment shows a high response that exceeds the average signal of the non-specific adsorption. However, it is difficult to identify the surface bound molecules with SPR. MALDI MS has shown to be a fast and accurate technique for molecular identification via mass to charge ratio. One solution is to combine the SPR with MALDI MS to perform quantitative analysis of protein adsorption on the SPR sensing surface and then identify surface bound proteins on the SPR substrate surface with MALDI MS. However, due to the thickness limitation of substrates required by a commercial MALDI MS system, the combination of MFCA-SPRM with MALDI MS was challenging. The preliminary experiments were done using arrays prepared *ex situ* with the MFCA. Chapter 5 presented the result of using MALDI MS to identity proteins on microspots of an antibody array created by the MFCA on a gold-coated microscope slide. It was found that it was possible to identify the antibodies on the microarray created by the MFCA. Further investigation could probe important factors to improve the detection limit of MALDI MS. This preliminary work also demonstrated the versatility of applying MFCA as a microspotter in MALDI MS sample preparation.

Characterization of vesicles adsorption on solid surfaces by MFCA-SPRM was reported in Chapter 6. The mobility of vesicles leads to the formation of bilayers, flattened vesicles or intact vesicles at surface. SPR can only detect changes caused by refractive index, so it is challenging to determine the structure of vesicles on the surface. Compared with reported result of vesicle structure characterized by atomic force microscopy and SPR spectroscopy, a calculation model was proposed to correlate SPR signals with the structure of the vesicles on the surface. Experiments with AFM to

analyze the vesicles structure under tested conditions could further prove the accuracy of the model.

This dissertation has demonstrated the setup of an integrated MFCA-SPRM system, the optimization of experimental conditions for microarray analysis of biomolecular interactions. The optimized conditions and developed methods can be applied for future large-scale sample analysis, such as development of immunogenicity assay and characterization of vesicle adsorption. The MFCA-SPRM system is also a versatile tool to be combined with other analytical instruments like MALDI MS for application in many research fields such as fundamental biomedical research, drug discovery and biomarker diagnostics.